

University of Massachusetts Medical School

eScholarship@UMMS

GSBS Dissertations and Theses

Graduate School of Biomedical Sciences

2016-07-29

The Role of MDM2 Phosphorylation in P53 Responses to DNA Damage and Tumor Suppression: A Dissertation

Michael I. Carr

University of Massachusetts Medical School

Let us know how access to this document benefits you.

Follow this and additional works at: https://escholarship.umassmed.edu/gsbs_diss



Part of the [Biochemistry Commons](#), [Cancer Biology Commons](#), and the [Cell Biology Commons](#)

Repository Citation

Carr MI. (2016). The Role of MDM2 Phosphorylation in P53 Responses to DNA Damage and Tumor Suppression: A Dissertation. GSBS Dissertations and Theses. <https://doi.org/10.13028/M2KK55>.

Retrieved from https://escholarship.umassmed.edu/gsbs_diss/847

This material is brought to you by eScholarship@UMMS. It has been accepted for inclusion in GSBS Dissertations and Theses by an authorized administrator of eScholarship@UMMS. For more information, please contact Lisa.Palmer@umassmed.edu.

**THE ROLE OF MDM2 PHOSPHORYLATION IN P53
RESPONSES TO DNA DAMAGE AND TUMOR SUPPRESSION**

A Dissertation Presented

By

MICHAEL IAN CARR

Submitted to the Faculty of the
University of Massachusetts Graduate School of Biomedical Sciences, Worcester
in partial fulfillment of the requirements for the degree of

DOCTOR OF PHILOSOPHY

JULY 29, 2016

CELL AND DEVELOPMENTAL BIOLOGY

**THE ROLE OF MDM2 PHOSPHORYLATION IN P53 RESPONSES TO DNA
DAMAGE AND TUMOR SUPPRESSION**

A Dissertation Presented
By
MICHAEL IAN CARR

This work was undertaken in Graduate School of Biomedical Sciences
Cell Biology Program

Under the mentorship of

Stephen Jones, Ph.D., Thesis Advisor

The signatures of the Dissertation Defense Committee signify
completion and approval as to style and content of the Dissertation

Sharon Cantor, Ph.D., Member of Committee

Roger Davis, Ph.D., Member of Committee

Michelle Kelliher, Ph.D., Member of Committee

Manabu Kurokawa, Ph.D., External Member of Committee

The signature of the Chair of the Committee signifies that the written dissertation
meets the requirements of the Dissertation Committee

Hong Zhang, Ph.D., Chair of Committee

The signature of the Dean of the Graduate School of Biomedical Sciences signifies
that the student has met all graduation requirements of the school.

Anthony Carruthers, Ph.D.
Dean of the Graduate School of Biomedical Sciences

July 29, 2016

Acknowledgments

I am grateful to the many people who have contributed to my development as a graduate student. I would like to thank my mentor Dr. Stephen Jones for his support and guidance. I would also like to thank the current and former members of the Jones lab for fostering a supportive and collaborative research environment. I thank Drs. Michelle Kelliher and Justine Richardson for their expertise and advice in our collaborations, and members of the Department of Cell and Developmental Biology for helpful discussions. Finally, I would like to thank my family for their enduring support.

Abstract

The p53 tumor suppressor protein is upregulated in response to DNA damage and other stress signals. The upregulation of p53 involves freeing it from negative regulation imposed by Mdm2 and MdmX (Mdm4). Accumulating evidence indicates that phosphorylation of Mdm proteins by different stress-activated kinases such as ATM or c-Abl significantly impacts p53 functions. We have previously shown that ATM phosphorylation of Mdm2 Ser394 is required for robust p53 stabilization and activation following DNA damage.

This dissertation describes *in vivo* examination of the mechanism by which Mdm2 Ser394 phosphorylation impacts p53 activities and its contribution to suppression of oncogene and DNA damage-induced tumors. We determine that phosphorylation of Mdm2 Ser394 regulates p53 activity by modulating Mdm2 stability and paradoxically delays Myc-driven lymphomagenesis while increasing lymphomagenesis in sub-lethally irradiated mice.

c-Abl phosphorylates the residue neighboring Mdm2 Ser394, Mdm2 Tyr393.

This dissertation describes the generation of a novel *Mdm2*^{Y393F} mutant mouse to determine if c-Abl phosphorylation of Mdm2 regulates p53-mediated DNA damage responses or tumor suppression *in vivo*. *Mdm2*^{Y393F} mice develop accelerated spontaneous and oncogene-induced tumors, yet display no defects in p53 stabilization and activity following acute genotoxic stress. Furthermore, the effects of these phosphorylation events on p53 regulation are not additive, as *Mdm2*^{Y393F/S394A} mice and *Mdm2*^{S394A} mice display similar phenotypes.

The studies presented herein further our understanding of the mechanisms by which DNA damage-associated kinases stabilize and activate p53, and influence p53-dependent responses and tumor suppression. A better understanding of the *in vivo* effects of Mdm2 phosphorylation may facilitate the development of novel therapeutics capable of stimulating p53 anti-tumor activity or alleviating p53-dependent toxicities in non-malignant tissues.

TABLE OF CONTENTS

Signature Page	ii
Acknowledgments	iii
Abstract	iv
Table of Contents	vi
List of Tables	vii
List of Figures	viii
Copyrighted Materials Produced by the Author	xii
Chapter I: Introduction	1
Chapter II: Mdm2 Ser394 Phosphorylation Regulates Mdm2 Stability and has Contrasting Effects on Oncogene and Radiation-Induced Tumorigenesis	35
Results	36
Methods	64
Chapter III: Phosphorylation of Mdm2 Tyr393 by c-Abl regulates p53 tumor suppression and the radiosensitivity of mice	69
Results	70
Methods	100
Chapter IV: Discussion	106
Bibliography	128

List of Tables

Chapter II

Table 2.1. Antibodies used for flow cytometry in Chapter II

Chapter III

Table 3.1. Viability of *Mdm2*^{Y393F} mice

Table 3.2. *Mdm2*^{Y393F} tumors

Table 3.3. Viability of *Mdm2*^{Y393F/S394A} mice

Table 3.4. *Mdm2*^{Y393F/S394A} tumors

Table 3.5. Antibodies used for flow cytometry in Chapter III

List of Figures

Chapter I

Figure 1.1: Diagram of the p53 protein.

Figure 1.2: Diagram of the Mdm2 protein.

Figure 1.3: Diagram of the MdmX protein.

Chapter II

Figure 2.1: Western blot of thymus extracts.

Figure 2.2: Quantification of thymus Mdm2 and p53 protein levels.

Figure 2.3: Relative expression levels of p53 target genes in thymi.

Figure 2.4: Apoptosis in thymi.

Figure 2.5: Western blot of spleen extracts.

Figure 2.6: Mdm2 protein stability in untreated thymocytes.

Figure 2.7: Mdm2 protein stability in irradiated thymocytes.

Figure 2.8: p53 protein stability in untreated thymocytes.

Figure 2.9: p53 protein stability in irradiated thymocytes.

Figure 2.10: Reciprocal co-immunoprecipitation of Mdm2 and p53 from thymus extracts.

Figure 2.11: Co-immunoprecipitation of Mdm2 and p53 with MdmX from thymus extracts.

Figure 2.12: Lymphomagenesis in *Eμ-myc* and *Eμ-myc;Mdm2^{S394A}* mice.

Figure 2.13: Representative staining of *Eμ-myc* and *Eμ-myc;Mdm2^{S394A}* lymphomas.

Figure 2.14: *Eμ-myc;Mdm2^{S394A}* tumor analysis.

Figure 2.15: Schematic outlining the proposed methods of p53 activation by Myc.

Figure 2.16: IR-induced tumorigenesis.

Figure 2.17: H&E staining of IR-induced lymphomas.

Figure 2.18: Immunohistochemical staining of IR-induced lymphomas.

Figure 2.19: Relative expression levels of p53-target genes in bone marrow.

Figure 2.20: Haematoxylin and eosin stained bone marrow following exposure to 8 Gy IR.

Figure 2.21: Immunohistochemical staining for TER-119 in bone marrow.

Figure 2.22: Quantification of lineage-defined hematopoietic cells in bone marrow.

Figure 2.23: Quantification of L⁻S⁻K (CMP) and L⁻SK (HSPC) cells in bone marrow.

Figure 2.24: Colony-forming cell (CFC) assays.

Figure 2.25: Experimental design of bone marrow repopulation assays.

Figure 2.26: WT and *Mdm2*^{S394A} competitive bone marrow reconstitution.

Figure 2.27: Post-IR relative contribution of WT and *Mdm2*^{S394A} chimeric bone marrow.

Chapter III

Figure 3.1: Sequence of wild-type and mutant Mdm2 alleles surrounding codon 393.

Figure 3.2: Diagram of the targeting strategy used to generate the *Mdm2*^{Y393F} allele.

Figure 3.3: Southern blot analysis of targeted ES cells.

Figure 3.4: Southern blot analysis of mouse DNA.

- Figure 3.5: Genotyping *Mdm2*^{Y393F} mice.
- Figure 3.6: Spontaneous tumorigenesis in *Mdm2*^{Y393F} mice.
- Figure 3.7: *Mdm2*^{Y393F} tumor histology.
- Figure 3.8: *Mdm2*^{Y393F} tumor staining.
- Figure 3.9: *Eμ-myc*-driven lymphomagenesis in *Mdm2*^{Y393F} mice.
- Figure 3.10: Western blots of irradiated *Mdm2*^{Y393F} spleens and thymi.
- Figure 3.11: Gene expression in irradiated *Mdm2*^{Y393F} spleens and thymi.
- Figure 3.12: Apoptosis in irradiated *Mdm2*^{Y393F} spleens and thymi.
- Figure 3.13: Quantification of apoptosis in irradiated *Mdm2*^{Y393F} spleens and thymi.
- Figure 3.14: Cell-cycle arrest in MEFs.
- Figure 3.15: Primary MEF proliferation.
- Figure 3.16: Radioresistance in *Mdm2*^{Y393F} mice.
- Figure 3.17: Gene expression in bone marrow.
- Figure 3.18: Relative bone marrow cellularity.
- Figure 3.19: Quantification of lineage-defined hematopoietic cells in bone marrow.
- Figure 3.20: Quantification of L S K hematopoietic progenitor cells in bone marrow.
- Figure 3.21: Quantification of L SK hematopoietic progenitor cells in bone marrow.
- Figure 3.22: Haematoxylin and eosin stained bone marrow following IR.
- Figure 3.23: Sequence of wild-type and mutant *Mdm2* alleles surrounding codons 393 and 394.

- Figure 3.24: Diagram of the targeting strategy used to generate the *Mdm2*^{Y393F/S394A} allele.
- Figure 3.25: Southern blot analysis of targeted ES cells.
- Figure 3.26: Southern blot analysis of mouse DNA.
- Figure 3.27: Genotyping *Mdm2*^{Y393F/S394A} mice.
- Figure 3.28: Spontaneous tumorigenesis in *Mdm2*^{Y393F/S394A} mice.
- Figure 3.29: *Mdm2*^{Y393F/S394A} tumor histology.
- Figure 3.30: *Mdm2*^{Y393F/S394A} tumor staining.
- Figure 3.31: Western blots of irradiated *Mdm2* mutant thymi.
- Figure 3.32: Gene expression in irradiated *Mdm2* mutant thymi.
- Figure 3.33: Apoptosis in irradiated *Mdm2* mutant thymi.
- Figure 3.34: Quantification of apoptotic *Mdm2* mutant thymocytes.
- Figure 3.35: Radioresistance in *Mdm2* mutant mice.
- Figure 3.36: Gene expression in irradiated *Mdm2* mutant bone marrow.
- Figure 3.37: Quantification of L SK hematopoietic progenitor cells in *Mdm2* mutant bone marrow.
- Figure 3.38: Haematoxylin and eosin stained *Mdm2*^{S394A} and *Mdm2*^{Y393F/S394A} bone marrow.
- Figure 3.39: Quantification of lineage-defined hematopoietic cells in *Mdm2* mutant bone marrow.
- Figure 3.40: Quantification of L S K hematopoietic progenitor cells in *Mdm2* mutant bone marrow.
- Chapter IV
- Figure 4.1: Graphical summary of the effects of *Mdm2* Tyr393 and *Mdm2* Ser394 phosphorylation on p53-dependent DNA damage responses and tumor suppression.

Copyrighted Materials Produced by the Author

Some data and analysis in this thesis have been submitted as manuscripts not yet in print. All submitted data and analysis presented in this thesis were originally obtained and analyzed by the author. Final analysis included contributions from co-authors listed.

Chapter II and some related portions of Chapters I and IV have been submitted as a manuscript not yet in print:

Carr, M.I., Roderick, J.E., Gannon, H.S., Kelliher, M.A., and Jones, S.N. (2016). Mdm2 phosphorylation regulates its stability and has contrasting effects on oncogene and radiation-induced tumorigenesis. *Cell Rep.* (in press)

Chapter III and some related portions of Chapters I and IV have been submitted as a manuscript not yet in print:

Carr, M.I., Roderick, J.E., Woda, B.A., Kelliher, M.A., and Jones, S.N. (2016). Phosphorylation of Mdm2 by c-Abl regulates p53 tumor suppression and the radiosensitivity of mice. (submitted)

CHAPTER I

Introduction

p53

The p53 protein was first identified in 1979, through studies examining the transforming ability of the simian virus 40 (SV40) tumor virus. p53 was found to be bound by the SV40 large T antigen, and p53 protein levels were elevated in a number of SV40-transformed cell lines (Melero et al., 1979; Lane and Crawford, 1979; Linzer and Levine, 1979; Chang et al., 1979; Kress et al., 1979). Several groups proceeded to clone the p53 cDNA (Pennica et al., 1984; Bienz et al., 1984; Parada et al., 1984; Jenkins et al., 1984), and ensuing studies with several of these clones demonstrated that p53 cooperated with Ha-Ras in transforming primary rat cells in culture (Eliyahu et al., 1984; Parada et al., 1984; Jenkins et al., 1984). Accordingly, p53 was initially perceived to be oncogenic. However, further experimentation determined that the p53 sequences that facilitated transformation included mutations, and that those mutations were responsible for the cooperation with Ras (Finlay et al., 1988; Hinds et al., 1989). Moreover, transformation studies using the wild-type (WT) p53 sequence showed that p53 actually blocked the ability of Myc or E1A plus Ras to transform cells (Finlay et al., 1989; Eliyahu et al., 1989). These results, coupled with accumulated evidence of p53 mutation in tumors from a Friend leukemia virus-driven mouse tumor model (Mowat et al., 1985; Chow et al., 1987; Munroe et al., 1988; Ben

David et al., 1988), as well as the first evidence of p53 mutation contributing to human cancer (Baker et al., 1989), ultimately led to a reversal of the field's interpretation of p53 and the recognition of p53 as a tumor suppressor.

p53 structure and function

Shortly after p53's identification as a tumor suppressor, studies focused on the biochemical properties of p53 showed that it could bind DNA in a sequence-specific manner (Kern et al., 1991; El-Deiry et al., 1992; Funk et al., 1992) and stimulate the expression of genes downstream of its binding site (Kern et al., 1992; Funk et al., 1992; Zambetti et al., 1992). The 20 base pair p53 consensus-binding sequence is comprised of two copies of the palindromic 10 base pair sequence 5'-PuPuPuC(A/T)(T/A)GPyPyPy-3' separated by up to 13 base pairs (El-Deiry et al., 1992; Funk et al., 1992). The site-specific binding of p53 to DNA is dependent upon a central DNA-binding domain spanning residues 102-292 (Pavletich et al., 1993; Bargonetti et al., 1993; Cho et al., 1994). The majority of cancer-associated p53 mutations are missense mutations within this domain which ablate DNA binding. Approximately 30% of these mutations occur at six residues (Arg175, Gly245, Arg248, Arg249, Arg273 and Arg282) known as 'hotspots' (Vousden and Lu, 2002). This emphasizes a critical role for p53 transcriptional activities in tumor suppression, and follows with the observation that the sequence-specific DNA binding ability of various p53 mutants positively correlates with growth-suppressor activity (Pietenpol et al., 1994).

The highly acidic nature of the N-terminal region of p53 led to its early identification as the region of p53 containing its transcription activating domain (Fields and Jang, 1990; Raycroft et al., 1990). Later studies confirmed that this region of p53 contains a pair of transcriptional activation domains (TADs), TAD1 and TAD2, which span amino acid residues 1-40 and 40-60, respectively (Candau et al., 1997; Zhu et al., 1998; Venot et al., 1999). These domains act to promote the transcription of p53 target genes by recruiting components of the basal transcriptional machinery (Lu and Levine, 1995; Thut et al., 1995; Di Lello et al., 2006), histone-modifying enzymes such as CREB-binding protein (p300/CBP) (Gu et al., 1997; Teufel et al., 2007), and coactivator complexes, such as STAGA and Mediator (Gamper and Roeder, 2008; Meyer et al., 2010). In addition to activating transcription, p53 can repress gene expression by binding to specific p53 response elements and recruiting co-repressors such as histone deacetylases and by obstructing binding sites for other transcriptional activators (Ho and Benchimol, 2003; Riley et al., 2008). The N-terminus of p53 is also the site of a multitude of phosphorylation events by stress-responsive kinases, as well as binding by the negative regulators of p53, Mdm2 and MdmX (discussed below).

Located between the N-terminal TADs and the central DNA binding domain is a proline-rich domain (PRD; residues 60-95). This domain was originally proposed to participate in protein-protein interactions on the basis of the presence of PXXP motifs which create binding sites for Src homology 3

(SH3) domain-containing proteins (Walker and Levine, 1996). The PRD has been implicated in the regulation of p53 activity through interaction with the histone acetyl transferase p300, promoting p53 acetylation (Dornan et al., 2003). The PRD has also been shown to modulate Mdm2-mediated degradation of p53 (Berger et al., 2001). This is attributed to the the prolyl isomerase Pin1 binding the PRD after stress and effecting a conformational change in p53 to reduce Mdm2 binding (Zheng et al., 2002; Zacchi et al., 2002). Cells expressing p53 lacking the PRD display increased colony formation (Walker and Levine, 1996) and reduced apoptosis in response to activated oncogenes as well as various DNA damage-inducing anti-neoplastic agents (Sakamuro et al., 1997; Roth et al., 2000; Baptiste et al., 2002). However, while complete deletion of this domain in mice disrupts p53 growth arrest and tumor-suppressor function, knock-in mice carrying proline-to-alanine point mutations in all PXXP motifs of this domain appear normal, suggesting that the contributions of this domain to p53 function may be largely structural (Toledo et al., 2006; Toledo et al., 2007).

C-terminal to the DNA-binding domain is a tetramerization domain (residues 325-356) which directs p53 oligomerization and binding of its response elements as a tetramer (Stenger et al., 1992; Friedman et al., 1993; Pavletich et al., 1993). Interestingly, the majority of p53 mutants retain an intact tetramerization domain, allowing mutant p53 proteins to assemble into tetramers along with wild-type p53 proteins. As a result, mutant p53 can display a dominant-negative effect on p53 DNA binding and transactivation function

(Sturzbecher et al., 1992; Shaulian et al., 1992).

Finally, the extreme C-terminus of p53 contains a basic, lysine-rich domain (residues 363-393). This domain is proposed to regulate the DNA-binding ability of p53 by altering its conformation, or sterically interfering with DNA binding (Luo et al., 2004; McKinney et al., 2004; Friedler et al., 2005). This activity is linked to post-translational modification of the domain. Six C-terminal lysines of p53 are acetylated by p300/CBP (Gu and Roeder, 1997), in a sequence dependent on phosphorylation of the same region by kinases such as protein kinase C and casein kinase II (Baudier et al., 1992; Hupp et al., 1992; Sakaguchi et al., 1998). Accordingly, p53 acetylation levels are elevated in response to stress, promoting p53 activation (Sakaguchi et al., 1998; Ito et al., 2001). Importantly, these same lysine residues are principle sites of ubiquitin ligation by Mdm2 (Rodriguez et al., 2000; Nakamura et al., 2000), the primary regulator of p53 stability (discussed below). Acetylation and ubiquitination are mutually exclusive modifications, and competition between these modifications is thought to regulate p53 stability and activity (Ito et al., 2001; Li et al., 2002b). Several other lysines located in the DNA binding and tetramerization domains of p53 are also targets of acetylation (Tang et al., 2008). Acetylation of these residues is reported to influence the relative activation of different p53 target genes (Meek, 2015).

Since the identification of p53 as a transcription factor, a multitude of p53-responsive genes have been identified, implicating p53 in the control of

numerous cellular responses to a wide range of stresses, such as various forms of DNA damage, ribosomal stress, activated oncogenes and hypoxia. Among the first p53-responsive genes to be discovered was *CDKN1A*, encoding the cyclin dependent kinase inhibitor p21 (WAF1/CIP1) (El-Deiry et al., 1993), which governs cell cycle arrest in response to DNA damage (Deng et al., 1995; Brugarolas et al., 1995) and mediates cellular senescence (Noda et al., 1994; Fang et al., 1999; Wang et al., 1999). Additional p53-targets involved in cell cycle arrest and senescence include the growth arrest-related genes *Gadd45* (growth-arrest and DNA damage-inducible protein 45) (Kastan et al., 1992), *14-3-3 σ* (Hermeking et al., 1997), *Reprimo* (Ohki et al., 2000), and senescence associated *PAI-1* (plasminogen activator inhibitor-1) (Kortlever et al., 2006). p53 is also capable of transactivating the expression of several genes involved in apoptosis, such as the Bcl-2 family members *Bax* (Miyashita and Reed, 1995), *Noxa* (Oda et al., 2000), and *Puma* (Nakano and Vousden, 2001; Yu et al., 2001). p53-targets involved in DNA repair include *Ercc5* (Excision repair cross-complementing rodent repair deficiency complementation group 5) and *Mgmt* (O(6)-methylguanine-DNA methyltransferase) (Valente et al., 2013). p53-targets involved in metabolic processes and regulation of oxidative stress include *TIGAR* (TP53-induced glycolysis regulator) (Bensaad et al., 2006), *Sco2* (synthesis of cytochrome c oxidase) (Matoba et al., 2006), *Gls2* (Glutaminase 2) (Hu et al., 2010; Suzuki et al., 2010), *Aldh4* (aldehyde dehydrogenase 4) (Yoon et al., 2004) and the Sestrins, *Sesn1* (Sestrin-1/PA26) and *Sesn2* (Sestrin-2/Hi95) (Velasco-

Miguel et al., 1999; Peeters et al., 2003; Budanov et al., 2002; Bodanov et al., 2004). Novel p53-dependent target genes encoding proteins involved in a growing number of signaling pathways and cellular functions, are constantly being described. The relative contribution of these pathways and functions to the tumor suppressive effect of p53 is still being elucidated (Brady et al., 2011; Li et al., 2012; Jiang et al., 2015).

p53 tumor suppression

Proper coordination of p53-responsive gene expression provides a crucial barrier to tumor development. This is evidenced by the fact that more than 50% of human cancers harbor mutations in p53 (Levine, 1997; Soussi and Beroud, 2001). Moreover, in cancers in which p53 is wild-type, p53 function is frequently compromised through mutations of associated positive regulators, or amplification of negative regulators of p53 (Levine, 1997). A number of p53-null mouse models have been developed and characterized (Donehower et al., 1992; Clarke et al., 1993; Jacks et al., 1994). While it was initially reported that $p53^{-/-}$ mice developed normally both prenatally and postnatally, it was subsequently shown that a primarily female subset of $p53^{-/-}$ mice die *in utero* due to exencephaly (Sah et al., 1995; Armstrong et al., 1995). In all cases, mice homozygous for the null allele rapidly developed spontaneous tumors, with similar spectrums and latencies (Donehower et al., 1992; Purdie et al., 1994; Jacks et al., 1994). All $p53^{-/-}$ mice develop tumors by 10 months of age, with a

mean time to tumorigenesis of approximately 4.5 months. These tumors are primarily lymphomas (~70-80%, largely T-cell in origin), with some incidence of sarcomas and other tumor types. $p53^{+/}$ mice develop tumors later than $p53^{/}$ mice, with the earliest tumor presentation around 12 months of age (Harvey et al., 1993a; Purdie et al., 1994; Jacks et al., 1994). The majority of $p53^{+/}$ mice (~95%) develop tumors by 24 months of age, with a mean time to tumorigenesis of approximately 17 months. These animals present with lymphomas (primarily of B cell origin), osteosarcomas, soft-tissue sarcomas and a range of carcinomas (Donehower and Lozano, 2009). Interestingly, one study observed that while the remaining wild-type $p53$ allele is deleted in approximately half of $p53^{+/}$ tumors, supporting the Knudson hypothesis, the other half retain a functional wild-type allele (Venkatachalam et al., 1998). While this may suggest that perturbation of other members of the p53 signaling axis accounts for functional loss of p53 in these tumors, it has been suggested that in certain contexts p53 may be haploinsufficient, and that a reduction in p53 dosage is sufficient to increase the susceptibility of $p53^{+/}$ cells to tumorigenesis (Venkatachalam et al., 2001).

In agreement with the early observations that p53 impaired the ability the ability of oncogenes to transform cells (Finlay et al., 1989; Eliyahu et al., 1989), numerous studies have shown that combining the p53-null allele with mouse models of cancer, such as those driven by PTEN deficiency, activated BRAF^{V600E}, or Myc overexpression, leads to accelerated tumor development (Chen et al., 2005b; Dankort et al., 2007; Eischen et al., 1999). Early *in vitro*

studies aimed at identifying the mechanism by which p53 impaired tumor formation identified p53 as a regulator of cell growth and senescence, as well as apoptosis. Overexpression of p53 was shown to inhibit the growth of a number of human cancer cell lines (Baker et al., 1990; Diller et al., 1990; Chen et al., 1990). Similar results were observed in cells expressing a temperature-sensitive p53 mutant (p53^{val135}) at the wild-type-permissive temperature, with growth arrest reported to occur primarily in G1 (but also G2/M) (Michalovitz et al., 1990; Martinez et al., 1991). Additionally, biochemical experiments identified p53 as a substrate of cyclin-dependent kinase 1 (CDK1) (Bischoff et al., 1990; Sturzbecher et al., 1990).

An early indication of the role for p53 in senescence came from the observation that p53 mutation was a common event in the spontaneous immortalization of MEFs (Harvey and Levine, 1991). This was further supported by studies showing that *p53*^{-/-} fibroblasts are more readily immortalized in culture (Harvey et al., 1993b; Tsukada et al., 1993), that mutant p53 extends the proliferative life span of fibroblasts (Bond et al., 1994), and that p53 expression (Kulju and Lehman, 1995) and transactivation activity (Bond et al., 1996, Atadja et al., 1995) increase as cells approach senescence. Reintroduction of wild-type p53 triggers rapid senescence in certain human tumor cells lacking functional p53 (Sugrue et al., 1997), and p53 is essential for oncogene-induced senescence in cells overexpressing Ras, E2F1 and constitutively active β -catenin (Serrano et al., 1997; Dimri et al., 2000; Damalas et al., 2001). A role for p53-dependent

senescence in tumor suppression in mice has been suggested by a study in which mice expressing a mutant p53 protein (p53^{R172P}), defective for apoptosis but retaining growth arrest capabilities, displayed delayed *Eμ-myc*-driven B cell lymphomagenesis compared to mice heterozygous for p53 (Post et al., 2010). Lymphomas from p53^{R172P} expressing mice displayed increased levels of senescence-associated β-galactosidase activity relative to mice heterozygous for p53.

The influence of p53 on growth arrest and senescence has been largely attributed to p21. p21 protein levels increase in normal fibroblasts as they approach senescence (Noda et al., 1994) and *p21*^{-/-} cells display reduced growth arrest in response to DNA damage (Deng et al., 1995; Brugarolas et al., 1995). Furthermore, tumor cell lines lacking functional p53 failed to arrest in response to forced expression of p53 when the *p21* gene was disrupted (Polyak et al., 1996), and induced expression of p21 promotes senescence in tumor cells lacking functional p53 (Fang et al., 1999; Wang et al., 1999).

Induced expression of p53 has also been shown to stimulate apoptosis *in vitro* in various human cancer cell lines (Yonish-Rouach et al., 1991; Shaw et al., 1992; Yang et al., 1995; Liu et al., 1995). By expressing p53, either under the control of a metal ion-inducible rat MT promoter (Shaw et al., 1992), or through adenoviral delivery (Yang et al., 1995; Liu et al., 1995), several of these groups further showed that p53 expression in tumor cells inhibits tumor formation in nude mice, and that established tumor xenografts undergo regression and

display histological features of apoptosis when p53 expression is induced. Studies in primary murine cells have shown p53 accumulation and stabilization, along with increased apoptosis, in response to adenovirus E1A expression (Lowe and Ruley, 1993), as well as induction of apoptosis in cells co-expressing E1A and the temperature-sensitive p53val135 mutant at the wild-type-permissive temperature (Debbas and White, 1993). A subsequent study using *p53*^{-/-} MEFs confirmed the p53-dependence of E1A-induced apoptosis, and demonstrated that reduced apoptosis increases the tumorigenic potential of cells in nude mice (Lowe, et al., 1994). Similar results to those observed with E1A *in vitro* were observed in cells expressing c-Myc fused to the hormone binding domain of the human estrogen receptor (c-MycER). Activation of c-Myc in wild-type MEFs induces apoptosis not observed in similarly transfected *p53*^{-/-} MEFs (Hermeking and Eick, 1994; Wagner et al., 1994).

Additional results implicating p53-dependent apoptosis in tumor suppression have been reported from a number of studies in mice. p53-dependent apoptosis has been shown to suppress *Eμ-myc*-driven B cell lymphomagenesis (Schmitt et al., 1999), E2F1 driven skin carcinomas (Pierce et al., 1998), and brain tumorigenesis driven by a mutant SV40 T antigen (non p53-binding TgT₁₂₁) (Symonds, et al., 1994). Furthermore, the development of TgT₁₂₁ and *Eμ-myc*-driven tumors is accelerated in mice null for the p53-responsive apoptotic gene *Bax* (Yin et al., 1997; Eischen et al., 2001). A similar acceleration of *Eμ-myc*-driven tumors has been described in mice null for the p53-responsive

apoptotic gene *Puma* (Hemann et al., 2004; Garrison et al., 2008; Michalak et al., 2009).

The aforementioned results detailing the contributions of p53-dependent growth arrest, senescence and apoptosis to tumor suppression in various tissues and cell-types, highlight the importance of these tumor-suppressive mechanisms. However, the relative contribution of these mechanisms is likely to be tissue- or cell-type-dependent. This is exemplified by a series of studies in which p53 reactivation in established tumors resulted in apoptosis in lymphomas and senescence in sarcomas, respectively (Martins et al., 2006; Xue, et al., 2007; Ventura, et al., 2007). More recently, a number of studies have questioned the influence of cell cycle arrest, senescence and apoptosis in tumor suppression, and implicated additional p53-dependent mechanisms in impairing tumor growth. Gu and colleagues have described a knock-in mouse in which three p53 acetylation sites in the p53 DNA-binding domain were mutated to arginine ($p53^{3KR}$ mice) (Li et al., 2012). $p53^{3KR}$ mice and cells fail to transactivate the majority of p53 target genes, and induce growth arrest or apoptosis. However, these mice do not develop cancer, suggesting that tumor suppression by p53 may occur independently of growth arrest or apoptosis. It is proposed that as these animals retain the ability to transactivate the metabolic targets *Gls2* and *TIGAR*, p53 may display tumor suppressive activity through the regulation of energy metabolism and reactive oxygen species (ROS) levels (Li et al., 2012). Similar findings have been reported using, triple knock-out mice deficient for p21,

Puma, and Noxa (*p21^{-/-} puma^{-/-} noxa^{-/-}* mice) (Valente, et al., 2013). These mice are profoundly resistant to DNA damage-associated apoptosis and growth arrest, and largely (but not entirely) resistant to p53-dependent senescence, yet do not develop spontaneous tumors. These authors noted that induction of p53 target genes involved in DNA repair was unperturbed in *p21^{-/-} puma^{-/-} noxa^{-/-}* mice, and propose that coordination of DNA repair is an essential tumor suppressive activity of p53. More recently, Gu and colleagues have identified the ability of p53 to transcriptionally repress the cysteine/glutamate antiporter SLC7A11 and induce ferroptosis (an iron-dependent mechanism of non-apoptotic cell death (Dixon, et al., 2012)) in response to reactive oxygen species as another mechanism by which *p53^{3KR}* mice may suppress tumorigenesis (Jiang, et al., 2015).

p53 responses to DNA damage

Following the identification of p53 as a tumor suppressor protein, and in concert with the aforementioned studies elucidating the tumor suppressive activities of p53, a series of studies showed that p53 levels and activity increased in response to DNA damage. Treatment of cells with DNA damaging agents such as ultraviolet light (UV), ionizing radiation (IR), and numerous cancer therapeutic and/or DNA damage-inducing compounds such as diamminedichloroplatinum (cisplatin), mitomycin C, etoposide, hydroxyurea (HU), methyl methanesulfonate (MMS) and actinomycin D results in increased p53

protein levels and associated cell cycle arrest (Maltzman and Czyzyk, 1984; Kastan, et al., 1991; Fritsche et al., 1993; Zhan et al., 1993). Tumor cells lacking p53 fail to induce growth arrest following IR, a result that can be reversed by transfection with wild-type p53 (Kastan et al., 1991; Kuerbitz et al., 1992). Furthermore, p53^{-/-} MEFs are resistant to oncogene-sensitized apoptosis in response to serum withdrawal or a variety of genotoxic agents (Lowe et al., 1993a; Lowe et al., 1994). Analyses of p53^{-/-} mice determined that p53 governs IR-induced apoptosis in both thymocytes (Lowe et al., 1993b; Clarke et al., 1993; Lotem and Sachs, 1993) and epithelial stem cells of the small intestine (Merritt et al., 1994). Further studies have identified additional radiosensitive cell populations in the spleen, bone marrow, and hair follicles (Komarova et al., 2000).

An early indication of the signaling pathways governing the p53 response to DNA damage came from a study that showed cells from patients with ataxia-telangiectasia (an autosomal recessive disorder resulting in neuronal degeneration, sensitivity to ionizing radiation, premature ageing, increased incidence of cancer and other pathologies) do not display increased p53 levels and activity following IR exposure (Kastan et al., 1992). Mice null for *ATM* (ataxia telangiectasia mutated), the gene responsible for ataxia-telangiectasia, are extremely sensitive to IR-induced lethality, and cells and tissues from these mice show profound defects in DNA damage-induced growth arrest and apoptosis (Barlow et al., 1996; Elson et al., 1996; Xu and Baltimore, 1996;

Herzog et al., 1998). Similar to AT patient cells, p53 is not stabilized in *ATM*^{-/-} MEFs or thymocytes following IR (Xu and Baltimore, 1996; Gurley and Kemp, 2007). Furthermore, these animals succumb to T-cell lymphomas by 6 months of age (Barlow et al., 1996; Elson et al., 1996). Research aimed at identifying the mechanism by which ATM leads to p53 stabilization is discussed below.

Mdm proteins regulate p53

Mdm2

The chief negative regulator of p53 stabilization and activity is widely considered to be the Mdm2 oncoprotein. The *Mdm2* (murine double minute 2) gene was initially identified as an amplified DNA sequence associated with double minutes (small, acentromeric extrachromosomal nuclear bodies) present in a spontaneously immortalized mouse 3T3 cell line and shown to originate from mouse chromosome 10 (Cahilly-Snyder et al., 1987). The Mdm2 protein was initially observed as a cellular protein of approximately 90 kDa which co-immunoprecipitated with p53 from rat embryo fibroblasts (Hinds et al., 1990). This protein was subsequently purified from cells overexpressing p53 and identified by sequence homology as the product of the predicted open reading frame of *Mdm2* (Momand et al., 1992). In this same study, co-expression of Mdm2 with p53 was shown to inhibit the ability of p53 to transactivate a reporter plasmid. These findings closely coincided with the identification of *Mdm2* as an oncogene. Mdm2 overexpression is capable of conferring tumorigenicity on cells

(Fakharzadeh et al., 1991), and *Mdm2* is amplified in a significant fraction (~30%) of soft tissue sarcomas (Oliner et al., 1992; Leach et al., 1993; Cordon-Cardo et al., 1994). Further studies have identified *Mdm2* amplification in a variety of other tumor types, including breast carcinomas (Sheikh et al., 1993), glioblastomas and astrocytomas (Reifenberger et al., 1993), myeloid neoplasms (Bueso-Ramos et al., 1993), B cell lymphomas (Watanabe et al., 1994) and oral carcinomas (Matsumura et al., 1996).

Shortly after the identification of Mdm2's interaction with p53, mapping of the p53 and Mdm2 interaction domains, by yeast two-hybrid and co-immunoprecipitation experiments, determined that the N-terminus of Mdm2 bound to the transactivation domain of p53 (Oliner et al., 1993; Chen et al., 1993). These same groups further showed that this interaction inhibited the transactivation ability of p53 in reporter assays. Accordingly, Mdm2 overexpression cooperates with Ras in transforming primary cell lines, despite the presence of wild-type p53 (Finlay, 1993). Mdm2 overexpression also inhibits p53-dependent growth arrest and apoptosis in various cell lines, in response to either DNA damage or activated oncogenes (Chen et al., 1994; Haupt et al., 1996; Chen et al., 1996). It has since been determined that the central acidic domain of Mdm2 also interacts with p53, though with a weaker affinity than that observed with the N-terminal. This interaction is thought to further stabilize the Mdm2-p53 interaction (Yu et al., 2006).

It was subsequently shown that in addition to inhibiting the transactivation ability of p53, Mdm2 promotes the proteasomal degradation of p53 (Haupt et al., 1997; Kubbutat et al., 1997). Mdm2 functions as an E3 ubiquitin ligase capable of directing p53 polyubiquitination (Honda et al., 1997). This E3 activity of Mdm2 is dependent on its C-terminal RING finger domain (Fang et al., 2000). The Mdm2 RING finger has also been shown to promote the nuclear export of p53 by directing its monoubiquitination (Boyd et al., 2000; Geyer et al., 2000; Lohrum et al., 2001; Gu et al., 2001). It is proposed that low levels of Mdm2 activity induce monoubiquitination and nuclear export of p53, whereas high levels promote polyubiquitination and nuclear degradation of p53 (Li et al., 2003). As discussed above, the principle sites of ubiquitin ligation by Mdm2 are a series of C-terminal lysines also targeted by acetylation, creating one of many layers of regulation of p53 stability and activity (Rodriguez et al., 2000; Nakamura et al., 2000; Ito et al., 2001; Li et al., 2002b). Notably, the *Mdm2* gene is itself a target of the p53 transcription factor (Wu et al., 1993; Juven et al., 1993). As p53 becomes stabilized and active, it increases the levels of its own negative regulator Mdm2, forming an autoregulatory feedback loop that returns p53 protein and activity to basal levels. Furthermore, Mdm2 has also been shown to be capable of directing its own degradation (Fang et al., 2000; Honda and Yasuda, 2000).

The crucial role of Mdm2 in regulating p53 activity is illustrated by the p53-dependent lethality of Mdm2-null mice during early embryogenesis. *Mdm2*^{-/-} mice display embryonic lethality at E5.5-6.5 of early development (Montes de

Oca Luna et al., 1995; Jones et al., 1995). This loss of viability is due to unregulated p53 activity in developing embryos, as crossing these mice with the p53-null allele completely rescues Mdm2-null mice (Montes de Oca Luna et al., 1995; Jones et al., 1995). Mice null for both Mdm2 and p53 develop spontaneous tumors of similar incidence and spectrum as p53-null mice (Jones et al., 1996). Furthermore, primary p53-null and Mdm2/p53 double-null cells display similar growth characteristics in culture and are indistinguishable in their response to genotoxic agents (Jones et al., 1996). These results highlight regulation of p53 as the primary role of Mdm2. *Mdm2*^{+/-} mice display delayed Myc-driven lymphomagenesis (Alt et al., 2003), an observation ascribed to increased p53-dependent apoptosis in Myc expressing B cells. In another study employing a hypomorphic Mdm2 allele, mice expressing reduced levels of Mdm2 displayed p53-dependent sensitivity to radiation-induced lethality and apoptosis in lymphopoietic tissues (Mendrysa et al., 2003). Thus, perturbations in the levels of Mdm2 can significantly impact p53 responses to oncogenes and DNA damage.

In contrast with Mdm2-null mice, mice overexpressing an *Mdm2* transgene are viable, but succumb to spontaneous tumors (Jones et al., 1998). The rate of tumorigenesis in Mdm2-transgenic mice is slower than that observed in p53^{-/-} mice, with 50% of Mdm2-transgenics developing tumors by 19 months (as opposed to 4.5 months for p53^{-/-} mice). It is suggested that this may be due to the relatively modest levels of Mdm2 overexpression (approximately 4 fold)

present in the Mdm2-transgenics. Mdm2-transgenics present with a large percentage of lymphomas, similar to what is observed in p53^{-/-} mice, as well as a large number of sarcomas (predominantly hemangiosarcomas). Notably, while the Mdm2-transgene does not accelerate spontaneous tumorigenesis in p53^{-/-} mice, it does increase the number of sarcomas observed (in addition to the previously observed tumor spectrum and incidence), suggesting a possible p53-independent contribution of Mdm2 overexpression to tumorigenesis. Mdm2 overexpressing mice also display accelerated Myc-driven lymphomagenesis (Wang et al., 2008). This same study showed that elevated levels of Mdm2 resulted in reduced p53 protein levels and activity in B cells, and reduced B cell apoptosis following IR.

MdmX

Similar to Mdm2, the related protein MdmX (Mdm4) is also capable of binding p53 and inhibiting p53 transactivation of target genes (Shvarts et al., 1996; Shvarts et al., 1997). MdmX and Mdm2 share 34% protein homology and contain highly homologous p53-binding, acidic, zinc finger, and RING finger domains (Shvarts et al., 1996). As with Mdm2, the *MdmX* gene is amplified or overexpressed in a variety of tumor types, including brain and breast cancers, soft tissue sarcomas, retinoblastoma and melanoma (Riemenschneider et al., 2003; Danovi et al., 2004; Bartel et al., 2005; Laurie et al., 2006; Gembarska et al., 2012). However, unlike Mdm2, MdmX does not possess the ability to directly

ubiquitinate p53 (Jackson and Berberich, 2000; Stad et al., 2000).

Mice null for *MdmX* display a similar p53-dependent embryonic lethality as observed in *Mdm2*^{-/-} mice, albeit slightly later in development (E9.5-10.5), and are rescued by deletion of *p53* (Parant et al., 2001; Migliorini et al., 2002; Finch et al., 2002). Notably, the lethality in *MdmX*^{-/-} embryos appears to be predominantly associated with a lack of proliferation, as opposed to aberrant apoptosis (as reported for *Mdm2*^{-/-} embryos (de Rozières et al., 2000)). Accordingly, a subsequent study revealed that co-deletion of *p21* can significantly delay the embryonic lethality of *MdmX*-null mice (Steinman et al., 2004). *MdmX*^{+/-} MEFs display a decreased growth rate and increased levels of UV-induced apoptosis (Finch et al., 2002). This is attributed to elevated protein levels of p53 and several p53 target gene products including p21 and Bax. As observed with mice heterozygous for *Mdm2*, *MdmX*^{+/-} cells and mice display decreased oncogene-driven transformation and *Eμ-myc*-driven lymphomagenesis, respectively (Terzian et al., 2007). Furthermore, *MdmX*^{+/-} mice are similarly sensitized to radiation induced lethality as observed with *Mdm2*^{+/-} mice (Terzian et al., 2007).

Mdm2 and *MdmX* have been shown to interact via their C-terminal RING domains (Tanimura et al., 1999; Sharp et al., 1999). This interaction was initially reported to stabilize both *Mdm2* (Tanimura et al., 1999; Sharp et al., 1999; Stad et al., 2000) and p53 (Sharp et al., 1999; Jackson and Berberich, 2000; Stad et al., 2000). However, it was later shown that the observed stabilization of p53 by

MdmX was likely due to exceedingly high levels of MdmX generated in transfection-based studies, and that stabilization of Mdm2 by heterodimerization with MdmX actually increases the ability of Mdm2 to degrade p53 (Gu et al., 2002; Linares et al., 2003; Kawai et al., 2007; Wang et al., 2011b). Notably, the turnover of MdmX is mediated by Mdm2 (Pan and Chen, 2003; de Graaf et al., 2003; Kawai et al., 2003).

Recently, a series of Mdm2 and MdmX knock-in mouse models have been generated that display altered Mdm2-MdmX interactions and/or Mdm2 E3 ligase activity (Itahana et al., 2007; Pant et al., 2011; Huang et al., 2011; Tollini et al., 2014). Analyses of these models have revealed that Mdm2-MdmX interactions are crucial for inhibiting p53 activity during development and tissue homeostasis, whereas the E3 ligase function of Mdm2 is vital for regulating p53 protein levels and activity in cellular and organismal responses to DNA damage (Tollini et al., 2014).

p53 stabilization and activation in response to stress

The inhibitory role of Mdm proteins on p53 protein stabilization and activities must be interrupted in order for p53 to become elevated and activated in response to DNA damage or other forms of stress.

Oncogene-induced ARF-Mdm2 interaction

An important mediator of oncogene-dependent activation of p53 is the

tumor suppressor protein p19^{ARF} (p14^{ARF} in humans). Oncogenes including c-*Myc*, *Ras* and *E1A* induce ARF and cause p53-dependent growth arrest and apoptosis (Zindy et al., 1998; de Stanchina et al., 1998; Palmeiro et al., 1998). ARF binds to Mdm2 and can block its ubiquitin ligase activity towards p53 (Pomerantz et al., 1998; Zhang et al., 1998; Kamijo et al., 1998; Stott et al., 1998; Honda and Yasuda, 1999; Midgley et al., 2000) as well as sequester Mdm2 in the nucleolus (Weber et al., 1999; Tao and Levine, 1999). This facilitates p53 protein stabilization and activation in order to limit the transformative effects of aberrant oncogene activity.

DNA damage-induced modifications of p53

The cellular response to DNA damage is primarily governed by the PI3K-related serine/threonine kinases (PIKKs) ATM and ATR (ataxia telangectasia and Rad3-related protein). ATM is activated by DNA damaging agents that create double-strand breaks (DSBs), while ATR is activated following recruitment to ssDNA regions. The related protein DNA-PKcs (DNA-dependent protein kinase catalytic subunit) primarily regulates a smaller group of proteins involved in DSB end joining. Following the recognition of DNA damage by different sensor proteins, these kinases trigger the direct or indirect phosphorylation of numerous effector proteins involved in a multitude of signaling networks that promote different DNA repair processes, cell-cycle arrest and programmed cell death (Jackson and Bartek, 2009; Ciccia and Elledge, 2011). Though the majority of

the understanding of these DNA damage-associated PIKKs pertains to their specific canonical damage response pathways, these kinases are increasingly being implicated in the regulation of additional signaling pathways. Activation of ATM is observed in response to replication stress resultant from hypoxia or chloroquine treatment (in the absence of apparent DSBs), as a step in the mitotic spindle checkpoint, and is implicated in insulin signaling and regulation of oxidative stress (Shiloh and Ziv, 2013). ATR has a role in coordinating DNA replication origin firing and maintaining replication fork stability (Nam and Cortez, 2011), and DNA-PK is implicated in regulating cell proliferation and regulation of oxidative stress (Shiloh and Ziv, 2013).

Included among the various PIKK substrates is p53. p53 is phosphorylated on a number of residues, primarily clustered in the N- and C-terminal regions (Figure 1.1), in response to various DNA-damaging agents (Meek and Anderson, 2009; Meek, 2015). Phosphorylation of C-terminal residues is primarily thought to influence site-specific DNA binding by p53, whereas N-terminal phosphorylation events have been implicated in regulating the Mdm2-p53 interaction as well as p300/CBP recruitment (Meek and Anderson, 2009; Meek, 2015). Seven serines (Ser6, 9, 15, 20, 33, 37, 46) and two threonines (Thr18 and 81) in the N-terminal region of human p53 are phosphorylated in response to exposing cells to ionizing radiation or UV light (Meek and Anderson, 2009). These majority of these phosphorylation events occur directly by ATM, ATR, or DNA-PK (Lees-Miller et al., 1992; Banin et al.,

1998; Canman et al., 1998; Tibbetts et al., 1999) or indirectly by the ATR- and ATM-activated checkpoint kinases Chk1 or Chk2 (Shieh et al., 2000; Hirao et al., 2000; Saito et al., 2002). Additionally, Casein kinase 1 (CK1) has also been shown to phosphorylate a number of these residues (Dumaz et al., 1999; Higashimoto et al., 2000).

Of particular interest in the search for the mechanism of p53 stabilization following DNA damage were residues Ser15 and Ser20 (Ser18 and Ser23 in mice). *In vitro* experiments revealed phosphorylation of Ser15, a target of both ATM and ATR, inhibits the p53-Mdm2 interaction (Shieh et al., 1997) and coincides with p53 activation (Siliciano et al., 1997). Similar experiments have shown phosphorylation of Ser20, a target of Chk2, leads to reduced Mdm2-mediated degradation of p53 and increased p53 activity (Unger et al., 1999; Chebab et al., 1999; Hirao et al., 2000). Furthermore, Thr18 phosphorylation, which occurs through CK1 and can disrupt Mdm2-p53 binding, was shown to be dependent on prior Ser15 phosphorylation (Dumaz et al., 1999; Sakaguchi et al., 2000).

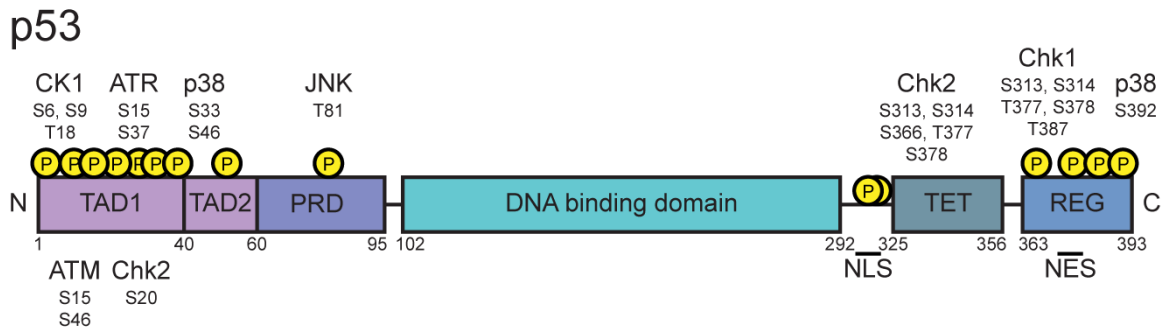


Figure 1.1: Diagram of the p53 protein. Shown are the major functional domains along with sites of phosphorylation relevant to the DNA damage response (P, yellow circles). TAD, transcriptional activation domain; PRD, proline-rich domain; TET, tetramerization domain; REG, C-terminal regulatory region; NLS, nuclear localization sequence; NES, nuclear export sequence.

As these p53 residues are located within, or immediately adjacent to, the Mdm2-p53 binding interface (Kussie et al., 1996), it was hypothesized that phosphorylation of these residues was sufficient to account for p53 stabilization and activation following DNA damage. However, analysis of various genetically engineered mouse models, which allowed for the examination of these phosphorylation events under endogenous conditions, revealed that these phosphorylation events were insufficient to account for the full effects of DNA damage on p53 stabilization and activation or for p53 tumor suppression (Wu et al., 2002; Chao et al., 2003; Sluss et al., 2004; MacPherson et al., 2004; Chao et al., 2006).

$p53^{S18A}$ mice in which serine 18 (Ser15 in humans) is replaced with alanine show no significant defects in p53 protein stabilization in thymocytes or MEFs in response to DNA damage (Chao et al., 2003; Sluss et al., 2004). MEFs from $p53^{S18A}$ mice show no defects in proliferation or growth arrest after DNA

damage, while thymocytes show an intermediate (compared to $p53^{-/-}$) defect in apoptosis. However, the ability of p53 to transactivate a number of target genes is compromised in $p53^{S18A}$ mice. A recent report suggests that this may be due to a role for p53 Ser15 in transcription and promoter relaxation as opposed to p53 stabilization (Loughery et al., 2014). Additionally, while $p53^{S18A}$ mice do not develop spontaneous tumors, they do develop *Eμ-myc*-driven B cell lymphomas at an accelerated rate, possibly due to their apoptotic defects (Sluss et al., 2010).

$p53^{S23A}$ mice in which serine 23 (Ser20 in humans) is replaced with alanine, show a similar absence of defects in p53 stabilization or growth arrest MEFs (Wu et al., 2002; MacPherson et al., 2004). However, $p53^{S23A}$ mice do show reduced stabilization of p53 and apoptosis in thymocytes in response to IR, though intermediate compared to $p53^{-/-}$ thymocytes (MacPherson et al., 2004). Furthermore, $p53^{S23A}$ mice develop spontaneous tumors (predominantly B cell lymphomas) with an earliest onset of approximately 12 months and approximately 70% of animals having developed tumors by 24 months. Interestingly, $p53^{S18A/S23A}$ mice, in which both Ser18 and Ser23 have been substituted, display more profound deficiencies in p53 stabilization and function, indicating an additive effect of phosphorylation of these two residues in regulating p53 function (Chao et al., 2006). While still intermediate to the phenotypes observed in $ATM^{-/-}$ and $p53^{-/-}$ cells, thymocytes from $p53^{S18A/S23A}$ mice show more significantly impaired p53 stabilization, transactivation of target genes, and apoptosis in response to irradiation than either single-mutant alone. However,

p53 stabilization and activities are still unperturbed in MEFs. These mice are similarly tumor prone as reported for Ser23 mutant mice, and again present primarily with lymphomas.

DNA damage-induced modifications of Mdm proteins

As the *in vivo* results obtained from p53 knock-in mice failed to replicate the profound defects in DNA damage-induced p53 stabilization and activity predicted by *in vitro* studies, additional signaling events must contribute to this process. In addition to p53, its primary negative regulators Mdm2 and MdmX are also subject to a multitude of phosphorylation events in response to DNA damage (Figures 1.2, 1.3).

Phosphorylation of the Mdm2 acidic domain

Located in the acidic domain of Mdm2 is a cluster of residues that are phosphorylated under homeostatic conditions (Hay and Meek, 2000). Phosphorylation of these residues is known to occur through the activities of the kinases Glycogen Synthase Kinase 3 β (GSK-3 β), Casein Kinase 1 (CK1), and CK2 (Hjerrild et al., 2001; Winter et al., 2004; Allende-Vega et al., 2005; Kulikov et al., 2005). Phosphorylation of these residues improves Mdm2-mediated turnover of p53 in the absence of stress stimuli (Blattner et al., 2002; Hjerrild et al., 2001; Kulikov et al., 2005), and hypo-phosphorylation of this region of Mdm2 is reported to coincide with DNA damage-induced p53 stabilization (Blattner et

al., 2002). Accordingly, inhibition of GSK-3 β leads to p53 stabilization in cells (Kulikov et al., 2005). Notably, GSK-3 β is inhibited through phosphorylation by Akt, which is activated by DNA-PK following DNA damage (Boehme et al., 2008). Akt-mediated inhibition of Mdm2 activity in this context contrasts with other reports in which the direct phosphorylation of Mdm2 Ser166 and Ser186 by Akt is proposed to inhibit p53 activity by facilitating Mdm2 translocation into the nucleus (Mayo and Donner, 2001; Zhou et al., 2001) and by inhibiting Mdm2 self-ubiquitination and degradation (Feng et al., 2004).

Mdm protein phosphorylation by ATM

In response to DNA damage, human MdmX is phosphorylated at Ser342 and Ser367 by Chk2 (Chen et al., 2005a; Okamoto et al., 2005; LeBron et al., 2006; Pereg et al., 2006) and Ser403 by ATM (Pereg et al., 2005). These phosphorylation events lead to MdmX degradation, concurrent with p53 stabilization and activation (Chen et al., 2005a; Okamoto et al., 2005). This phosphorylation-dependent degradation of MdmX is proposed to be directed by Mdm2, and possibly mediated by changes in MdmX binding by 14-3-3 and the deubiquitinase HAUSP (Meulmeester et al., 2005; Okamoto et al., 2005; LeBron et al., 2006; Pereg et al., 2006). Wahl and colleagues have generated an *MdmX*^{3SA} mouse model in which all three of these serine residues are replaced with alanine (Wang et al., 2009). *MdmX*^{3SA} mice display impaired p53 stabilization and decreased p53 activity in response to IR. Furthermore,

MdmX^{3SA} mice are resistant to lethal doses of IR, and though not prone to spontaneous tumorigenesis, these mice display increased *Eμ-myc*-driven lymphomagenesis. Thus, DNA damage-induced phosphorylation of MdmX, a negative regulator of p53, can impact p53 stabilization and activity.

As observed with MdmX, ATM-dependent phosphorylation of Mdm2 precedes p53 stabilization after DNA damage (Khosravi et al., 1999). It was initially shown that ATM directly phosphorylates Ser395 of human Mdm2 (Ser394 in mouse) in response to DNA damage (Maya et al., 2001). Furthermore, in transfection-based assays, Mdm2 with an aspartic acid in place of Ser395 (mimicking phosphorylation) shows a decreased capacity to induce p53 degradation and nuclear export (Maya et al., 2001). The phosphatase Wild-type p53-induced phosphatase 1 (Wip1) can dephosphorylate Mdm2 Ser395, and dephosphorylated Mdm2 has increased stability and affinity for p53, facilitating p53 ubiquitination and degradation (Lu et al., 2007). This result trends with another study that showed that DNA damage-induced p53 stabilization is preceded by the destabilization of Mdm2, a phenomenon that could be inhibited with the PIKK inhibitor wortmannin (Stommel and Wahl, 2004). However, a subsequent study identified five additional residues in the C-terminal region of human Mdm2 that are phosphorylated by ATM (Ser386, Ser407, Thr419, Ser425 and Ser 429) (Cheng et al., 2009) and *in vitro* work in which all six residues were replaced with alanine or aspartic acid suggests that ATM phosphorylation of this series of residues inhibits RING domain oligomerization and E3 ligase activity

(Cheng et al., 2009; Cheng et al., 2011). Thus, ATM phosphorylation of Mdm2 is proposed to influence both Mdm2 stability and activity towards p53.

Mdm2

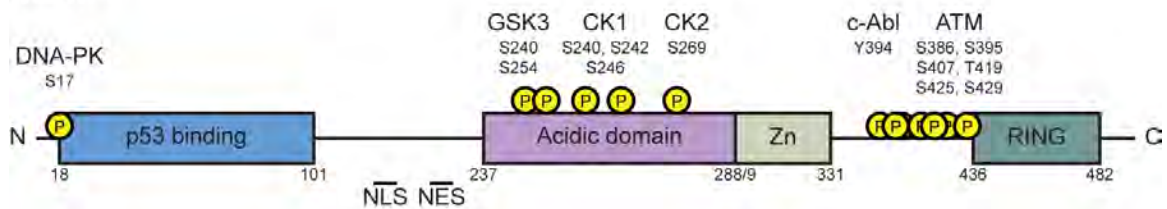


Figure 1.2: Diagram of the Mdm2 protein. Shown are the major functional domains along with sites of phosphorylation relevant to the DNA damage response (P, yellow circles). Zn, zinc finger; NLS, nuclear localization sequence; NES, nuclear export sequence.

MdmX

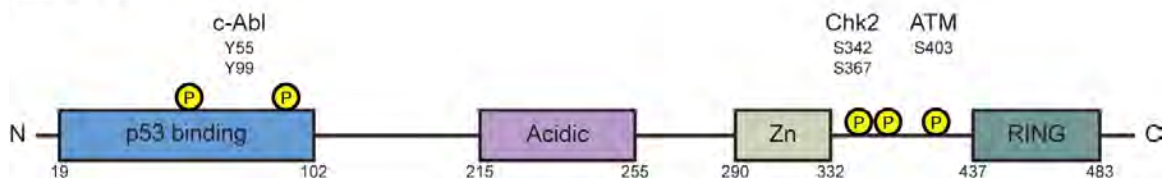


Figure 1.3: Diagram of the MdmX protein. Shown are the major functional domains along with sites of phosphorylation relevant to the DNA damage response (P, yellow circles). Zn, zinc finger.

In order to examine the impact of Mdm2 Ser395 phosphorylation under endogenous conditions, our lab has previously reported the generation and initial characterization of a mouse model wherein ATM phosphorylation of Mdm2 at serine residue 394 (the equivalent of human Mdm2 Ser395) was abolished (*Mdm2^{S394A}* mice) (Gannon et al., 2012). Cells and tissues in *Mdm2^{S394A}* mice display profound defects in DNA damage-induced p53 protein stabilization and

p53 target gene activation. This failure to induce a robust p53 response translates to less p53-dependent apoptosis in hematopoietic tissues, radio-resistance, and increased spontaneous lymphomagenesis. Furthermore, replacing Mdm2 Ser394 with aspartic acid (*Mdm2^{S394D}* mice), mimicking constitutive phosphorylation at this residue, results in prolonged p53 activity following damage and suggests dephosphorylation of this residue is involved in resolving the p53 response. Therefore, ATM phosphorylation of the negative regulator of p53, Mdm2, can profoundly impact p53 stabilization and activation in response to stress *in vivo*.

Mdm protein phosphorylation by c-Abl

Similar to ATM, the c-Abl tyrosine kinase is activated by a variety of DNA damaging agents (Kharbanda et al., 1995; Liu et al., 1996; Wang et al., 2011a). c-Abl is a member of the Src family of non-receptor tyrosine kinases and was discovered as the product of the cellular proto-oncogene from which the *Gag-v-Abl* oncogene of the Abelson murine leukemia virus originated (Wang, 2014). This finding, coupled with Abl's role in the Bcr-Abl oncoprotein resultant from the Ph⁺ chromosomal translocation, have led to extensive studies of the oncogenic functions of Abl fusion proteins and the current understanding that either Gag or Bcr fusion to N-terminally truncated Abl adds to and alters Abl function (Wang, 2014). c-Abl is ubiquitously expressed and is ascribed pleiotropic functions associated with activity in both the nucleus and cytoplasm (Levav-Cohen et al.,

2005). A large number of proteins that are phosphorylated by c-Abl have been identified, and include other kinases, adapters, transcription factors, chromatin modifiers and cytoskeletal proteins (Wang, 2014). c-Abl interacts with ATM and is phosphorylated on Ser465, leading to its activation (Baskaran et al., 1997; Shafman et al., 1997). This initially led to c-Abl activities in the DNA damage response being viewed as downstream of ATM. However, more recent work has shown c-Abl to phosphorylate both ATM and ATR, and that these phosphorylation events are required for maximal activity of either PIKK (Wang et al., 2011a). Overexpression studies indicate c-Abl promotes growth arrest in a p53-dependent manner, and apoptosis by p53-dependent and independent mechanisms (Sawyers et al., 1994; Wen et al., 1996; Yuan et al., 1997). c-Abl mediated p53-independent apoptosis is attributed to the p53 homolog p73, which is directly phosphorylated by c-Abl on Tyr99 (Gong et al., 1999; Agami et al., 1999; Yuan et al., 1999). However, no c-Abl target residues have been identified on p53.

MdmX is phosphorylated by c-Abl on Tyr55 and Tyr99 in response to DNA damage. These residues are located within the p53 binding domain of MdmX, and Tyr99 phosphorylation impairs p53 binding in a transfection-based assay (Zuckerman et al., 2009). Similar co-expression studies have shown that c-Abl protects p53 from Mdm2 mediated degradation, and overcomes the inhibitory effect of Mdm2 on p53 transcriptional activity and p53-dependent apoptosis (Sionov et al., 1999). Additionally, c-Abl is required for maximal p53

accumulation in response to ionizing radiation (IR), doxorubicin, and mitomycin C in MEFs, and co-expression of c-Abl overcomes Mdm2 mediated ubiquitination and nuclear export of p53 (Sionov et al., 2001). *In vitro* studies have shown that c-Abl phosphorylates human Mdm2 on Tyr394 (Tyr393 in mouse) as well as Tyr276 and Tyr405 (Goldberg et al., 2002; Dias et al., 2006), and that c-Abl phosphorylation of Mdm2 Tyr394 impairs Mdm2's ability to inhibit p53's stabilization and transactivation, and p53-mediated apoptosis (Goldberg et al., 2002). It has since been proposed that c-Abl phosphorylation of Mdm2 increases Mdm2-MdmX binding and promotes Mdm2-directed MdmX ubiquitination. This increase in MdmX ubiquitination ultimately destabilizes the Mdm2-MdmX complex, promoting p53 stabilization (Waning et al., 2011). However, the contribution of these proposed c-Abl-dependent phosphorylation events to p53 stabilization and activation has not been examined under physiological conditions.

Aims of this dissertation

The principal aim of this dissertation is to further the understanding of the mechanisms by which DNA damage response-related kinase signaling affects p53 stabilization and activation, and its impact on p53 responses and tumor suppression. Specifically, this dissertation describes the use of several knock-in mouse models to examine the effects of Mdm2 phosphorylation by the ATM and c-Abl kinases on Ser394 and Tyr393, respectively, under endogenous conditions.

Our lab's previous findings of reduced p53 stabilization and activity, radioresistance, and spontaneous tumor susceptibility in *Mdm2*^{S394A} mice highlight a significant role for Mdm2 phosphorylation in regulating p53 activation.

In Chapter II of this dissertation, we use *Mdm2*^{S394A} mice to explore *in vivo* the mechanism by which Mdm2 Ser394 phosphorylation alters p53 functions in a radiosensitive tissue. Furthermore, we address whether ATM-Mdm2-p53 signaling in mice impacts tumorigenesis induced by activated oncogenes or ionizing radiation (IR), and explore the role of ATM-Mdm2-p53 signaling in promoting IR-mediated bone marrow failure. Our results indicate that Mdm2 Ser394 phosphorylation has dramatically different and stress-dependent effects in tumorigenesis.

In Chapter III of this dissertation we present a novel knock-in mouse that cannot be phosphorylated at Tyr393 (*Mdm2*^{Y393F} mice). Experiments with *Mdm2*^{Y393F} mice allow us to examine the influence of c-Abl phosphorylation of Mdm2 on the regulation of p53-mediated DNA damage responses and p53 tumor suppression *in vivo*. Furthermore, we describe the generation of mice in which both Tyr393 and Ser394 cannot be phosphorylated (*Mdm2*^{Y393F/S394A} mice), allowing for the determination of whether phosphorylation of these residues has additive effects.

CHAPTER II

Mdm2 Ser394 Phosphorylation Regulates Mdm2 Stability and has Contrasting Effects on Oncogene and Radiation-Induced Tumorigenesis

ATM phosphorylation of Mdm2 Ser394 is required for robust p53 stabilization and activation in DNA damaged cells. We have now utilized *Mdm2*^{S394A} knock-in mice to determine that phosphorylation of Mdm2 Ser394 regulates p53 activity and the DNA damage response in lymphatic tissues *in vivo* by modulating Mdm2 stability. Mdm2 Ser394 phosphorylation delays lymphomagenesis in *Eμ-myc* transgenic mice, and preventing Mdm2 Ser394 phosphorylation obviates the need for p53 mutation in Myc-driven tumorigenesis. However, irradiated *Mdm2*^{S394A} mice also have increased hematopoietic stem and progenitor cell functions, and decreased lymphomagenesis in sub-lethally irradiated *Mdm2*^{S394A} mice. These findings document contrasting effects of ATM-Mdm2 signaling on p53 tumor suppression, and reveal that destabilizing Mdm2 by promoting its phosphorylation by ATM would be effective in treating oncogene-induced malignancies, while inhibiting Mdm2 Ser394 phosphorylation during radiation exposure or chemotherapy would ameliorate bone marrow failure and prevent the development of secondary hematological malignancies.

Results

ATM-Mdm2 signaling regulates the p53-response in lymphatic tissues

To further explore the effects of Mdm2 Ser394 phosphorylation on p53 protein levels and activity *in vivo*, we analyzed thymi of mice treated with a low dose (1.75 Gy) of IR. Although p53 protein levels were elevated in the thymus of *Mdm2*^{S394A} mice at 3 hours and 6 hours following IR, there was considerably less total p53 protein and phosphorylated p53 phosphorylation (S18) in treated *Mdm2*^{S394A} mice than in irradiated wild-type (WT) mice (Figure 2.1). This is similar to what we observed previously in these mice using higher dosages of IR (Gannon et al., 2012). However, we also noted that basal levels of p53 appeared slightly lower in *Mdm2*^{S394A} thymi than in WT thymi, and more Mdm2 protein appeared to be present in *Mdm2*^{S394A} thymi in the absence of acute DNA-damage and following IR treatment (Figure 2.1).

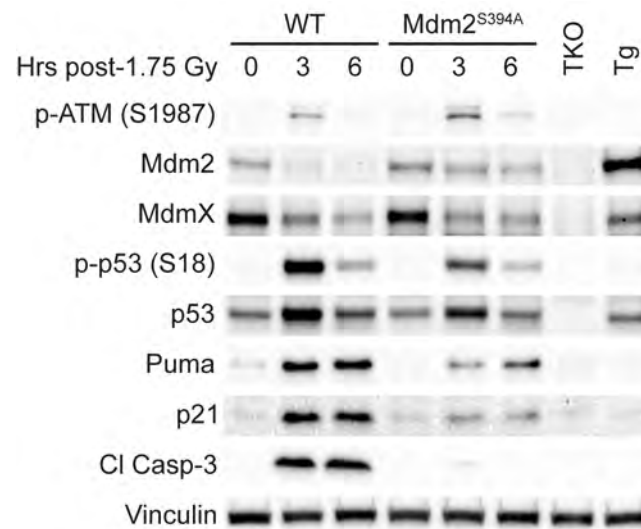


Figure 2.1: Western blot of thymus extracts. WT and *Mdm2*^{S394A} mice were left untreated or exposed to 1.75 Gy ionizing radiation (IR) and thymi were harvested at 3 and 6 hours. Protein levels were analyzed by western blotting. TKO indicates *Mdm2*^{-/-}, *MdmX*^{-/-}, *p53*^{-/-} control; Tg indicates *Mdm2*^{Tg/+} Mdm2 overexpressing control.

There was a significant decrease in WT Mdm2 protein levels in whole thymus following DNA damage, an observation that has been made in cell culture settings by several groups (Stommel and Wahl, 2004; Itahana et al., 2007; Inuzuka et al., 2010; Malonia et al., 2015). However, Mdm2 protein levels appeared to diminish after IR at a lesser rate in *Mdm2*^{S394A} thymus than in WT thymus. To more definitively quantify the observed differences in thymic Mdm2 and p53 levels, we analyzed biological triplicates of untreated and irradiated WT and *Mdm2*^{S394A} thymi. This confirmed that Mdm2 protein levels were higher in *Mdm2*^{S394A} thymi both before and after treatment, and that the IR-induced relative decrease in Mdm2 protein levels was far less in *Mdm2*^{S394A} thymi (Figure 2.2). In

contrast, the reduction of MdmX levels induced by DNA damage (Wang et al., 2009) appears to be similar in WT and *Mdm2*^{S394A} thymi. Though not statistically significant, p53 levels are slightly lower in untreated *Mdm2*^{S394A} thymi (Figure 2.2, lower panel), and are significantly lower in irradiated *Mdm2*^{S394A} thymi.

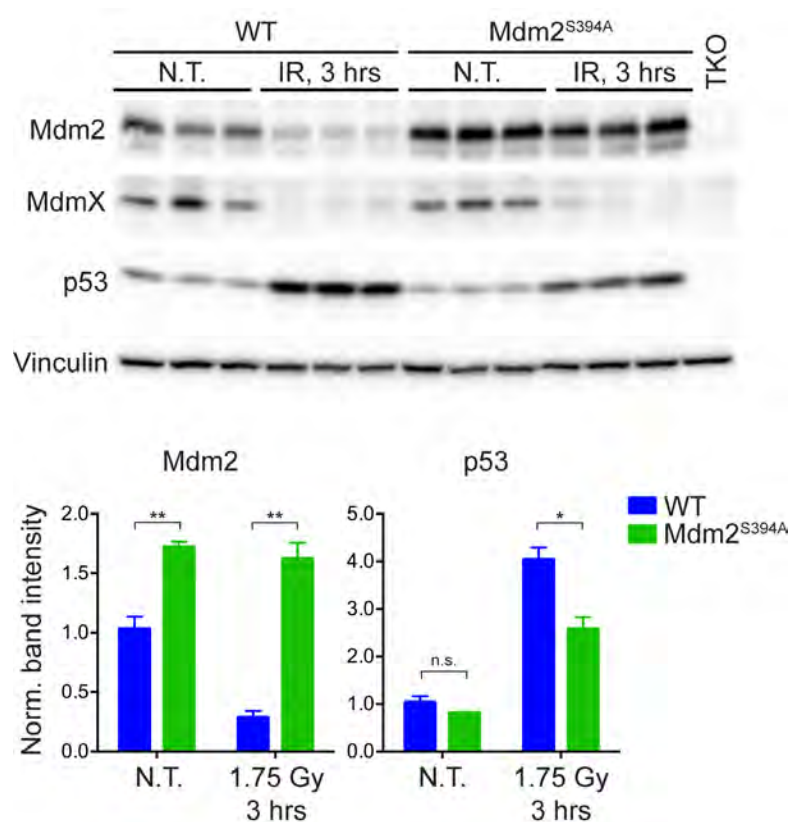


Figure 2.2: Quantification of thymus Mdm2 and p53 protein levels.

Biological triplicates of WT and *Mdm2*^{S394A} mice left untreated or 3 hours after exposure to 1.75 Gy were analyzed by western blotting. Band intensities were determined by densitometry. Mdm2 and p53 levels were normalized for Vinculin levels and average values plotted (\pm SEM). * $P < 0.05$, ** $P < 0.01$ (Student's t -tests).

Although p53 target gene expression was similar in non-damaged WT and *Mdm2*^{S394A} thymi (Figure 2.3), a reduction in IR-activation of p53 target genes

was seen in *Mdm2*^{S394A} thymi. Reduced expression levels of *Mdm2*, the cell cycle regulator *Cdkn1a* (p21), and the pro-apoptotic genes *Puma*, *Noxa*, and *Bax* are in agreement with reduced levels of p21, Puma, and cleaved Caspase-3 protein (Figure 2.1), and with a clear reduction in DNA damage-induced apoptosis in *Mdm2*^{S394A} thymi following exposure of mice to low-level IR (Figure 2.4).

To explore whether these effects were unique to the thymus, we also examined protein levels in spleens of WT and *Mdm2*^{S394A} mice. As observed in the thymus, there appeared to be less total p53 in *Mdm2*^{S394A} spleens before and after irradiation (Figure 2.5), and Mdm2 levels were higher in both untreated and irradiated *Mdm2*^{S394A} spleens. Intriguingly, while no induction of Mdm2 protein was observed in thymi of WT and *Mdm2*^{S394A} mice in response to IR, spleens of both genotype displayed a more 'classic' induction of Mdm2 often seen in cultured cells after genotoxic stress. Similar to what was observed in the thymus, decreased levels of p53 and increased levels of Mdm2 in irradiated *Mdm2*^{S394A} spleens correlate with reduced p53 activation (phospho-S18 p53), reduced levels of Puma and p21, and reduced levels of cleaved Caspase-3 (Figure 2.5).

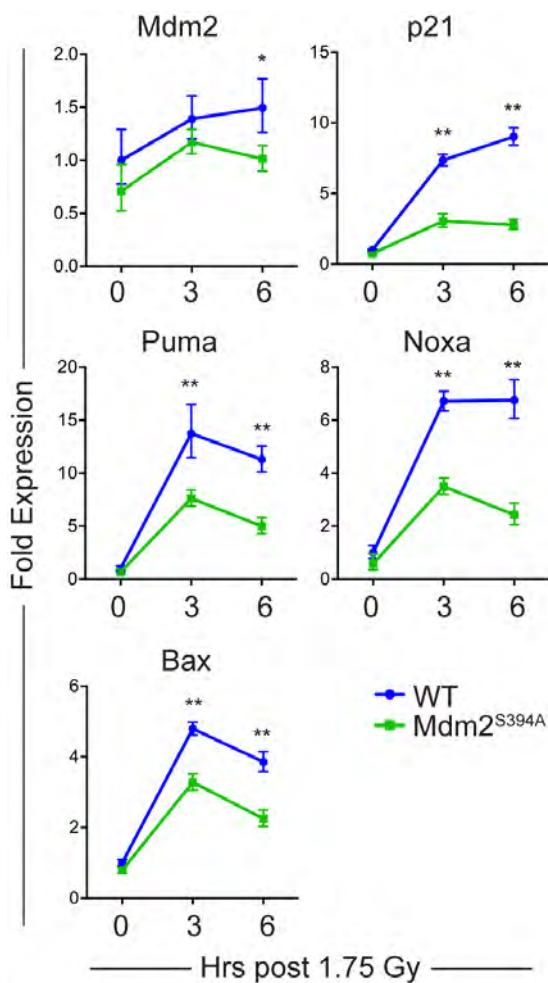


Figure 2.3: Relative expression levels of p53 target genes in thymi. WT and *Mdm2*^{S394A} mice were treated as in Figure 2.1 and fold expression of p53-target genes was determined by real-time quantitative PCR, relative to untreated WT samples and using *Rplp0* as internal reference ($n = 3$, \pm SEM). * $P < 0.05$, ** $P < 0.01$ (Student's *t*-tests).

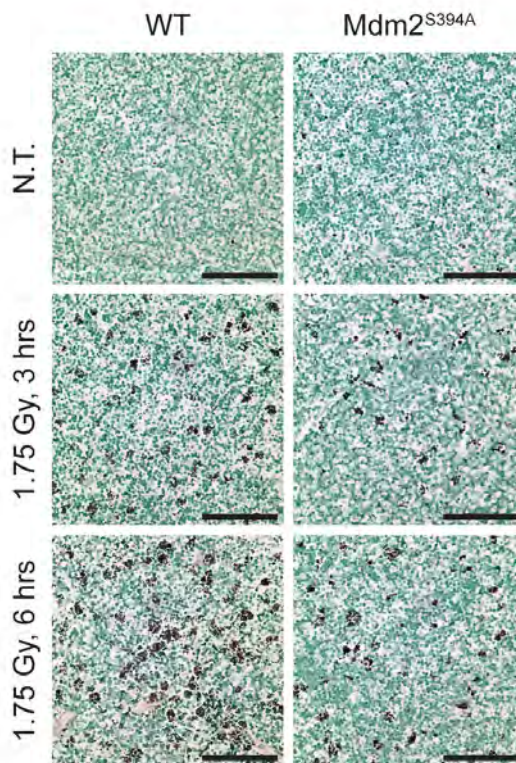


Figure 2.4: Apoptosis in thymi. TUNEL staining of thymi from WT and *Mdm2*^{S394A} mice treated as in Figure 2.1. Scale bars represent 100 μ m.

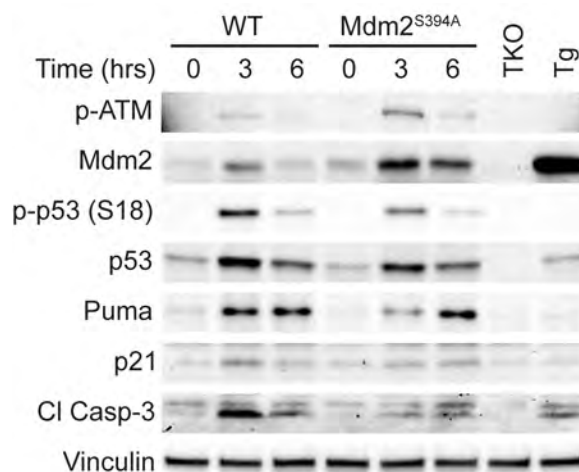


Figure 2.5: Western blot of spleen extracts. WT and *Mdm2*^{S394A} mice were left untreated or exposed to 1.75Gy ionizing radiation (IR) and spleens were harvested at 3 and 6 hours. Protein levels were analyzed by western blotting. TKO indicates *Mdm2*^{-/-}, *MdmX*^{-/-}, *p53*^{-/-} control; Tg indicates *Mdm2*^{Tg/+} Mdm2 overexpressing control.

ATM phosphorylation of Mdm2 Ser394 governs Mdm2 levels and stability

In order to directly analyze the effects of Mdm2 Ser394 phosphorylation on the stability of Mdm2 in the presence and absence of exogenous DNA damage, we measured the half-life of Mdm2 proteins using the protein synthesis inhibitor cycloheximide. Although basal levels of Mdm2 transcription are similar in WT and *Mdm2*^{S394A} thymi, Mdm2 protein levels are elevated in non-damaged *Mdm2*^{S394A} mice (Figures 2.1 and 2.2), suggesting that the mutant Mdm2 protein is more stable in the absence of exogenous DNA damage. However, we observed no significant difference in the half-lives of WT Mdm2 and *Mdm2*^{S394A} in untreated thymocytes (80 and 65 minutes respectively, overlapping 95% confidence intervals) (Figure 2.6). But following treatment of the thymocytes with 2.5 Gy IR, the half-life of WT Mdm2 decreased by more than 50 percent (29

minutes) whereas the half-life of Mdm2^{S394A} remained unchanged (69 minutes) (Figure 2.7). These data show that phosphorylation of Mdm2 Ser394 by ATM is a crucial event in DNA damage-induced destabilization of Mdm2 under physiological conditions.

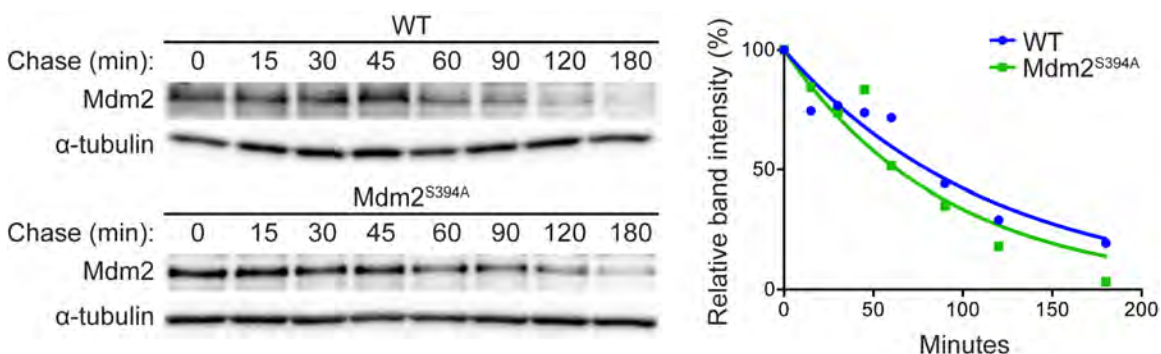


Figure 2.6: Mdm2 protein stability in untreated thymocytes. Thymocytes harvested from WT and *Mdm2*^{S394A} mice ($n = 6$) were treated with 100 mg/mL cycloheximide and harvested at the indicated time points. The levels of Mdm2 and α -tubulin were analyzed by western blotting. Band intensities were determined by densitometry and Mdm2 levels normalized to α -tubulin were plotted. One-phase decay curves were fitted using GraphPad Prism software.

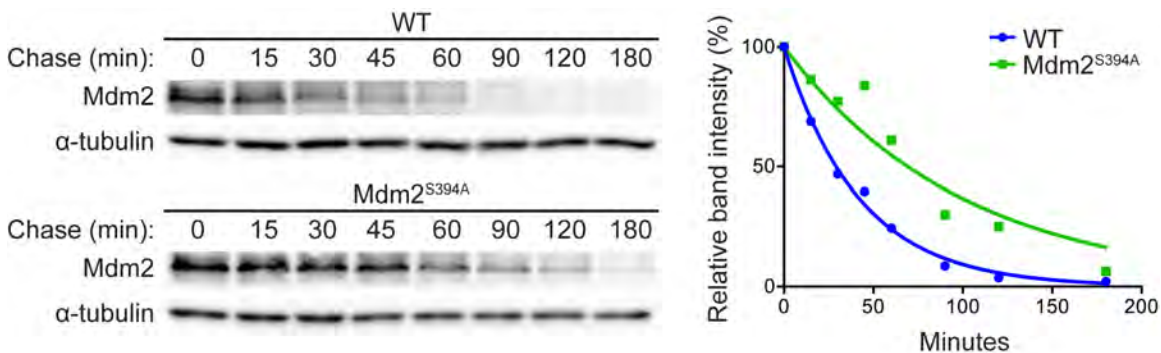


Figure 2.7: Mdm2 protein stability in irradiated thymocytes. Thymocytes harvested from WT and *Mdm2*^{S394A} mice ($n = 6-8$) were exposed to 2.5Gy IR and treated with 100 mg/mL cycloheximide and harvested at the indicated time points. Normalized Mdm2 levels were plotted as in Figure 2.6.

As previous studies have shown ATM phosphorylation of Mdm2 to impact the ability of Mdm2 to promote p53 degradation (Maya et al., 2001; Cheng et al., 2009; Cheng et al., 2011), we also examined whether p53 stability was affected in the presence and absence of DNA damage. We observed no difference in the half-life of p53 in non-treated WT versus *Mdm2*^{S394A} thymocytes (Figure 2.8). As expected, DNA damage stabilized p53 levels in WT cells (Figure 2.9). Likewise, DNA damage stabilized p53 levels in *Mdm2*^{S394A} thymocytes, albeit to a lower level than seen in WT thymocytes.

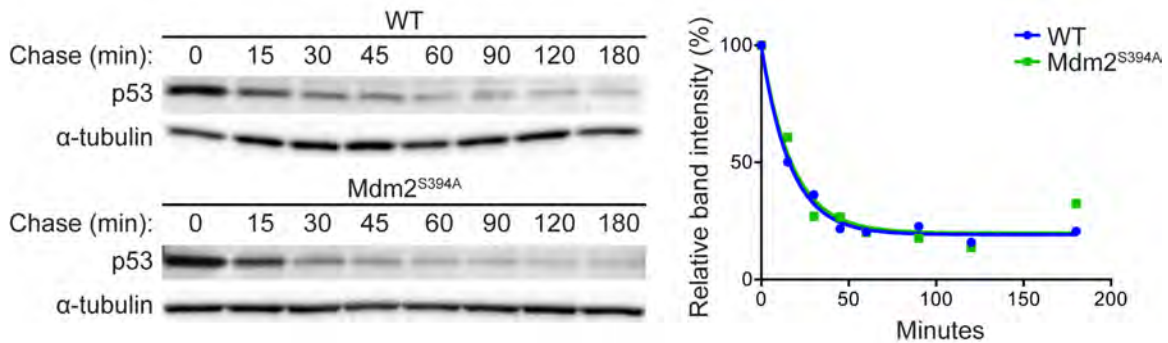


Figure 2.8: p53 protein stability in untreated thymocytes. Thymocytes harvested from WT and *Mdm2*^{S394A} mice ($n = 6$) were treated with 100 mg/mL cycloheximide and harvested at the indicated time points. The levels of p53 and α -tubulin were analyzed by western blotting. Band intensities were determined by densitometry and p53 levels normalized to α -tubulin were plotted. One-phase decay curves were fitted using GraphPad Prism software.

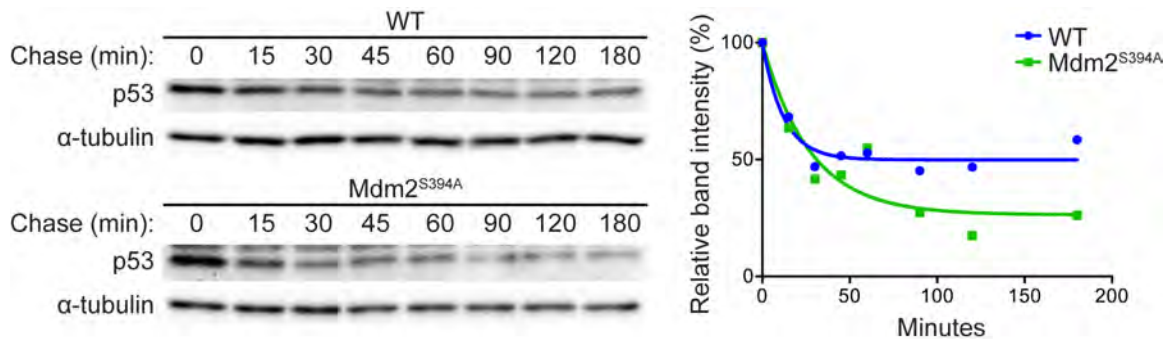


Figure 2.9: p53 protein stability in irradiated thymocytes. Thymocytes harvested from WT and *Mdm2*^{S394A} mice ($n = 6-8$) were exposed to 2.5Gy IR and treated with 100 mg/mL cycloheximide and harvested at the indicated time points. Normalized p53 levels were plotted as in Figure 2.8.

Since we observed no difference in the rate of p53 decay in *Mdm2*^{S394A} and WT thymocytes, it is possible that phosphorylation of Mdm2 Ser394 upregulates p53 activity not only by altering p53 protein stability but by also inhibiting Mdm2-p53 complex formation and Mdm2-mediated steric inhibition of p53 transcriptional activation. Therefore, we examined the effects of Mdm2 Ser394 phosphorylation on Mdm2-p53 binding in the presence and absence of DNA damage in whole tissue extracts. In an effort to control for potential differences in antibody affinity following IR-induced modification of Mdm2, Mdm2 was immunoprecipitated from untreated and irradiated thymus lysates in separate experiments with two distinct antibodies whose epitopes reside in opposing termini of Mdm2 (Figure 2.10, left). In both cases, more p53 co-immunoprecipitated with Mdm2^{S394A} than WT Mdm2 in untreated thymi, whereas similar amounts of p53 co-immunoprecipitated with Mdm2 in irradiated *Mdm2*^{S394A} and WT thymi. As there was less p53 observed in the total lysates of

untreated and irradiated *Mdm2*^{S394A} thymi relative to WT thymi (Figure 2.10, right), this result reveals increased levels of Mdm2-bound p53 (relative to total p53) in undamaged and IR-treated *Mdm2*^{S394A} thymi. We confirmed this finding by performing the reciprocal experiment using p53 immunoprecipitation, and observed that equivalent amounts of Mdm2 co-immunoprecipitated with lesser amounts of p53 in untreated and irradiated *Mdm2*^{S394A} thymi. Additional immunoprecipitation experiments against MdmX detected no effect on the relative amounts of Mdm2-bound MdmX or p53-bound MdmX before or after DNA damage (Figure 2.11).

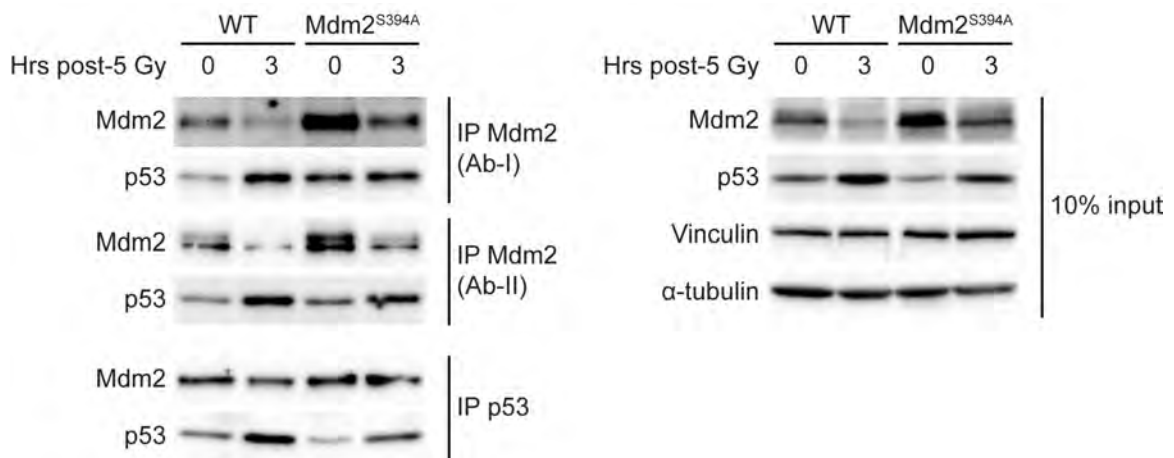


Figure 2.10: Reciprocal co-immunoprecipitation of Mdm2 and p53 from thymus extracts. Thymus protein extracts from WT and *Mdm2*^{S394A} mice untreated or exposed to 5 Gy IR were immunoprecipitated with antibodies for Mdm2 (NBP1-02158 (Ab-I) and Ab-5 (Ab-II)) and p53 (left). Immunoprecipitates were analyzed by western blotting for Mdm2 and p53. Total lysate (10% input) was analyzed by western blotting (right).

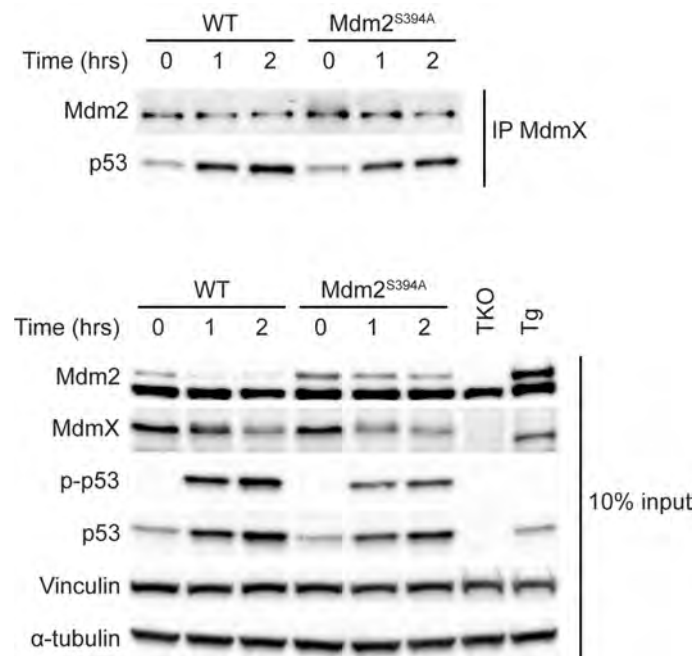


Figure 2.11: Co-immunoprecipitation of Mdm2 and p53 with MdmX from thymus extracts. Thymus protein extracts from WT and *Mdm2*^{S394A} mice untreated and exposed to 5Gy IR were immunoprecipitated with an antibody for MdmX (MDMX-82; Sigma) (top). Immunoprecipitates were analyzed by western blotting for Mdm2 and p53. Total lysate (10% input) was analyzed by western blotting (bottom).

Collectively, these data reveal that phosphorylation of Mdm2 Ser394 under basal conditions and following acute IR exposure reduces Mdm2 stability, thereby reducing the relative amount of Mdm2-bound p53. This reduction in Mdm2-p53 complex negatively impacts Mdm2 inhibition of p53 target gene transactivation as well as Mdm2 destabilization of p53.

Accelerated *Eμ-myc* driven lymphomagenesis in *Mdm2*^{S394A} mice

We have previously described an increased susceptibility to spontaneous tumorigenesis in *Mdm2*^{S394A} mice (Gannon et al., 2012). We next sought to examine the effects of Mdm2 Ser394 phosphorylation on oncogene-induced tumorigenesis. *Mdm2*^{S394A} mice were bred to *Eμ-myc* transgenic mice to generate *Eμ-myc* and *Eμ-myc;Mdm2*^{S394A} mice. *Eμ-myc* mice succumb to pre-B/B-cell lymphomas within 3-6 months of age. We observed a median time to tumor presentation of 126 days in *Eμ-myc* mice, consistent with previous studies (Adams et al., 1985; Eischen et al., 1999; Sluss et al., 2010) (Figure 2.12). In contrast, the median time to tumor presentation in *Eμ-myc;Mdm2*^{S394A} mice was only 71 days. This represents a nearly 50% reduction in the time to Myc-induced tumorigenesis when ATM phosphorylation of Mdm2 Ser394 is inhibited. All tumor-bearing *Eμ-myc* mice and *Eμ-myc;Mdm2*^{S394A} mice presented with enlarged lymph nodes and spleens, and representative tumors were examined histologically by haematoxylin and eosin (H&E) staining. Both genotypes developed similar, high-grade lymphomas, composed of monotonous populations of pre-B/B cells. Tumors displayed high levels of mitosis and apoptosis, and the characteristic “starry-sky” pattern resultant from abundant tingible body-laden macrophages. The cell type was further confirmed by immunohistochemistry (IHC) through positive staining for B220/CD45R (Figure 2.13).

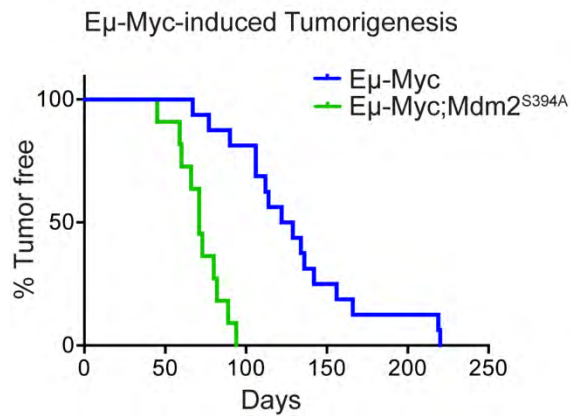


Figure 2.12: Lymphomagenesis in *Eμ-myc* and *Eμ-myc;Mdm2^{S394A}* mice. Kaplan-Meier survival curves of *Eμ-myc* ($n = 16$) and *Eμ-myc;Mdm2^{S394A}* ($n = 11$) mice. Median survival times were as follows: *Eμ-myc* (125.5 days) and *Eμ-myc;Mdm2^{S394A}* (71 days). Curves were compared by Log-rank test: $P < 0.0001$.

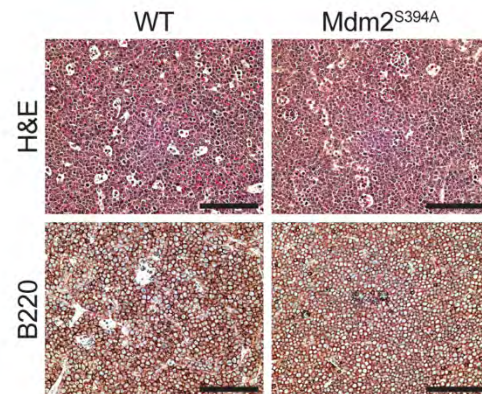


Figure 2.13: Representative staining of *Eμ-myc* and *Eμ-myc;Mdm2^{S394A}* lymphomas. B cell lymphomas from lymph nodes of *Eμ-myc* (98 days) and *Eμ-myc;Mdm2^{S394A}* (80 days) mice were stained by haematoxylin and eosin (top) and with an antibody specific for B220 (bottom). Scale bars represent 100 μm .

Myc-driven B cell tumors face selective pressure to inactivate the p53 pathway through p53 mutation, Mdm2 overexpression, or by loss of Arf (Eischen et al., 1999). We examined the status of p53, Mdm2 and Arf in a panel of ten tumors that developed in *Eμ-myc;Mdm2^{S394A}* mice (Figure 2.14). No marked differences in p53 protein levels were observed in any of the ten tumors examined. However, Arf levels appeared more variable, with loss of detectable Arf protein seen in four of the ten tumors. RT-PCR confirmed that three of those four tumors did not express full length Arf mRNA. Arf levels have been shown previously to be elevated in cases where p53 is mutant and the negative feedback loop between p53 and Arf is disrupted, and we identified several

tumors wherein Arf appeared to be increased. However, sequencing of the entire p53 coding sequence of all ten tumors revealed no mutations in p53 gene transcripts. Thus, the observed variability in Arf levels within the Myc tumors was not a result of p53 status. Furthermore, Mdm2 protein levels did not vary significantly between tumors, and qPCR analysis also failed to detect alterations in *Mdm2* transcript levels in any tumor (data not shown). Thus, ATM phosphorylation of Mdm2 Ser394 strongly suppresses Myc oncogene-induced tumorigenesis in mice, and inhibition of this signaling event obviates the need for mutation of the Mdm2-p53 tumor suppressor axis in Myc-driven B cell lymphomagenesis (Figure 2.15).

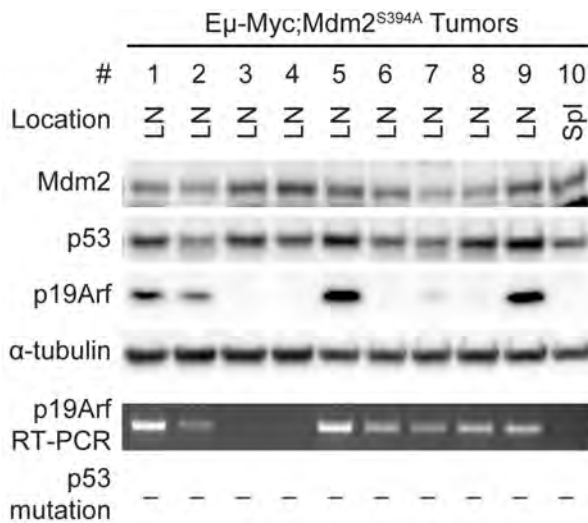


Figure 2.14: *Eμ-myc;Mdm2^{S394A}* tumor analysis. The levels of Mdm2, p53 and Arf were analyzed by western blotting in a panel of *Eμ-myc;Mdm2^{S394A}* tumors. RT-PCR confirmed that full-length *Arf* message was absent in 3 of 10 tumors (2nd from bottom). *p53* cDNA was sequenced for each tumor, revealing no mutations (bottom). LN, lymph node; Spl, spleen.

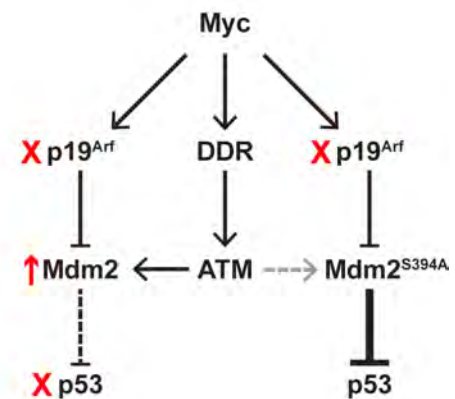


Figure 2.15: Schematic outlining the proposed methods of p53 activation by Myc. Tumors in mice in which Mdm2 is WT select for loss of Arf or p53, or Mdm2 overexpression (Eischen et al., 1999). We propose that *Mdm2^{S394A}* mice obviate the need for p53 loss or Mdm2 overexpression by mitigating the effects of the DDR arm of Myc signaling to p53.

***Mdm2^{S394A}* mice are resistant to IR-induced lymphomagenesis**

We next sought to examine the effects of ATM phosphorylation of Mdm2 Ser394 on IR-induced tumorigenesis. Exposure of mice to repeated low-dose IR promotes the development of thymic lymphomas (Kaplan and Brown, 1952). This lymphomagenesis is significantly enhanced in the absence of p53 (Kemp et al., 1994; Labi et al., 2010; Michalak et al., 2010). As we have shown that IR-induced p53 activity is diminished in both the thymus and spleen of *Mdm2^{S394A}* mice, we anticipated a heightened sensitivity to IR-induced lymphomagenesis in

this model. Cohorts of WT, *Mdm2*^{S394A}, *p53*^{+/-} and *p53*^{-/-} mice were subjected to four weekly doses of 1.75 Gy IR and monitored over time for tumor presentation. 89% of WT mice developed lymphomas by 400 days, with a median survival of 197 days (Figure 2.16), consistent with a previous study employing this dosing strategy (Labi et al., 2010). Also consistent with previous studies was the significant acceleration of lymphomagenesis observed in the absence of p53 (Kemp et al., 1994; Labi et al., 2010; Michalak et al., 2010). All *p53*^{-/-} mice developed lymphomas within 151 days, with a median survival of 131 days, whereas all *p53*^{+/-} mice developed lymphomas within 167 days, with a median survival of 154 days. Surprisingly, *Mdm2*^{S394A} mice proved to be highly resistant to IR-induced thymic lymphomagenesis. Although tumor presentation in *Mdm2*^{S394A} mice followed similar initial kinetics as observed in WT mice, only 42% of *Mdm2*^{S394A} mice developed lymphoma, with a median survival among tumor-bearing mice of 184 days. Tumor-bearing animals presented with profoundly enlarged thymi, as well as frequent splenomegaly and hepatomegaly. Histological analyses of H&E stained tissues showed disorganized, hyperplastic lymphatic tissues as well as significant lymphocyte infiltration in portal regions of the liver (Figure 2.17). Immunohistochemistry confirmed that the lymphomas arising in IR-treated mice were T cell-derived, with positive staining for CD3 and negative staining for B220 (Figure 2.18). Thus, in contrast to their increased rate of spontaneous and oncogene-induced tumorigenesis, *Mdm2*^{S394A} mice are

actually more resistant to radiation-induced T cell lymphomagenesis than WT mice, despite having clear defects in p53-mediated thymic apoptosis.

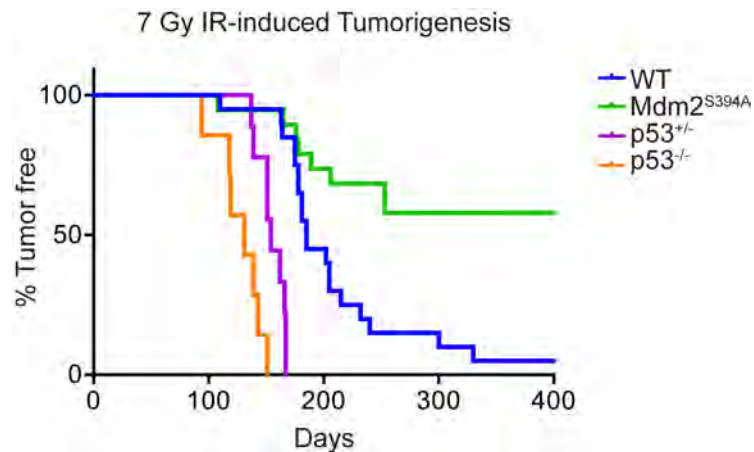


Figure 2.16: IR-induced tumorigenesis. Kaplan-Meier survival curves of WT ($n = 20$), *Mdm2*^{S394A} ($n = 19$), *p53*^{+/-} ($n = 9$) and *p53*^{-/-} ($n = 7$) mice exposed to 7 Gy cumulative IR. Median survival times were as follows: WT (185 days), *Mdm2*^{S394A} (n.d.), *p53*^{+/-} (154 days) and *p53*^{-/-} (131 days). Curves were compared by log-rank test: WT to *p53*^{-/-} ($P < 0.0001$), WT to *p53*^{+/-} ($P < 0.0001$), WT to *Mdm2*^{S394A} ($P = 0.0007$), *Mdm2*^{S394A} to *p53*^{+/-} ($P < 0.0001$), *Mdm2*^{S394A} to *p53*^{-/-} ($P < 0.0001$).

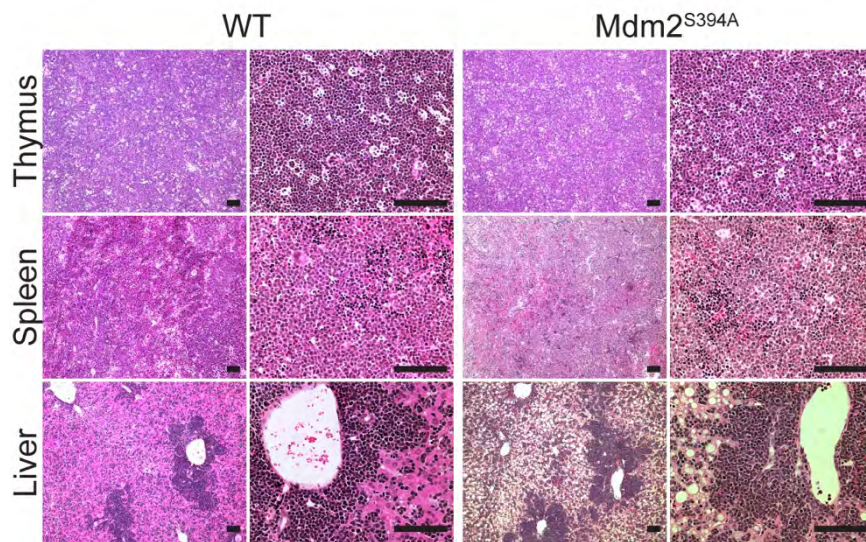


Figure 2.17: H&E staining of IR-induced lymphomas. Tissue sections of lymphomas that developed in the thymus, spleen and liver of WT and *Mdm2*^{S394A} mice stained with haematoxylin and eosin at 10X (left) and 40X (right) magnification. Scale bars represent 100 μ m.

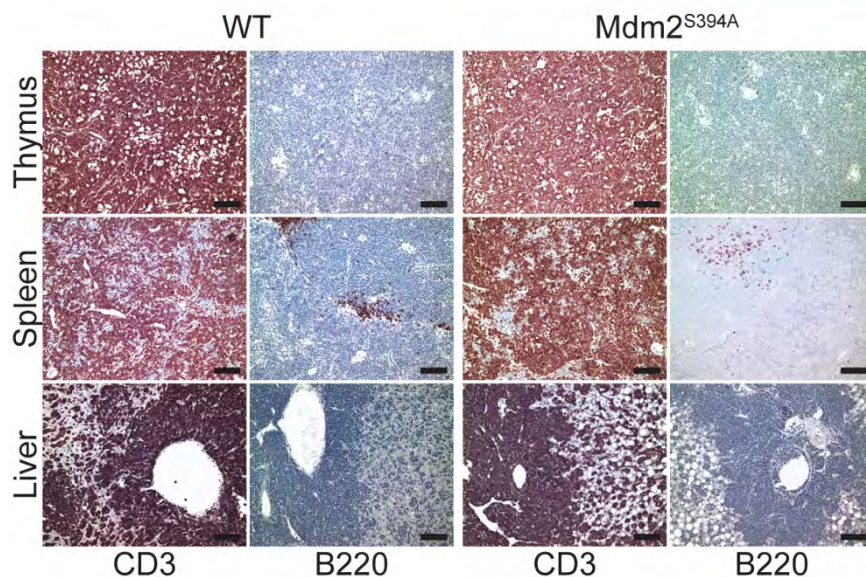


Figure 2.18: Immunohistochemical staining of IR-induced lymphomas. Tissue sections of lymphomas that developed in the thymus, spleen and liver of WT and *Mdm2*^{S394A} mice stained with antibodies specific for CD3 (left) and B220 (right). Scale bars represent 100 μ m.

Radiation resistance in *Mdm2*^{S394A} mice is dictated by improved bone marrow recovery following IR

We have previously reported that *Mdm2*^{S394A} mice are resistant to threshold-lethal doses (8 Gy) of radiation. To better understand why ATM phosphorylation of Mdm2 Ser394 would promote radiation-induced lymphomagenesis yet provide resistance to acute radiation, we decided to examine further the response of these mice to whole-body IR. The primary cause of lethality in mice subjected to IR doses as high as 10 Gy is a p53-dependent ablation of the bone marrow compartment, known as “hematopoietic syndrome” (Komarova et al., 2004). Previous reports have revealed that even small changes in p53 activity can profoundly impact the hematopoietic system (Mendrysa et al., 2003; Terzian et al., 2007; Wang et al., 2011c; Pant et al., 2013), and hematopoietic failure phenotypes have previously been described in mice bearing hypomorphic or reduced copies of functional *Mdm2* alleles (Mendrysa et al., 2003; Terzian et al., 2007). Furthermore, several p53 target genes, including those encoding p21 or Puma have been implicated in governing the radiosensitivity of murine bone marrow (Cheng et al., 2000; van Os et al., 2007; Shao et al., 2010; Yu et al., 2010; Wang et al., 2011c; Pant et al., 2013).

To elucidate the basis for the acute radioresistance of *Mdm2*^{S394A} mice, we examined the expression of the p53-target genes *Mdm2*, *p21*, *Puma* and *Noxa* by qPCR in the bone marrow of WT, *Mdm2*^{S394A} and *p53*^{-/-} mice before and after irradiation (Figure 2.19). As we observed in the thymus, no differences were

present in the expression levels of any of the examined p53 target genes in untreated $Mdm2^{S394A}$ bone marrow. Similar expression levels of the target genes were observed in untreated $p53^{-/}$ mice. Following whole body treatment of mice with 5 Gy IR, the expression levels of all four genes increased dramatically in WT bone marrow, indicative of a strong p53 response. However, lower levels of $p21$, $Puma$ and $Noxa$ transcripts were detected in $Mdm2^{S394A}$ bone marrow, indicating reduced p53 activity in this tissue. Although $Mdm2$ transcript levels did not appear to be overtly reduced in irradiated $Mdm2^{S394A}$ bone marrow, no induction of $Mdm2$, $p21$ or $Puma$ transcription was observed in the bone marrow of p53-deficient mice, pointing to the p53-dependence of their induction following irradiation.

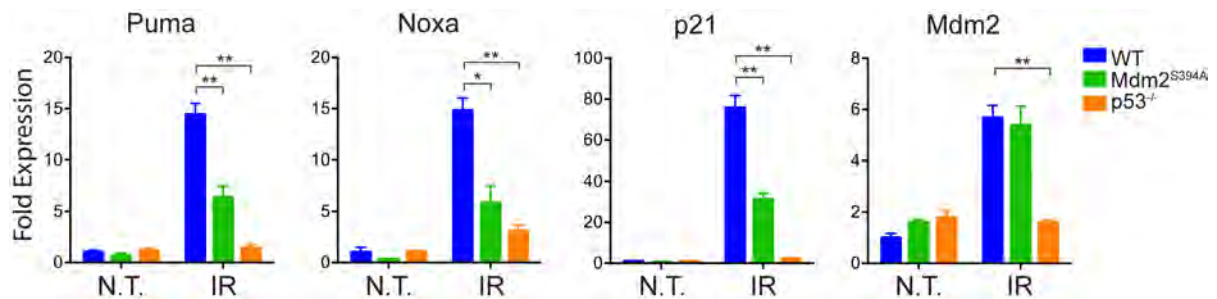


Figure 2.19: Relative expression levels of p53-target genes in bone marrow. Bone marrow was harvested from WT, $Mdm2^{S394A}$ and $p53^{-/}$ mice left untreated (N.T.) or 6 hours after 5Gy IR (IR). Fold expression was determined by real-time quantitative PCR, relative to untreated WT samples, using *Rplp0* as internal reference ($n = 3-4$ mice, \pm SEM). * $P < 0.05$, ** $P < 0.01$ (Student's *t*-tests of $\Delta\Delta Ct$ values).

We next examined the bone marrow of WT, *Mdm2*^{S394A} and *p53*[/] mice by H&E staining at intervals up to 9 days following exposure to 8 Gy IR (Figure 2.20). To our surprise, all mice examined showed a dramatic decrease in cellularity at 1 and 3 days following irradiation, to the point where the three genotypes were phenotypically indistinguishable. Although WT bone marrow continued to display a progressive loss of cellularity at day 6 after IR, large colonies of cells had appeared in the bone marrow of *Mdm2*^{S394A} and *p53*[/] mice at this time (Figure 2.20 - see arrows). By 9 days post-IR, the colonies present in *Mdm2*^{S394A} and *p53*[/] mice had expanded significantly and often bridged the medullary cavity, whereas only a few smaller colonies were observed in WT bone marrow. Immunohistochemical staining for CD45 confirmed that the colonies were of hematopoietic origin (data not shown). The timing of the increased bone marrow cellularity in *Mdm2*^{S394A} and *p53*[/] mice (but not in WT mice) is likely significant, as it precedes by one day the onset of mortality observed in WT mice treated with 8 Gy IR (Gannon et al., 2012).

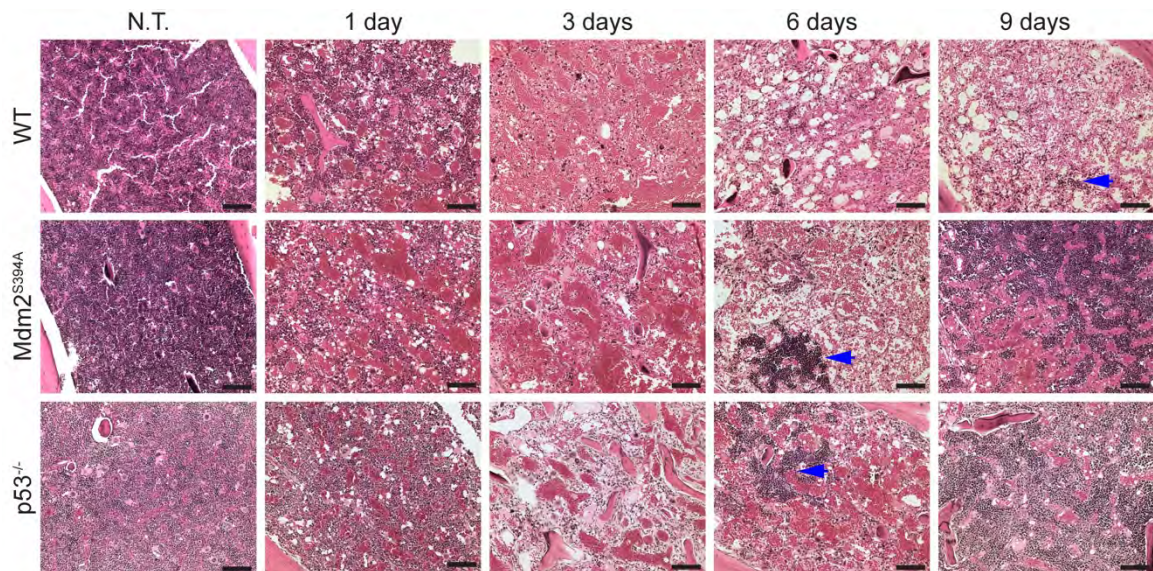


Figure 2.20: Haematoxylin and eosin stained bone marrow following exposure to 8 Gy IR. Femurs from WT, $Mdm2^{S394A}$ and $p53^{-/-}$ mice were harvested at daily intervals following exposure to 8 Gy IR. Blue arrows indicate nascent hematopoietic cell colonies. Scale bars represent 100 μ m.

It has been shown that mice undergoing hematopoietic recovery produce primarily myeloerythroid cells, and myeloerythroid-restricted progenitors are sufficient to confer radioprotection (Uchida et al., 1994; Na Nakorn et al., 2002). We further characterized the bone marrow colonies by IHC staining for the erythroid marker TER-119 (Figure 2.21). Consistent with previous findings, we found that approximately 25% of nucleated bone marrow cells and all mature erythrocytes stained positive for TER-119 in the untreated bone marrow of mice irrespective of their genotype (Kina et al., 2000). However, at 9 days post-8 Gy IR treatment, only the few remaining mature erythrocytes in the WT bone marrow stained positive for TER-119, whereas all of the large colonies present in $Mdm2^{S394A}$ and $p53^{-/-}$ bone marrow were predominantly TER-119 positive. Thus,

the p53-dependant resistance to hematopoietic syndrome observed in $Mdm2^{S394A}$ and $p53^{-/-}$ mice following whole body IR is linked to the increased capability of these models to repopulate their erythroid cell compartment.

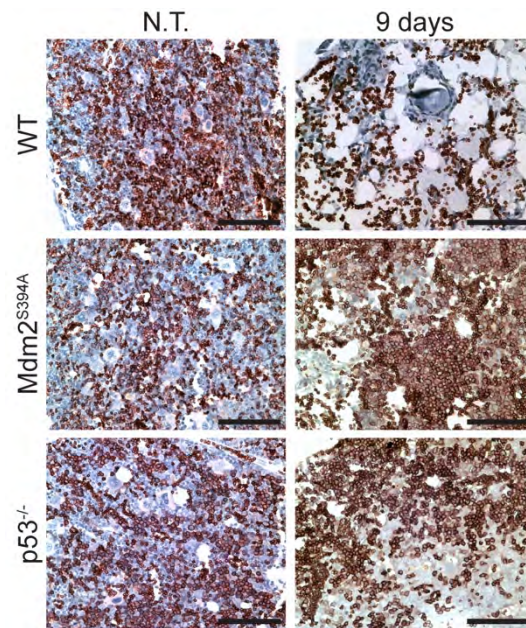


Figure 2.21: Immunohistochemical staining for TER-119 in bone marrow. Bone marrow sections from WT and $Mdm2^{S394A}$ mice left untreated, or 9 days after 8 Gy IR. Scale bars represent 100 μ m.

Radiation resistance in $Mdm2^{S394A}$ mice is governed by hematopoietic stem and progenitor cells

In order to characterize the cell type responsible for the increase in bone marrow repopulation and subsequent radioresistance observed in $Mdm2^{S394A}$ mice, we utilized flow cytometry to examine total bone marrow harvested 24 hours after treatment with IR. No differences were observed in the numbers of lineage-defined, mature hematopoietic cells in untreated WT or $Mdm2^{S394A}$ mice

(Figure 2.22). Furthermore, no differences were observed in the numbers of mature hematopoietic cells in irradiated WT or *Mdm2*^{S394A} bone marrow, save for slightly higher numbers of surviving B cells ($p=0.046$) in *Mdm2* mutant mice. These results are in keeping with the lack of a histopathological difference in the initial loss of cellularity in irradiated WT and *Mdm2*^{S394A} bone marrow.

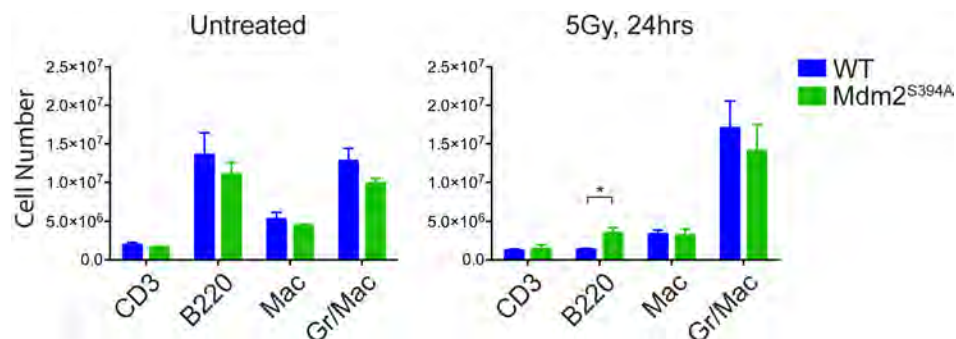


Figure 2.22: Quantification of lineage-defined hematopoietic cells in bone marrow. Bone marrow from WT and *Mdm2*^{S394A} mice was analyzed by flow cytometry in the absence of treatment (left) and 24 hours after exposure to 5 Gy IR (right) ($n = 3-4$, \pm SEM). * $P < 0.05$, ** $P < 0.01$ (Student's t -tests).

In addition, no difference was observed in the numbers of Lin⁻Sca1⁻cKit⁺ (L⁻S⁻K) common myeloid progenitors (CMPs) in untreated WT and *Mdm2*^{S394A} bone marrow, or in WT and *Mdm2*^{S394A} bone marrow following irradiation (Figure 2.23, left). This was confirmed by *in vitro* colony forming assays performed using the bone marrow of untreated and irradiated WT and *Mdm2*^{S394A} mice (Figure 2.24). While there was no difference in the numbers of Lin⁻Sca1⁺cKit⁺ (L⁻SK) hematopoietic stem and progenitor cells (HSPCs) in untreated WT and *Mdm2*^{S394A} bone marrow, there were significantly more HSPCs present in

$Mdm2^{S394A}$ bone marrow than in WT bone marrow following irradiation (Figure 2.23, right). This finding indicates that the radioresistance observed in $Mdm2^{S394A}$ mice is due to reduced loss and/or increased function of HSPCs in this model following IR exposure.

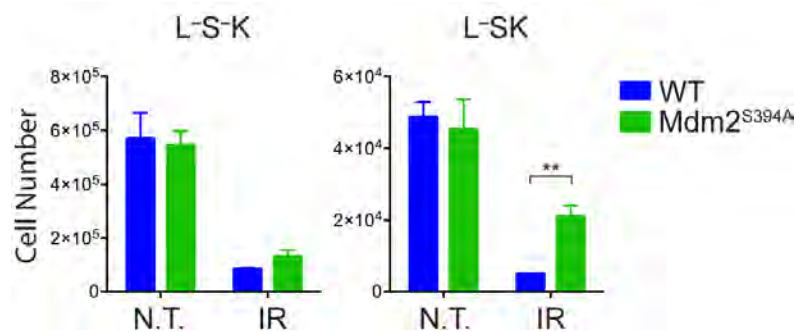


Figure 2.23: Quantification of L^{S-K} (CMP) and L^{SK} (HSPC) cells in bone marrow. Bone marrow from WT and $Mdm2^{S394A}$ mice was analyzed by flow cytometry in the absence of treatment (N.T.) and 24 hours after exposure to 5Gy IR (IR) ($n = 3-4$, \pm SEM). * $P < 0.05$, ** $P < 0.01$ (Student's t -tests).

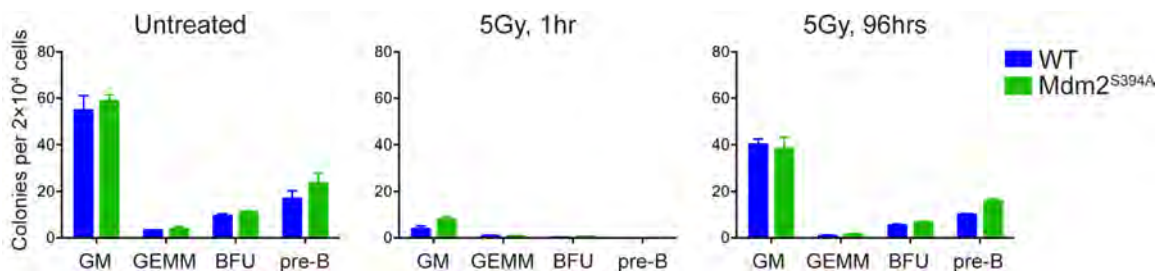


Figure 2.24: Colony-forming cell (CFC) assays. Total bone marrow was harvested from WT and $Mdm2^{S394A}$ mice left untreated, or 1 or 96 hours after exposure to 5 Gy IR. Colony-forming cell (CFC) assays (MethoCult 3434 and MethoCult 3630; StemCell Technologies) were carried out in accordance with manufacturer's instructions ($n = 3-6$, \pm SEM).

We further examined the HSPCs of *Mdm2*^{S394A} mice by performing *in vivo* competitive repopulation assays. *Mdm2*^{S394A} bone marrow expressing the CD45.2 leukocyte marker and WT bone marrow expressing the CD45.1 leukocyte marker were transplanted in a 1:1 ratio into lethally irradiated WT (CD45.1) recipient mice (Figure 2.25). Peripheral blood analysis at 4, 8 and 10 weeks following transplantation showed gradually increasing relative contributions to the hematopoietic lineage of *Mdm2*^{S394A} bone marrow (62%, 69% and 72%, respectively) (Figure 2.26). This indicated that *Mdm2*^{S394A} HSPCs have an inherent advantage relative to WT HSPCs in their ability to repopulate the hematopoietic compartment of lethally irradiated mice. In addition, we irradiated a cohort of the same bone marrow-chimeric mice at 8 weeks post-transplantation and assayed the relative contributions of WT and *Mdm2*^{S394A} bone marrow, 1 and 12 days later (Figure 2.27). Relative contributions of 21% WT and 78% *Mdm2*^{S394A} were observed in the untreated bone marrow of reconstituted mice. No significant changes were observed in the percentages of WT and *Mdm2*^{S394A} bone marrow at 1 day after IR (18% and 81%, respectively). However, a significant shift towards a greater proportion of *Mdm2*^{S394A} bone marrow was observed (8% WT, 91% *Mdm2*^{S394A}) in the reconstituted mice 12 days after IR.

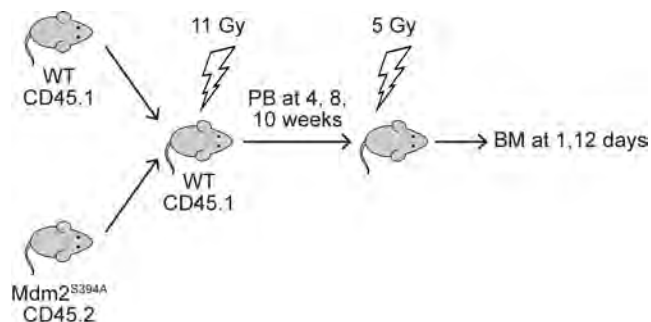


Figure 2.25: Experimental design of bone marrow repopulation assays.

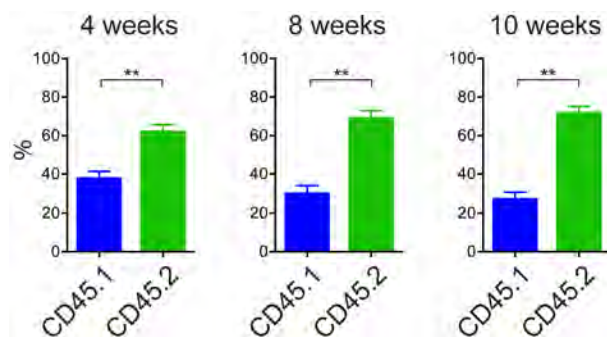


Figure 2.26: WT and *Mdm2*^{S394A} competitive bone marrow reconstitution. Leukocyte marker analysis of peripheral blood of recipient mice diagrammed in Figure 2.25 at 4 ($n = 15$), 8 ($n = 15$) and 10 ($n = 5$) weeks after bone marrow transplantation (\pm SEM). ** $P < 0.01$ (Student's t -tests).

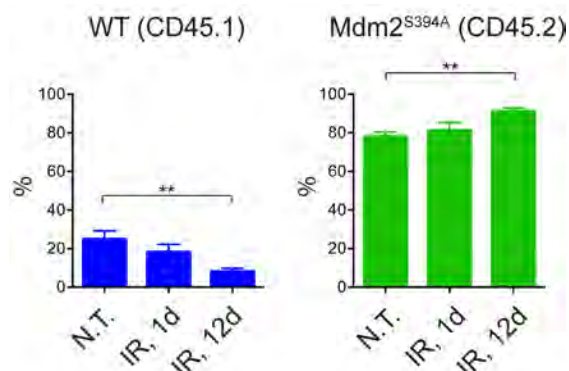


Figure 2.27: Post-IR relative contribution of WT and *Mdm2*^{S394A} chimeric bone marrow. Leukocyte marker analysis of total bone marrow of recipient mice diagrammed in Figure 2.25, untreated, 1 and 12 days after exposure to 5Gy IR ($n = 5$, \pm SEM). * $P < 0.05$, ** $P < 0.01$ (Student's t -tests).

These results confirm that *Mdm2*^{S394A} HSPCs have a greater capacity to repopulate irradiated bone marrow and determine that *Mdm2*^{S394A} HSPCs display greater stem cell function after genotoxic insult. Furthermore, increased *Mdm2*^{S394A} HSPC cell function is cell-autonomous, as *Mdm2*^{S394A} HSPCs outperform WT HSPCs in a WT microenvironment.

Materials and Methods

Mice and Animal Studies

All animals described in this study were on a C57Bl/6 background. Mice and cells were irradiated with a cesium-137 source (Gammacell 40). The generation of *Mdm2*^{S394A} mice has been previously described (Gannon et al, 2012). *Eμ-myc* mice were a gift from Christine Eischen (Vanderbilt University). Mice in *Eμ-myc* tumor assays were virgin and inherited the *Eμ-myc* allele paternally. For IR-induced tumor assays, mice 31±3 days of age were irradiated weekly with 1.75 Gy for 4 weeks (7 Gy cumulative dose). For bone marrow transplantation experiments, recipient CD45.1 mice received 11 Gy of whole body irradiation in a split dose (2 × 5.5 Gy, 4 hours apart). Irradiated recipients were reconstituted by i.v. injection of 2 × 10⁶ bone marrow cells (1:1 mixture of WT and *Mdm2*^{S394A}). All animals used in this study were maintained and assayed in accordance with federal guidelines and those established by the Institutional Animal Care and Use Committee at the University of Massachusetts Medical School.

Protein Analysis

Tissues and cells were lysed in NP-40 lysis buffer (50 mM Tris-HCl [pH 7.5], 150 mM NaCl, 0.5% NP-40) or in CelLytic MT Cell Lysis Reagent (Sigma), supplemented in both cases with protease and phosphatase inhibitor cocktail tablets (Roche). Protein extracts were analyzed by direct western blotting or immunoprecipitation/western blotting. Immunoprecipitations were performed on

500 µg whole thymus lysate with antibodies specific for Mdm2 (NBP1-02158; Novus (Ab-I) and Ab-5; Calbiochem (Ab-II)), p53 (CM5; Novocastra) and MdmX (MDMX-82; Sigma), using PureProteome Protein A/G Mix Magnetic Beads (Millipore). Mdm2 Ab-I immunoprecipitates were counterblotted with Mdm2 (Ab-5; Calbiochem (Ab-II)) and p53 (IMX25; Novocastra) antibodies. Mdm2 Ab-II immunoprecipitates were counterblotted with Mdm2 (NBP1-02158; Novus (Ab-I)) and p53 (CM5; Novocastra) antibodies. Western blotting was performed with antibodies specific for Mdm2 (NBP1-02158; Novus and Ab-5; Calbiochem), p53 (CM5; Novocastra), MdmX (MDMX-82; Sigma), p-ATM(S1981) (Cell Signaling), p-p53(S15) (#9284 or #12571; Cell Signaling), Vinculin (hVin-1; Sigma), α-tubulin (B-5-1-2; Sigma), p21 (SXM30; BD Pharmingen), Puma (#7467; Cell Signaling), Arf (5-C3-1; Santa Cruz) and Cleaved Caspase-3(Asp175) (#9661; Cell Signaling). For cycloheximide experiments, single cell suspensions of thymocytes from 6-8 thymi were generated maintained in DMEM supplemented with 10% FBS. Thymocyte pools were untreated or irradiated with 2.5 Gy IR and immediately treated with cycloheximide (100 µg/ml; Sigma). Pools were aliquoted and maintained in a 37°C incubator with 5% CO₂ and collected for protein analysis at the indicated time points. Blots were imaged on a Chemidoc MP (Bio-Rad) and relative band intensities determined by densitometry using Image Lab software (v4.1, Bio-Rad).

Gene Expression Analysis and Sequencing

Total RNA was isolated from tissues by RNeasy mini kit (QIAGEN) and cDNA synthesized by Superscript III First Strand Synthesis System (oligo-dT priming) (Invitrogen). Quantitative PCR was performed using SYBR Select Master Mix (Applied Biosystems) in conjunction with a 7300 Real-Time PCR System (Applied Biosystems). Thymus cDNA input was 10 ng and bone marrow cDNA input was 100 ng. Fold expression was calculated using the $\Delta\Delta C_t$ method relative to untreated WT samples using *Rplp0* as internal reference. Primers used were as follows: *Puma*, 5'ACGACCTCAACGCGCAGTACG3' and 5'GAGGAGTCCCATGAAGAGATTG3'; *Noxa*, 5'CTCAGGAAGATCGGAGACAAAG3' and 5'GCACACTCGTCCTTCAAGT3'; *Bax*, 5'GTGGTTGCCCTCTTCTACTTT3' and 5'CAGCCCATGATGGTTCTGAT3'; *p21*, 5'CTGAGCGGCCTGAAGATT3' and 5'ATCTGCGCTTGGAGTGATAG3'; *Mdm2*, 5'AGTCTCTGGACTCGGAAGATTA3' and 5'CTGTATCGCTTTCTCCTGTCTG3'; *Rplp0*, 5'CTGAGTACACCTTCCCCTTAC3' and 5'CTCTTCCTTTGCTTCAGCTTTG3'. *Arf* message was amplified from tumor sample cDNA using the following primer pair: 5'TCGCTTGTCACAGTGAGG3' and 5'CCGGATTTAGCTCTGCTCTT3'. *p53* message was amplified from tumor sample cDNA in overlapping fragments using three separate primer pairs: *p53seq1*, 5'TTCATTGGGACCATCCTGGCTGTA3' and 5'AGGCACAAACACGAACCTCAAAGC3'; *p53seq2*,

5'CTTATCCGGGTGGAAGGAAAT3' and 5'GAAGTAGACTGGCCCTTCTTG3';
p53seq3, 5'AGCTTTGAGGTTTCGTGTTTGTGCC3' and
5'ATGCAGACAGGCTTTGCAGAATGG3'. Amplified fragments were gel
extracted (QIAGEN) and sequenced by Sequegen, Inc (Worcester, MA).

Histopathology

Tissues samples were fixed in 10% formalin for 24 hr. The UMMS Morphology Core Laboratory performed embedding, sectioning, and staining. TUNEL staining was performed using the In Situ Cell Death Detection Kit, POD (Roche) according to manufacturer's instructions. Immunohistochemistry was performed with antibodies specific for B220 (550286; BD Pharmingen), CD3 (A0452; Dako) and TER-119 (553671; BD Pharmingen). Stained tissue was analyzed using an Olympus CX41 microscope fitted with a PixeLINK camera and software.

Flow Cytometry

Total bone marrow from both hind limbs was harvested, RBCs were lysed, and single-cell suspensions were stained with cell-surface antibodies for Gr-1, CD11B, CD3, and B220. For LSK analysis, bone marrow cells were stained with a biotin lineage mixture, and antibodies for Sca-1, c-Kit, CD34, and Flk2. To distinguish between WT and *Mdm2*^{S394A} hematopoietic cells in the reconstitution studies, peripheral blood and bone marrow was stained with antibodies specific for CD45.1 and CD45.2. All samples were run on a BD LSRII flow cytometer (BD

Bioscience) and analyzed using FlowJo software (Tree Star). A complete list of antibodies including clone numbers is given in Table 2.1.

Table 2.1. Antibodies Used for Flow Cytometry in Chapter II.

Antibody	Clone	Fluorophore	Source
CD3	145-2C11	Biotin, APC	BD Bioscience
B220	RA3-6B2	Biotin, PE	BD Bioscience
Ter119	TER-119	Biotin	Biolegend
Gr-1	RB6-8C5	Biotin, APC, PE	Biolegend
Mac-1	M1/70	Biotin, FITC	Biolegend
Sca-1	D7	APC/Cy7	Biolegend
CD117	2B8	APC	BD Bioscience
CD34	RAM34	FITC	BD Bioscience
Fk2	A2F10	PE	Biolegend
CD45.2	104	FITC, PE/Cy7	Biolegend
CD45.1	A20	PercP/Cy5.5	Biolegend

Statistical Analysis

Statistical analyses were performed using GraphPad Prism software, version 6.0d. Kaplan–Meier survival curves were analyzed by log-rank test. A *P*-value < 0.05 was considered statistically significant for Student’s t-tests.

CHAPTER III

Phosphorylation of Mdm2 by c-Abl regulates p53 tumor suppression and the radiosensitivity of mice.

The p53 tumor suppressor acts as a guardian of the genome by preventing the propagation of DNA damage-induced breaks and mutations to subsequent generations of cells. We have previously shown that ATM phosphorylation of Mdm2 Ser394 is required for robust p53 stabilization and activation in cells treated with ionizing radiation, and that inhibition of Mdm2 Ser394 phosphorylation event leads to spontaneous tumorigenesis and radioresistance in *Mdm2*^{S394A} mice. Previous *in vitro* data indicate that the c-Abl kinase phosphorylates Mdm2 at the neighboring residue (Mdm2 Tyr393) in response to DNA damage to regulate p53-dependent apoptosis. In this study, we have generated a novel Mdm2 mutant mouse (*Mdm2*^{Y393F}) to determine if c-Abl phosphorylation of Mdm2 regulates the p53-mediated DNA damage response or p53 tumor suppression *in vivo*. *Mdm2*^{Y393F} mice develop accelerated spontaneous and oncogene-induced tumors, yet display no defects in p53 stabilization and activity following acute genotoxic stress. Although apoptosis is unaltered in these mice, they recover more rapidly from radiation-induced bone marrow ablation, and are more resistant to whole body radiation-induced lethality. These data reveal an *in vivo* role for c-Abl phosphorylation of Mdm2 in regulation of p53 tumor suppression and bone marrow failure.

However, c-Abl phosphorylation of Mdm2-Y393 appears to play a lesser role in governing Mdm2-p53 signaling than ATM phosphorylation of Mdm2 Ser394. Furthermore, the effects of these phosphorylation events on p53 regulation are not additive, as *Mdm2*^{Y393F/S394A} mice and *Mdm2*^{S394A} mice display similar phenotypes.

Results

***Mdm2*^{Y393F} mice are viable and display increased spontaneous and oncogene-induced tumorigenesis.**

In order to investigate the role of Mdm2 Tyr393 phosphorylation under physiological conditions, we generated a mouse model in which this tyrosine residue is substituted with a phenylalanine residue (Y393F). Site-directed mutagenesis was performed to introduce an A to T missense mutation within the 393 codon, and a synonymous G to C mutation within the 397 codon of *Mdm2* exon 12 (Figure 3.1).

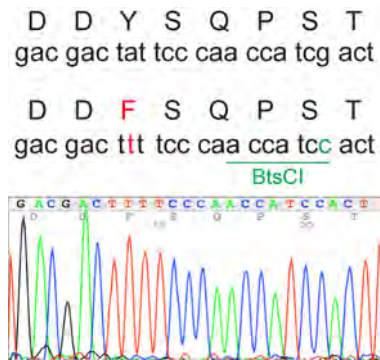


Figure 3.1. Sequence of wild-type and mutant *Mdm2* alleles surrounding codon 393. DNA sequence of WT and *Mdm2*^{Y393F} allele surrounding codon 393 (top). An A to T mutation changed codon 393 from Tyr to Phe. A silent G to C mutation in codon 397 introduced a BtsCI restriction site. Sequencing results of the corresponding region from *Mdm2*^{Y393F} spleen cDNA are shown (bottom).

A gene-replacement vector was constructed to replace the endogenous *Mdm2* exon 12 sequence with the mutated exon 12 (Figure 3.2). Gene targeting was performed in PC3 (129SV) embryonic stem (ES) cells (O’Gorman et al., 1997), and homologous recombination was confirmed in G418-resistant clones by Southern blotting (Figures 3.2 and 3.3). Blastocyst injection of targeted ES clones produced several high-degree male chimeras that passed the *Mdm2* Y393F allele through their germ line. Southern blotting further confirmed proper targeting in F1 and F2 generation mice, along with protamine-Cre directed deletion of the floxed neomycin cassette (Figure 3.4).

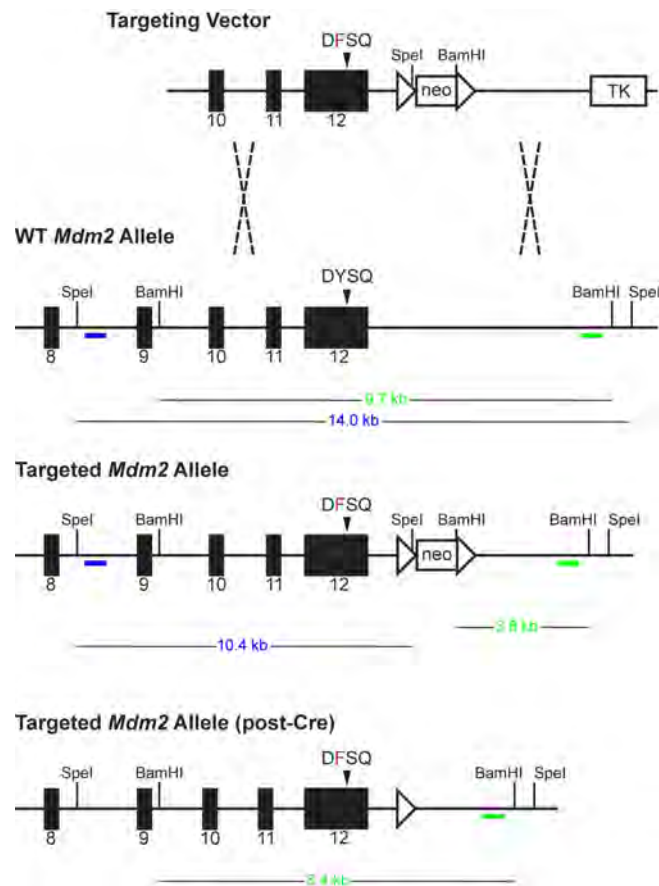


Figure 3.2. Diagram of the targeting strategy used to generate the *Mdm2*^{Y393F} allele. The targeting vector contained a floxed neomycin cassette (neo) and a 3' thymidine kinase cassette (TK) for positive and negative drug selection, respectively. The targeting vector was linearized and electroporated into PC3 ES cells. ES cell targeting was confirmed by BamHI digest and Southern blot analysis with a 3' external probe (green), as well as SpeI digest and Southern blot analysis with a 5' external probe (blue). Protamine-cre recombinase-directed excision of neo cassette was confirmed by BamHI digest of F1 and F2 generation tail DNA and Southern blot analysis with the same 3' external probe as in ES cells (green).

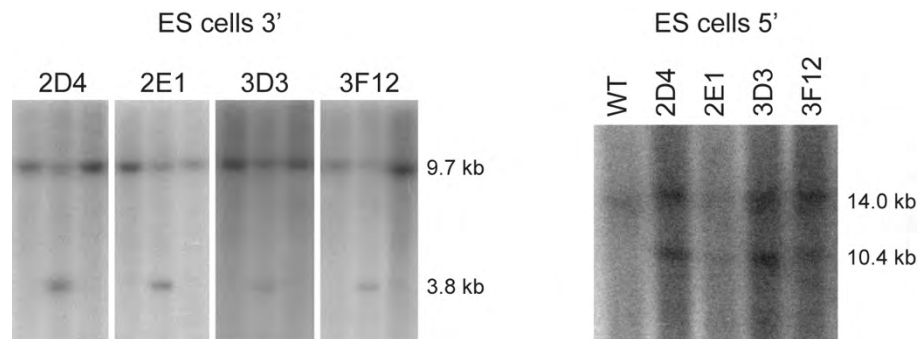


Figure 3.3. Southern blot analysis of targeted ES cells. BamHI digest and Southern blot analysis of ES cell genomic DNA (left). A 3' external probe (green bar from Figure 3.2) detects a 9.7 kb WT allele and 3.8 kb targeted allele. Four clones with correct 3' targeting are shown, each flanked by untargeted (WT) clones. SpeI digest and Southern blot analysis of ES cell genomic DNA (right). A 5' external probe (blue bar from Figure 3.2) detects a 14.0 kb WT allele and 10.4 kb targeted allele.

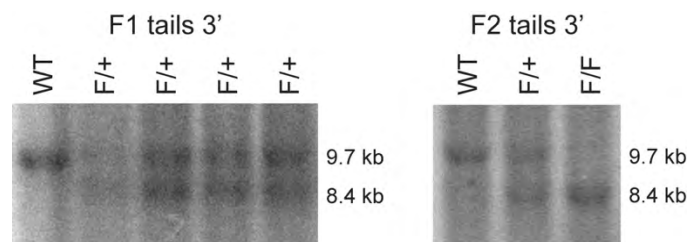


Figure 3.4. Southern blot analysis of mouse DNA. BamHI digest and Southern blot analysis of tail DNA from F1 generation mice (left) and F2 generation mice (right). A 3' external probe (green bar from Figure 3.2) detects a 9.7 kb WT allele and 8.4 kb targeted allele.

The presence of the additional synonymous G to C mutation within the 397 codon of the targeted allele introduced a novel BtsCI restriction digest site that allowed for identification of the *Mdm2*^{Y393F} allele by PCR-digest strategy (Figures 3.1 and 3.5). *Mdm2* transcripts from spleens of *Mdm2*^{Y393F} mice were sequenced, and confirmed as containing only the targeted mutations (Figure

3.1). Heterozygous intercrosses yielded homozygous *Mdm2*^{Y393F} mice at Mendelian ratios, indicating that *Mdm2*^{Y393F} is not compromised in its function during development (Table 3.1). Additionally, no differences were observed in average litter size, body weights at 6 weeks of age, or male-to-female sex distribution.

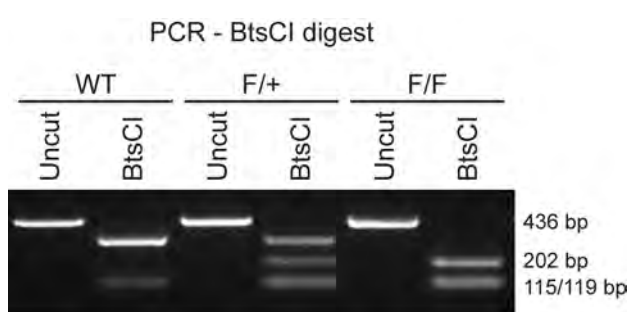


Figure 3.5. Genotyping *Mdm2*^{Y393F} mice. PCR-BtsCI digest analysis of F2 generation mice. Primers flanking *Mdm2* codon 393 amplify a 436 bp fragment of DNA. The WT *Mdm2* fragment contains a single BtsCI restriction site which generates 119 and 317 bp fragments. A silent mutation in the *Mdm2*^{Y393F} allele introduces an additional BtsCI restriction site which results in 115, 119 and 202 bp fragments.

Mendelian ratio

	Expected	Observed
+/+	25% (62.5/250)	28% (70/250)
F/+	50% (125/250)	50% (125/250)
F/F	25% (62.5/250)	22% (55/250)

Table 3.1. Viability of *Mdm2*^{Y393F} mice. The expected and observed Mendelian ratios from *Mdm2*^{Y393F} heterozygote breeding.

We have previously shown that mice deficient for phosphorylation of the neighboring residue (*Mdm2* Ser394) by the DNA damage activated kinase ATM are prone to spontaneous tumorigenesis (Gannon et al., 2012). Therefore, we sought to examine whether c-Abl phosphorylation of *Mdm2* Tyr393 impacted

tumor suppression. Cohorts of WT and *Mdm2*^{Y393F} mice were established and monitored for tumor formation. During the 24-month tumor assay, 8 of 21 (38%) *Mdm2*^{Y393F} mice developed spontaneous tumors (Figure 3.6), whereas only 1 of 28 (4%) WT mice presented with a tumor at 20 months of age. *Mdm2*^{Y393F} tumors arose between 14.5-24 months of age, a similar latency as seen in *Mdm2*^{S394A} mice (Gannon et al., 2012). The majority of tumors arose in lymphatic tissues, and 5 of the 6 tumors (83%) were identified as B cell lymphomas, with one of the B cell lymphomas also containing atypical T cells. Other tumor types seen in the cohort included a myeloid sarcoma, a hepatocellular carcinoma, and a papillary tumor of lacrimal origin (Figures 3.7 and 3.8, Table 3.2).

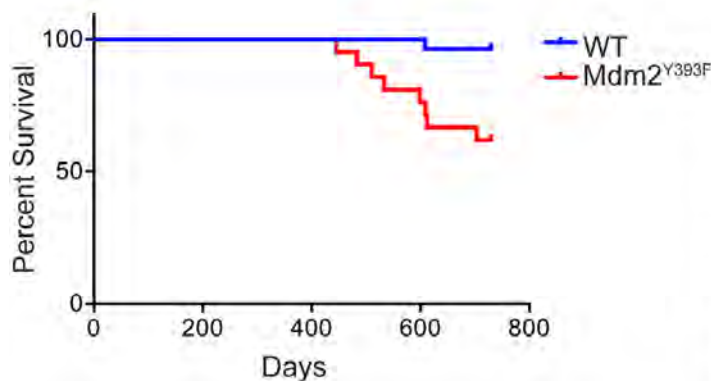


Figure 3.6. Spontaneous tumorigenesis in *Mdm2*^{Y393F} mice. Kaplan-Meier tumor-free survival curves of WT ($n = 28$) and *Mdm2*^{Y393F} ($n = 21$) mice. Curves were compared by Log-rank test: ($P < 0.01$).

Latency (days)	Location	Tumor
445	spleen/liver	myeloid
483	liver	HCC
510	spleen	B cell
533	mesenteric LN	B cell
599	mesenteric LN	B cell
609	lacrimal gland	papillary
612	mediastinal LN	B/T cell
703	mesenteric LN	B cell

Table 3.2. *Mdm2*^{Y393F} tumors. Table displaying the latency, location, and tumor type for spontaneous tumors arising in *Mdm2*^{Y393F} mice. LN, lymph node; HCC, hepatocellular carcinoma.

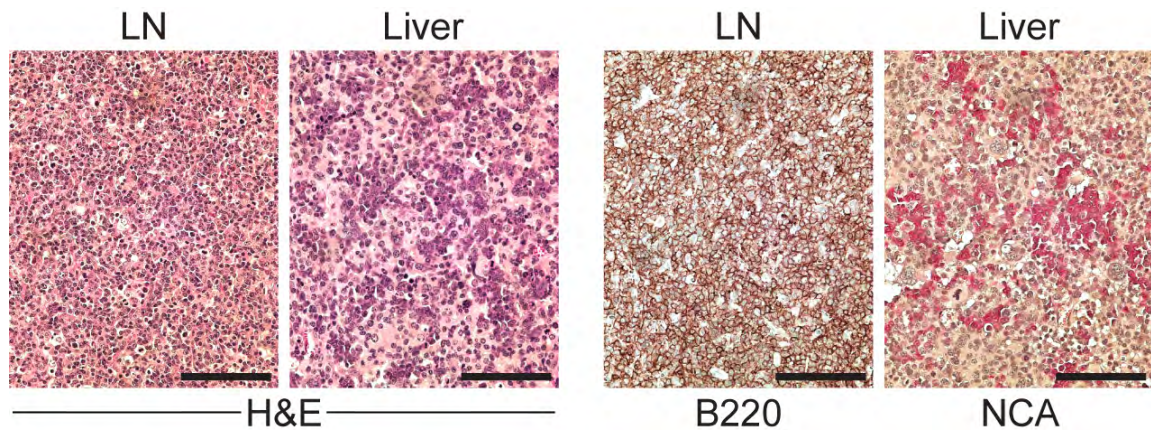


Figure 3.7. *Mdm2*^{Y393F} tumor histology. Representative H&E stained tissue sections of a lymph node exhibiting a B cell lymphoma (left) and myeloid sarcoma present in the liver sinusoids (right). Scale bars represent 100 μm. LN, lymph node.

Figure 3.8. *Mdm2*^{Y393F} tumor staining. The B cell lymphomas shows expression of B220 (left), and the myeloid neoplasms exhibit naphthol chloroacetate esterase (NCA) staining (right). Scale bars represent 100 μm.

As *Mdm2*^{Y393F} mice were prone to developing spontaneous tumors of lymphoid origin, we further examined the effects of Mdm2 Tyr393 phosphorylation on tumor suppression using the *Eμ-myc* mouse model (Adams et al., 1985). Cohorts of *Eμ-myc* and *Eμ-myc;Mdm2*^{Y393F} mice were generated (C57BL/6 background) and assayed for tumor formation. *Eμ-myc* mice develop pre-B/B cell lymphomas within 3-6 months of age, and we observed a median time to tumorigenesis of 125.5 days in the *Eμ-myc* model cohort (Figure 3.9), a duration in close agreement with previous studies (Adams et al., 1985; Eischen et al., 1999). However, *Eμ-myc;Mdm2*^{Y393F} mice displayed significantly accelerated tumorigenesis, with a median time to tumor formation of only 76.5 days. Thus, while dispensable for development, c-Abl phosphorylation of Mdm2

Tyr393 significantly impacts tumor suppression by preventing both spontaneous and oncogene-induced tumorigenesis.

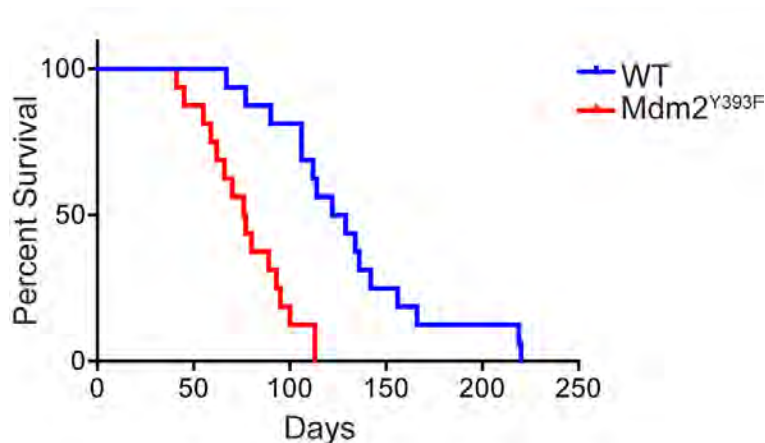


Figure 3.9. $E\mu$ -myc-driven lymphomagenesis in $Mdm2^{Y393F}$ mice. Kaplan-Meier tumor-free survival curves of $E\mu$ -myc ($n = 16$) and $E\mu$ -myc; $Mdm2^{Y393F}$ ($n = 16$) mice. Median survival times were as follows: $E\mu$ -myc (125.5 days), $E\mu$ -myc; $Mdm2^{Y393F}$ (76.5 days). Curves were compared by Log-rank test: ($P < 0.0001$).

c-Abl phosphorylation of Mdm2 Tyr393 does not influence DNA damage-induced p53 stabilization and activation in spleen and thymus.

Having observed increased lymphomagenesis in $Mdm2^{Y393F}$ mice, and as c-Abl is activated by a variety of DNA damaging agents (Kharbanda et al., 1995; Liu et al., 1996; Wang et al., 2011a), we next examined whether c-Abl phosphorylation of Mdm2 Tyr393 impacts DNA damage-induced p53 stabilization and activation in lymphatic tissues of $Mdm2^{Y393F}$ mice. WT and $Mdm2^{Y393F}$ mice were exposed to 5 Gy IR and spleens were analyzed for p53 and Mdm2 levels by immunoblotting (Figure 3.10). We observed similar induction of p53 following irradiation in both genotypes, with no significant differences detected in basal or

IR-induced p53 protein levels. Similarly, no obvious differences were observed in p53 activation as indicated by levels of p53 phosphorylation (S18). No differences were observed in the levels of Mdm2 protein, which increased at 2-4 hours following IR, before decreasing as p53 activity diminished, similar to what has previously been reported in this tissue (Gannon et al., 2012; Pant et al., 2013). Similar results were observed in thymi from these same animals, with no differences detected in the levels of total p53, phosphorylated p53 (S18), or Mdm2, save for slightly higher basal Mdm2 levels in *Mdm2*^{Y393F} mice (Figure 3.10). Consistent with equal levels of basal and IR-induced p53 protein stabilization and phosphorylation, real-time quantitative PCR on cDNA from untreated and irradiated spleens of WT and *Mdm2*^{Y393F} mice detected no differences in the basal or DNA damage-induced expression levels of the p53 target genes *Puma*, *Noxa*, *Cdkn1a* (*p21*) and *Mdm2* (Figure 3.11). Similar results were observed in thymi (Figure 3.11).

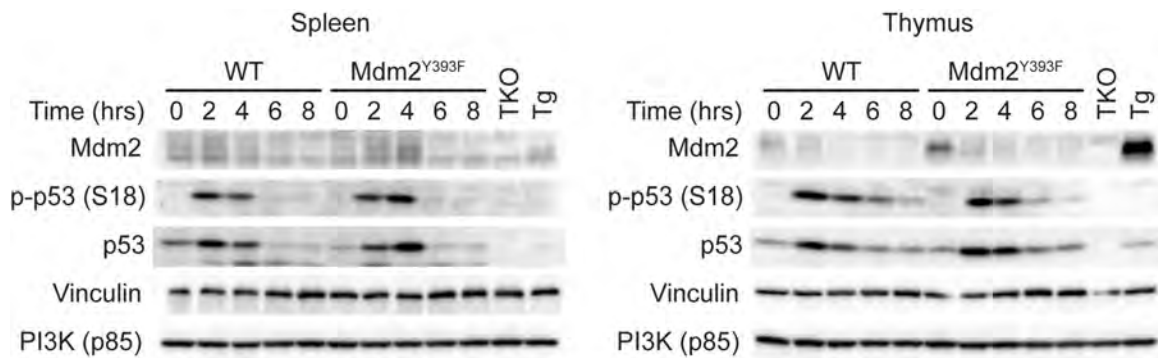


Figure 3.10. Western blots of irradiated spleens and thymi. WT and *Mdm2*^{Y393F} mice were left untreated or exposed to 5 Gy IR and spleens (left) and thymi (right) were harvested at 2 hour intervals. Protein levels were analyzed by western blotting. TKO indicates *Mdm2*^{-/-}, *MdmX*^{-/-}, *p53*^{-/-} control; Tg indicates *Mdm2*^{Tg/+} Mdm2 overexpressing control.

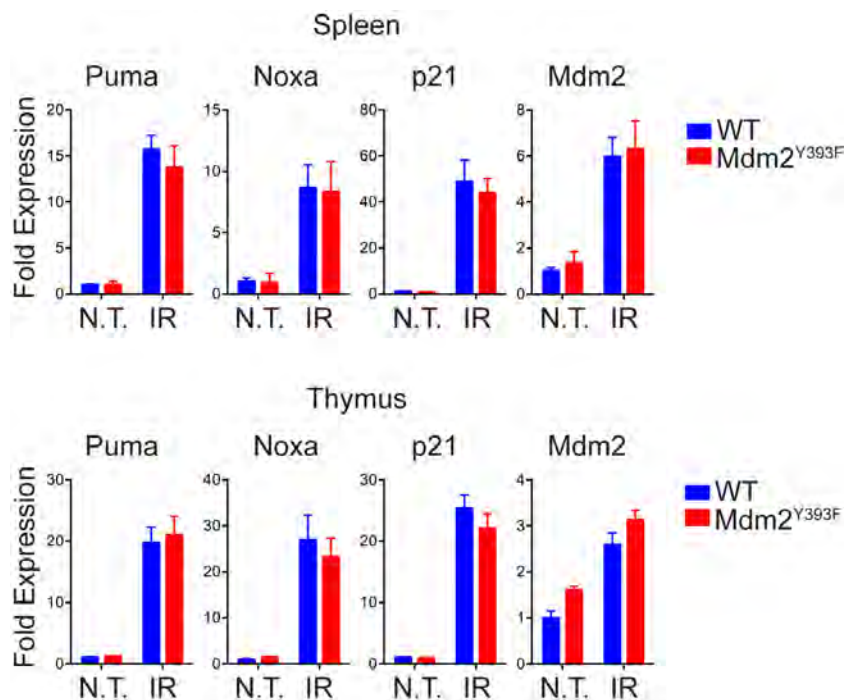


Figure 3.11. Gene expression in irradiated spleens and thymi. Mice were left untreated or exposed to 5 Gy IR and spleens (top) and thymi (bottom) were harvested at 4 hours. Fold expression of p53-target genes was determined by real-time quantitative PCR, relative to untreated WT samples using *Rplp0* as internal reference ($n = 3-4$, \pm SEM). Significance was determined by Student's *t*-test of $\Delta\Delta$ Ct values.

Hematopoietic organs are highly radiosensitive, and p53 activation in these tissues prompts widespread apoptosis following IR (Gudkov and Komarova, 2003). In keeping with the absence of observable differences in p53 stabilization and activation in *Mdm2*^{Y393F} spleens and thymi, we detected no differences in splenic or thymic apoptosis in untreated and irradiated *Mdm2*^{Y393F} mice by terminal deoxynucleotidyl transferase dUTP nick end labelling (TUNEL) (Figure 3.12). This observation was confirmed quantitatively by flow cytometry of Annexin V-FITC stained splenocytes and thymocytes (Figure 3.13). Thus, the IR-induced stabilization and activation of p53 and the resultant apoptotic response is unaltered in *Mdm2*^{Y393F} spleens and thymi.

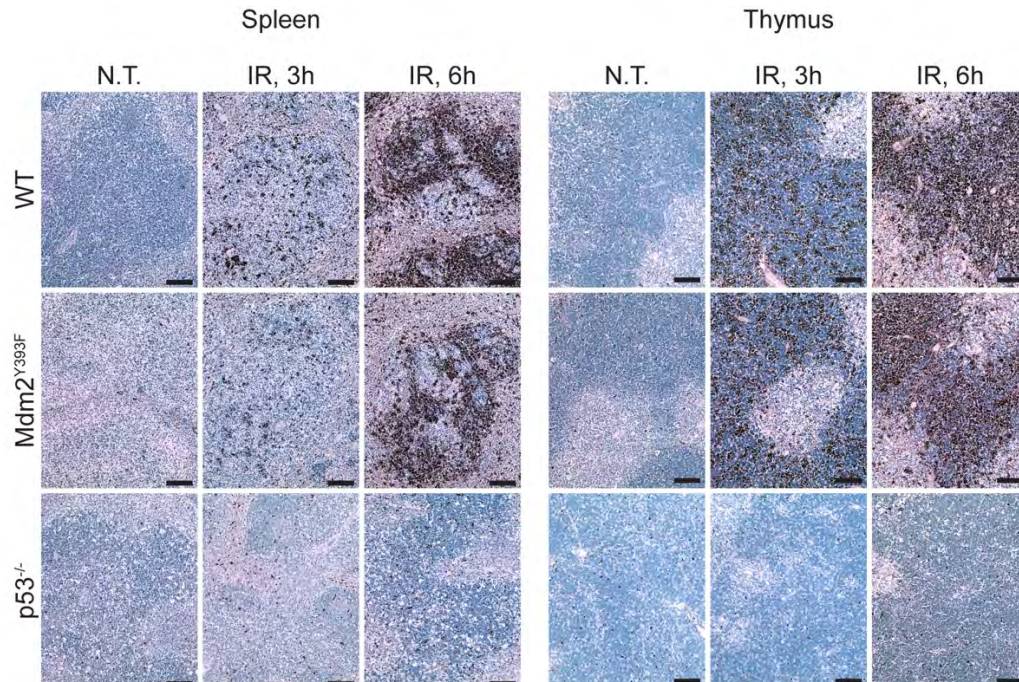


Figure 3.12. Apoptosis in irradiated spleens and thymi. TUNEL staining of spleens of mice treated as in Figure 3.10 and harvested at 3 and 6 hours.

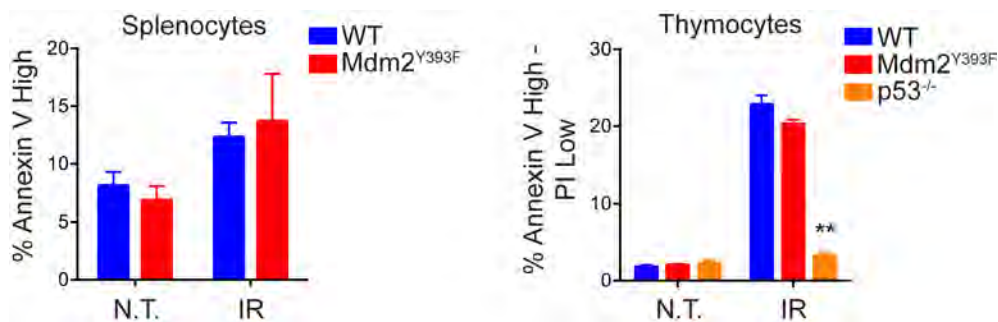


Figure 3.13. Quantification of apoptosis in irradiated spleens and thymi. WT, *Mdm2*^{Y393F} and *p53*^{-/-} mice were left untreated or irradiated with 5 Gy IR. Spleens or thymi were harvested 5 hours later and single cell suspensions of splenocytes (left) or thymocytes (right) were generated and stained with Annexin V-FITC and propidium iodide (PI) for FACS analysis. The percentage of Annexin V^{Hgh} - PI^{Low} cells were quantified ($n = 3$, \pm SEM). Significance was determined relative to similarly treated WT samples, ** $P < 0.01$ (Student's *t*-tests).

We also examined whether Mdm2 Tyr393 phosphorylation affected p53-dependent growth arrest. Mouse embryonic fibroblasts (MEFs) from WT, *Mdm2*^{Y393F} and *p53*^{-/-} mice were untreated or exposed to either 5 Gy IR or 150 nM doxorubicin for 18 hours. Flow cytometric cell cycle analysis of these cells revealed no differences in growth arrest in *Mdm2*^{Y393F} MEFs following either irradiation or treatment with doxorubicin (Figure 3.14). Furthermore, no differences were observed in the cell cycle populations of untreated WT and *Mdm2*^{Y393F} MEFs (data not shown). This indicated that WT and *Mdm2*^{Y393F} MEFs exhibit similar growth rates, and was confirmed by standard proliferation assays (Figure 3.15).

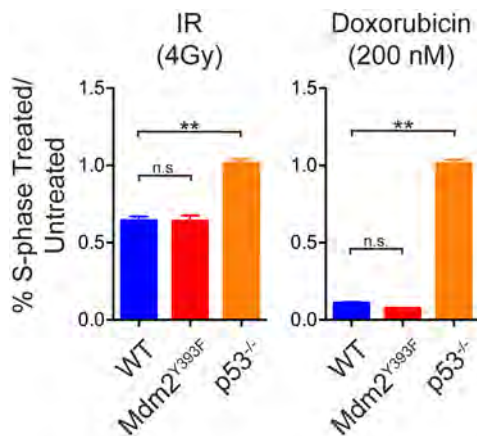


Figure 3.14. Cell-cycle arrest in MEFs. MEFs untreated or exposed to 4 Gy IR (left) or 200 nM doxorubicin (right) for 18 hours, were pulse labeled with 50 μ M BrdU for 3 hrs, harvested and fixed for FACS analysis. Fixed cells were stained with a FITC conjugated anti-BrdU antibody and PI, and analyzed by flow cytometry. Data are presented as the percentage of cells in S phase in the treated samples relative to untreated samples ($n = 3$, \pm SEM). ** $P < 0.01$ (Student's t -tests).

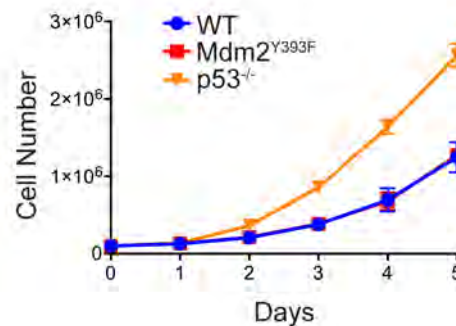


Figure 3.15. Primary MEF proliferation. 10^6 cells were seeded in 6-well plates and cell number per well was counted each day ($n = 3$, \pm SD).

***Mdm2*^{Y393F} mice are radioresistant and display enhanced bone marrow repopulating abilities following IR exposure.**

The proposed effects of c-Abl phosphorylation of Mdm2 on p53 are similar to those of ATM phosphorylation of Mdm2, namely p53 stabilization and activation. Conversely, our findings that DNA damage-induced p53 stabilization and activation in spleen and thymus, and p53-dependent apoptosis and growth arrest in *Mdm2*^{Y393F} tissues and cells, are unaltered, contrasts with what we have reported with *Mdm2*^{S394A} mice. Thus, c-Abl phosphorylation of Mdm2 Tyr393

may have limited effects on the p53-dependent DDR *in vivo*, or may be adequately compensated for by ATM phosphorylation of Mdm2 Ser394. However, when we challenged cohorts of WT and *Mdm2*^{Y393F} mice to a series of IR doses spanning the threshold-lethal range, we observed a significant resistance to whole-body IR-induced lethality in *Mdm2*^{Y393F} mice (Figure 3.16). Following treatment with 8 Gy IR, 74% of *Mdm2*^{Y393F} mice were surviving at 4 weeks as compared to 22% of WT mice. Similarly, following exposure to 9 Gy IR, 29% of *Mdm2*^{Y393F} mice were surviving at 4 weeks as compared to 7% of WT mice. All mice survived 7 Gy IR for both genotypes, whereas no mice of either genotype survived past 2 weeks following 10 Gy IR. The majority of mice succumbed between one and three weeks post-IR.

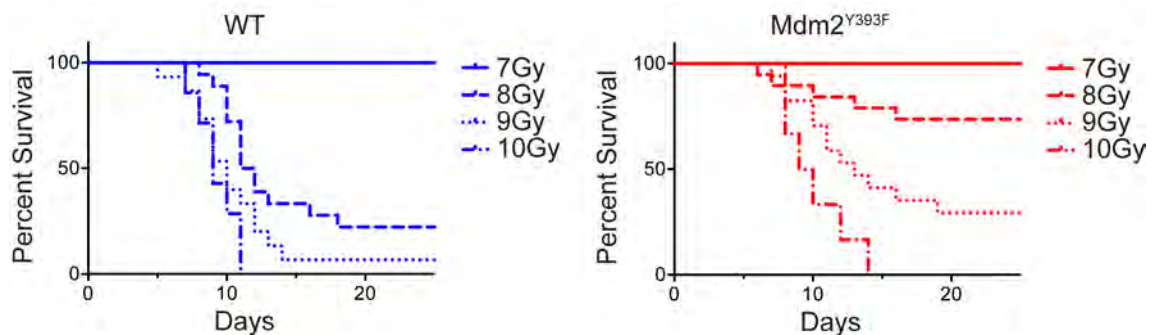


Figure 3.16. Radioresistance in *Mdm2*^{Y393F} mice. Kaplan-Meier survival curves of WT ($n = 7-18$) and *Mdm2*^{Y393F} ($n = 6-19$) mice exposed to 7, 8, 9 and 10 Gy whole-body IR. WT and *Mdm2*^{Y393F} curves were compared by Log-rank test: 7 Gy (n.s.), 8 Gy ($P = 0.003$), 9 Gy ($P = 0.030$), 10 Gy (n.s.).

Lethality in mice treated with this range of IR doses is attributed to p53-dependent bone marrow failure, referred to as ‘hematopoietic syndrome’ (Komarova et al., 2004). As we have described a similar resistance to whole-

body IR in *Mdm2*^{S394A} mice (Gannon et al., 2012), we next compared the effects of IR on bone marrow from WT, *Mdm2*^{Y393F}, *Mdm2*^{S394A} and *p53*[/] mice. Expression of p53 target genes *Puma* and *p21* are unaltered in *Mdm2*^{Y393F} bone marrow, in agreement with what was observed in irradiated spleen and thymus (Figure 3.17). Conversely, expression levels of those same genes are significantly reduced in *Mdm2*^{S394A} bone marrow, in keeping with the previously described reduction in IR-induced p53 responses in these animals (Gannon et al, 2012).

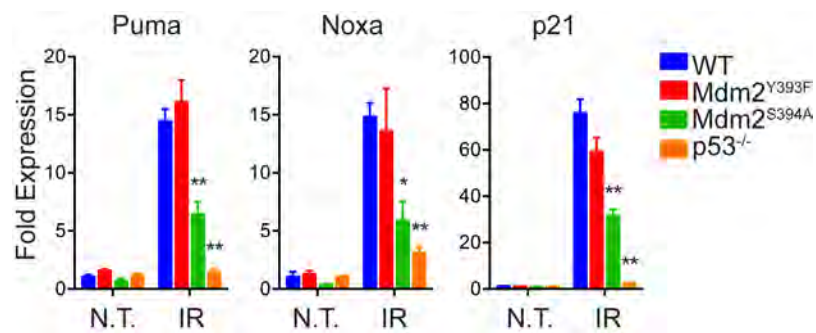


Figure 3.17. Gene expression in bone marrow. Fold expression of p53-target genes *Puma*, *Noxa* and *p21* in bone marrow of WT, *Mdm2*^{Y393F}, *Mdm2*^{S394A} and *p53*[/] mice, untreated and 6 hours after 5 Gy IR, was determined by real-time quantitative PCR. Fold expression was calculated relative to untreated WT samples using *Rplp0* as internal reference ($n = 3-4$ mice, \pm SEM). * $P < 0.05$, ** $P < 0.01$ (Student's t -tests of $\Delta\Delta$ Ct values).

However, similar initial reductions in bone marrow cellularity were observed in both mutants, as well as in WT mice and in *p53*[/] mice following treatment with 5 Gy IR (Figure 3.18). Thus, the initial reduction in gross cellularity appears, to some extent, independent of p53. Flow cytometry analysis of untreated bone marrow from WT, *Mdm2*^{Y393F}, *Mdm2*^{S394A} and *p53*[/] mice revealed no differences

in the populations of lineage-defined, mature hematopoietic cells, save for statistically fewer CD11b-positive cells in $p53^{-/-}$ mice (Figure 3.19, top). In agreement with the observed reduction in bone marrow cellularity in all genotypes, IR treatment induced a cumulative decline in populations of mature cells in bone marrow from each genotype (Figure 3.19, bottom). Only $p53^{-/-}$ mice displayed significantly more B220⁺ cells.

Relative Cellularity

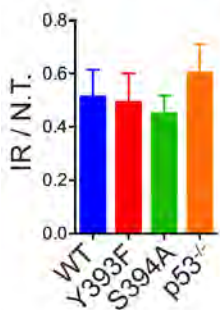


Figure 3.18. Relative bone marrow cellularity.

Quantification of numbers of nucleated cells in bone marrow from both hind limbs of WT, $Mdm2^{Y393F}$, $Mdm2^{S394A}$ and $p53^{-/-}$ mice either untreated or 8 hours after exposure to 5 Gy IR. ($n = 3-6$, \pm SEM).

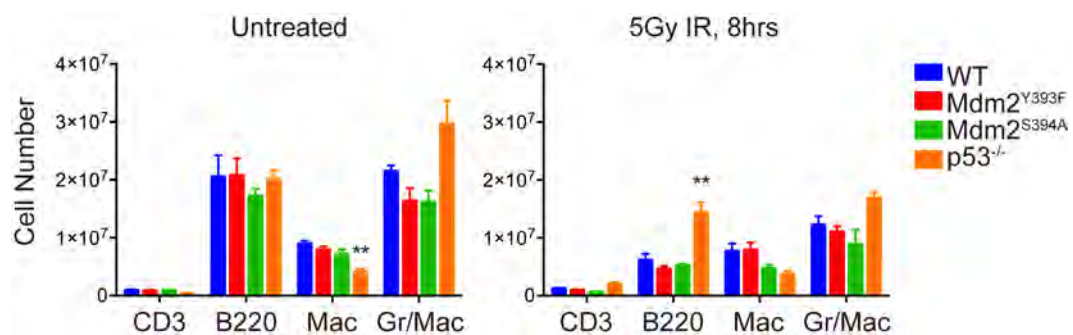


Figure 3.19. Quantification of lineage-defined hematopoietic cells in bone marrow.

Quantification of Lineage-defined hematopoietic cells in bone marrow of WT, $Mdm2^{Y393F}$, $Mdm2^{S394A}$ and $p53^{-/-}$ mice untreated (left) and 8 hours after 5 Gy IR (right) ($n = 3-4$, \pm SEM). ** $P < 0.01$ (Student's t -tests).

Again, no differences were observed in the absence of treatment, in the more primitive Lin⁻Sca1⁻cKit⁺ (L⁻S⁻K) progenitor populations of WT, *Mdm2*^{Y393F}, *Mdm2*^{S394A} or *p53*[/] mice (Figure 3.20). However, while L⁻S⁻K cell numbers decreased 70-80% in WT, *Mdm2*^{Y393F} and *Mdm2*^{S394A} bone marrows, bone marrow from *p53*[/] mice retained significantly more L⁻S⁻K cells following IR. This suggests that increased survival of hematopoietic progenitors underlies the resistance to IR-induced bone marrow failure in mice with compromised p53. Indeed, when Lin⁻Sca1⁺cKit⁺ (L⁻SK) hematopoietic stem and progenitor cells (HSPCs) were quantified in these same animals, we observed no decrease following irradiation in *p53*[/] mice (Figure 3.21). While greater numbers of HSPCs were observed in untreated *p53*[/] mice, no differences were observed in HSPC number in untreated WT, *Mdm2*^{Y393F} and *Mdm2*^{S394A} mice. However, there were significantly more HSPCs in *Mdm2*^{S394A} bone marrow following IR, and HSPC levels also appeared slightly (though not statistically) elevated in irradiated *Mdm2*^{Y393F} bone marrow.

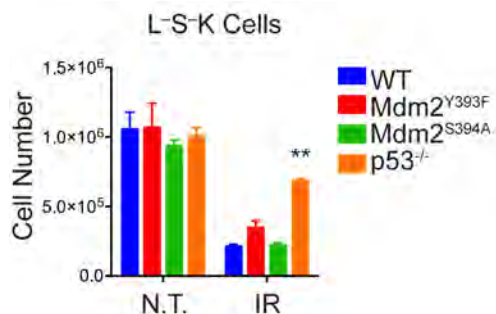


Figure 3.20. Quantification of L S K hematopoietic progenitor cells in bone marrow. Quantification of L S K hematopoietic progenitor cells in bone marrow of WT, $Mdm2^{Y393F}$, $Mdm2^{S394A}$ and $p53^{-/-}$ mice, either untreated or 8 hours after 5 Gy IR ($n = 3-4$, \pm SEM). $**P < 0.01$ (Student's t -tests).

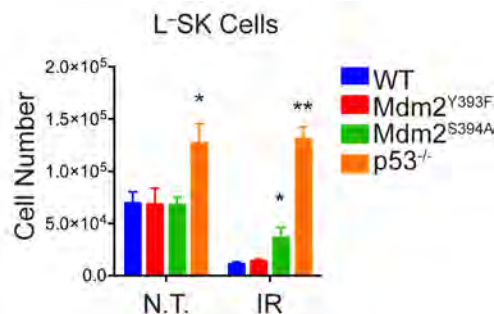


Figure 3.21. Quantification of L SK hematopoietic progenitor cells in bone marrow. Quantification of L SK (HSPC) hematopoietic progenitor cells in bone marrow of WT, $Mdm2^{Y393F}$, $Mdm2^{S394A}$ and $p53^{-/-}$ mice treated as described in (B). $*P < 0.05$, $**P < 0.01$ (Student's t -tests).

We examined whether the resistance to acute whole-body IR-associated lethality observed in $Mdm2^{Y393F}$ and $Mdm2^{S394A}$ mice was due to an increased capacity to repopulate irradiated marrow by performing haematoxylin and eosin (H&E) stains on bone marrow from mice either untreated or 6 and 9 days following 8 Gy IR (Figure 3.22). At 6 days post-IR, while mice of all three genotypes displayed evidence of a significant decrease in cellularity, both $p53^{-/-}$ and $Mdm2^{S394A}$ bone marrow, and to a lesser extent $Mdm2^{Y393F}$ bone marrow, contained multiple colonies of hematopoietic cells that were not apparent in WT bone marrow, as well as visibly more erythrocytes. By 9 days post-IR, coinciding with the period of observed morbidity in threshold-lethally irradiated animals, an even larger discrepancy in cellularity was observable between WT and mutant bone

marrows. Few hematopoietic colonies were visible in WT marrow, while colonies present in $p53^{-/-}$ and $Mdm2^{S394A}$ mice had expanded significantly and largely replenished the medullary cavity. While there was greater visible repopulation in $Mdm2^{Y393F}$ bone marrow as compared to WT, this repopulation appeared intermediate to that observed in $Mdm2^{S394A}$ bone marrow, trending with the observed improved HSPC survival following IR.

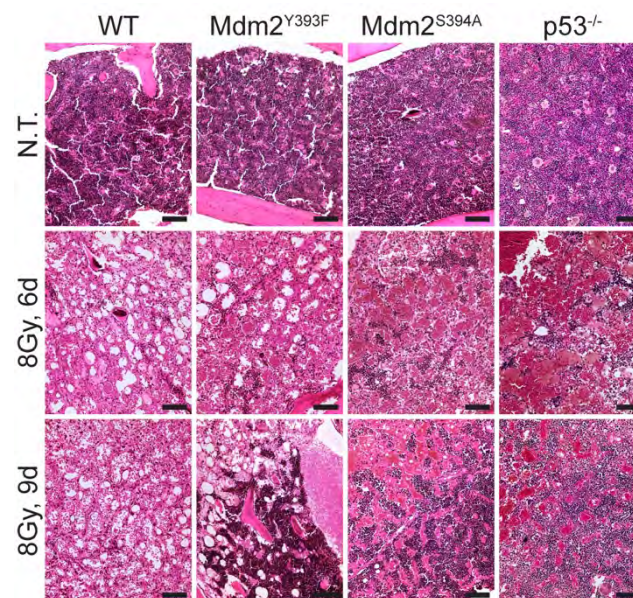


Figure 3.22. Haematoxylin and eosin stained bone marrow following IR. Haematoxylin and eosin stained bone marrow from WT, $Mdm2^{Y393F}$, $Mdm2^{S394A}$ and $p53^{-/-}$ mice exposed to 8Gy IR. Scale bars represent 100 μ m.

Mdm2 Tyr393 and Ser394 phosphorylations are not additive in their impact on tumor suppression and radioresistance.

To determine whether the shared effects of Mdm2 Tyr393 and Ser394 phosphorylation were redundant or additive, we generated a knock-in mouse in which both the Tyr393 residue is substituted with a phenylalanine residue

(Y393F) and the Ser394 residue is substituted with an alanine (S394A) (Figure 3.23). Gene targeting was carried out following a similar strategy as utilized for *Mdm2*^{Y393F} mice (Figures 3.24-3.27). The targeting construct coded for an A to T missense mutation within the 393 codon, a T to G missense mutation within the 394 codon, and a synonymous T to G mutation within the 398 codon of *Mdm2* exon 12, which also permitted PCR-digest genotyping of cells and mice. As observed for *Mdm2*^{S394A} mice (Gannon et al., 2012), *Mdm2*^{Y393F/S394A} mice were recovered from heterozygous intercrosses at Mendelian ratios (Table 3.3).

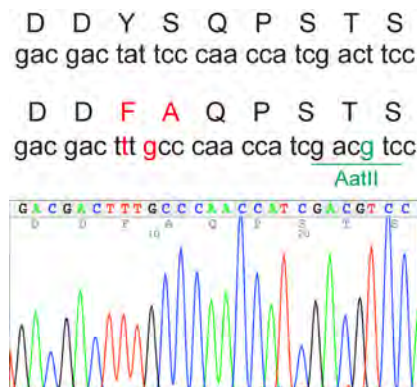


Figure 3.23. Sequence of wild-type and mutant *Mdm2* alleles surrounding codons 393 and 394. DNA sequence of WT and *Mdm2*^{Y393F/S394A} allele surrounding codons 393 and 394 (top). An A to T mutation changed codon 393 from Tyr to Phe. A T to C mutation changed codon 394 from Ser to Ala. A silent T to G mutation in codon 398 introduced a AatII restriction site. Sequencing results of the corresponding region from *Mdm2*^{Y393F/S394A} spleen cDNA are shown (bottom).

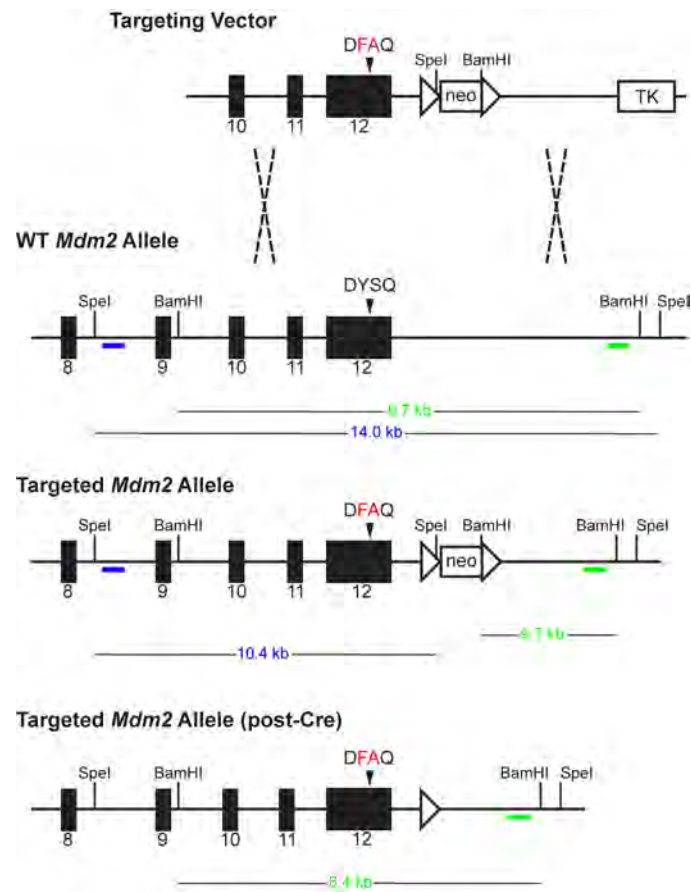


Figure 3.24. Diagram of the targeting strategy used to generate the *Mdm2*^{Y393F/S394A} allele. The targeting vector contained a floxed neomycin cassette (neo) and a 3' thymidine kinase cassette (TK) for positive and negative drug selection, respectively. The targeting vector was linearized and electroporated into PC3 ES cells. ES cell targeting was confirmed by BamHI digest and Southern blot analysis with a 3' external probe (green), as well as Spel digest and Southern blot analysis with a 5' external probe (blue). Protamine-Cre recombinase-directed excision of neo cassette was confirmed by BamHI digest of F1 generation tail DNA and Southern blot analysis with the same 3' external probe as in ES cells (green).

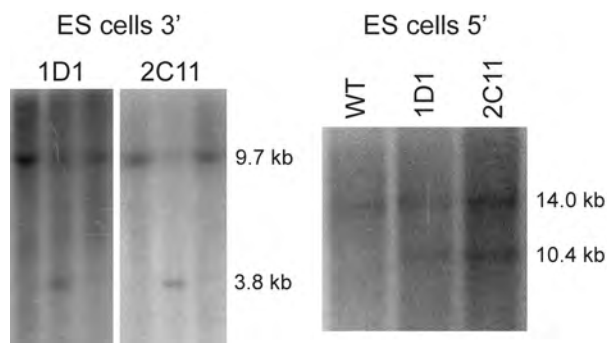


Figure 3.25. Southern blot analysis of targeted ES cells. BamHI digest and Southern blot analysis of ES cell genomic DNA (left). A 3' external probe (green bar from Figure 3.24) detects a 9.7 kb WT allele and 3.8 kb targeted allele. Two clones with correct 3' targeting are shown, each flanked by untargeted (WT) clones. SpeI digest and Southern blot analysis of ES cell genomic DNA (right). A 5' external probe (blue bar from Figure 3.24) detects a 14.0 kb WT allele and 10.4 kb targeted allele.

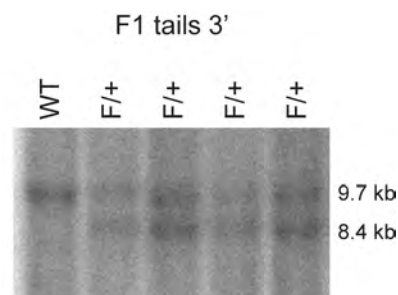


Figure 3.26. Southern blot analysis of mouse DNA. BamHI digest and Southern blot analysis of tail DNA from F1 generation mice. A 3' external probe (green bar from Figure 3.24) detects a 9.7 kb WT allele and 8.4 kb targeted allele.

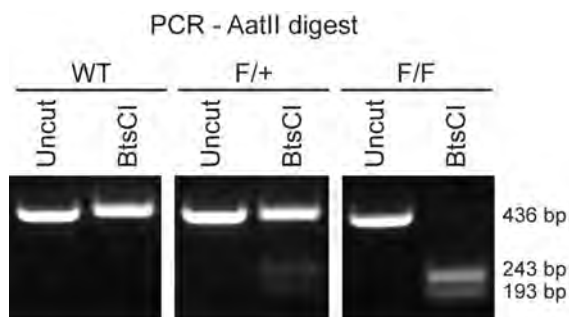


Figure 3.27. Genotyping *Mdm2*^{Y393F/S394A} mice. PCR-BtsCI digest analysis of F2 generation mice. Primers flanking *Mdm2* codons 393 and 394 amplify a 436 bp fragment of DNA. A silent mutation in the *Mdm2*^{Y393F/S394A} allele introduces a novel AatII restriction site which results in 193 and 243 bp fragments.

Mendelian ratio		
	Expected	Observed
+/+	25% (18/72)	26% (19/72)
FA/+	50% (36/72)	49% (35/72)
FA/FA	25% (18/72)	25% (18/72)

Table 3.3. Viability of *Mdm2*^{Y393F/S394A} mice. The expected and observed Mendelian ratios from *Mdm2*^{Y393F/S394A} heterozygote breeding.

A cohort of bi-allelic $Mdm2^{Y393F/S394A}$ mice were monitored for spontaneous tumor presentation, and by 24 months, 14 of 21 (67%) of these mice presented with tumors (Figure 3.28). This mirrors the 65% of $Mdm2^{S394A}$ mice that developed spontaneous tumors in our previous study (Gannon et al., 2012), as does the observed latency of 18-24 months for the majority of tumors. Consequently, the tumor suppressive effects of Mdm2 Tyr393 phosphorylation by c-Abl and Mdm2 Ser394 phosphorylation by ATM do not appear to be synergistic. The predominant tumor type in $Mdm2^{Y393F/S394A}$ mice was B cell lymphoma (6/15, 40%), along with myeloid sarcoma/lymphomas (5/15, 33%), hepatocellular carcinomas (3/15, 20%), and one tumor which appeared to be a liver metastasis of neuroendocrine cell origin (Table 3.4, Figures 3.29 and 3.30).

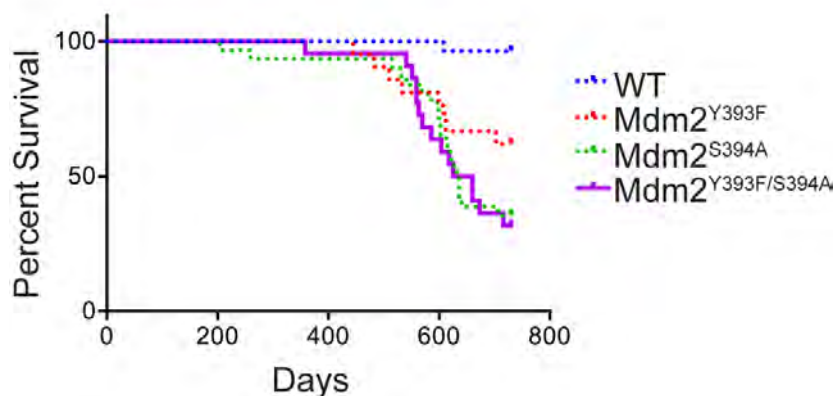


Figure 3.28. Spontaneous tumorigenesis in $Mdm2^{Y393F/S394A}$ mice. Kaplan-Meier tumor-free survival curve of $Mdm2^{Y393F/S394A}$ mice ($n = 21$). Included are tumor-free survival curves of WT and $Mdm2^{Y393F}$ mice described in Figure 3.6, and $Mdm2^{S394A}$ mice described previously (Gannon et al., 2012). Curves were compared by Log-rank test: $Mdm2^{Y393F/S394A}$ to WT ($P < 0.0001$), $Mdm2^{Y393F/S394A}$ to $Mdm2^{Y393F}$ ($P = 0.080$).

Latency (days)	Location	Tumor	Latency (days)	Location	Tumor
541	spleen/LN/liver	B cell	604	liver	HCC
551	liver	HCC	618	spleen/LN/liver	B cell
559	liver	HCC	625	mesenteric LN	B cell
559	LN	B cell	660	spleen/liver	Myeloid
563	spleen/liver	Myeloid	660	spleen/LN	Myeloid
570	liver	Islet cell	673	spleen/LN/liver	B cell
586	spleen/liver	Myeloid	716	spleen/liver	Myeloid

Table 3.4. *Mdm2*^{Y393F/S394A} tumors. Table displaying the latency, location, and tumor type for spontaneous tumors arising in *Mdm2*^{Y393F/S394A} mice.

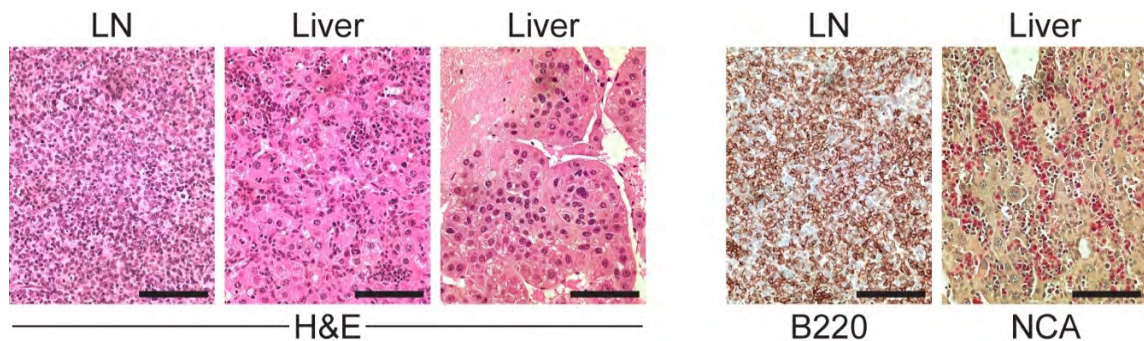


Figure 3.29. *Mdm2*^{Y393F/S394A} tumor histology. Representative H&E stained tissue sections of a B cell lymphoma (left), myeloid sarcoma (middle) and hepatoma (right) that developed in *Mdm2*^{Y393F/S394A} mice. Scale bars represent 100 μ m.

Figure 3.30. *Mdm2*^{Y393F/S394A} tumor staining. B cell lymphoma shows expression of B220 as detected by IHC (left), and a myeloid neoplasm exhibits NCA activity (right). Scale bars represent 100 μ m.

Irradiated thymi from *Mdm2*^{Y393F/S394A} mice were examined by immunoblotting, as well as by qPCR of p53 target gene transcripts, and showed a similar reduction of p53 stabilization and activity as observed in *Mdm2*^{S394A} mice (Figures 3.31 and 3.32). This is in keeping with the absence of observable defects in the p53 response to DNA damage in *Mdm2*^{Y393F} mice described in

Figures 3.10-3.13. Accordingly, while reduced in comparison to WT, no additional deficits in apoptosis were observed by TUNEL staining or Annexin V staining followed by flow cytometry of *Mdm2*^{Y393F/S394A} thymi relative to those seen in *Mdm2*^{S394A} thymi (Figures 3.33 and 3.34).

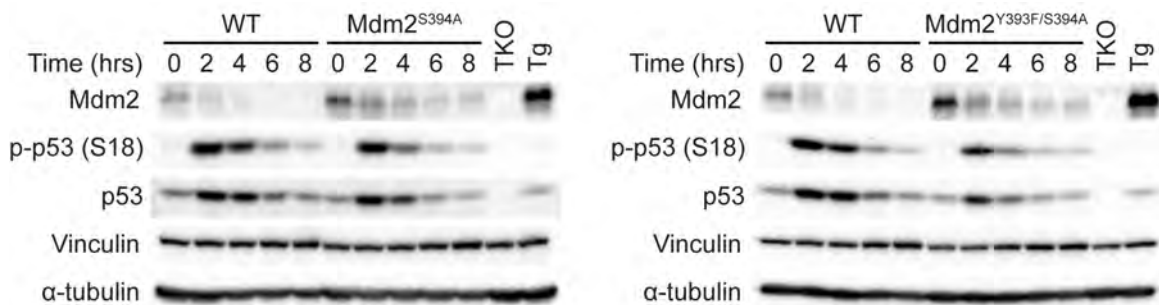


Figure 3.31. Western blots of irradiated Mdm2 mutant thymi. WT and *Mdm2*^{S394A} mice (left) or *Mdm2*^{Y393F/S394A} mice (right) were left untreated or exposed to 5 Gy IR and thymi were harvested at 2 hour intervals. Protein levels were analyzed by western blotting. TKO indicates *Mdm2*^{-/-}, *MdmX*^{-/-}, *p53*^{-/-} control; Tg indicates *Mdm2*^{Tg/+} Mdm2 overexpressing control.

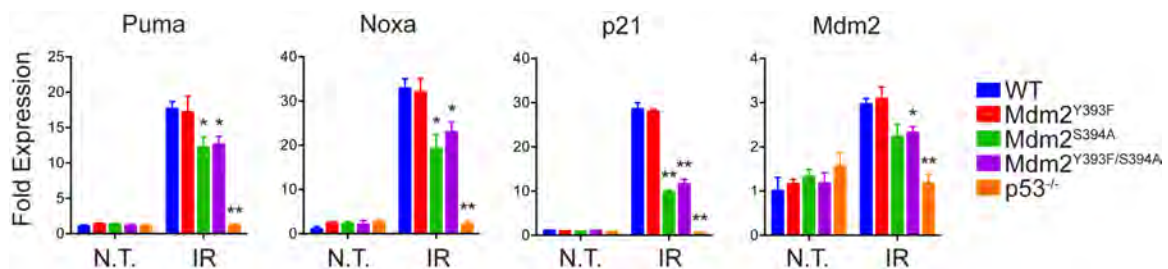


Figure 3.32. Gene expression in irradiated Mdm2 mutant thymi. WT, *Mdm2*^{Y393F}, *Mdm2*^{S394A}, *Mdm2*^{Y393F/S394A} and *p53*^{-/-} mice were left untreated or exposed to 5 Gy IR and thymi were harvested at 4 hours. Fold expression of p53-target genes was determined by real-time quantitative PCR, relative to untreated WT samples using *Rplp0* as internal reference ($n = 3-4$, \pm SEM). * $P < 0.05$, ** $P < 0.01$ (Student's t -tests of $\Delta\Delta$ Ct values).

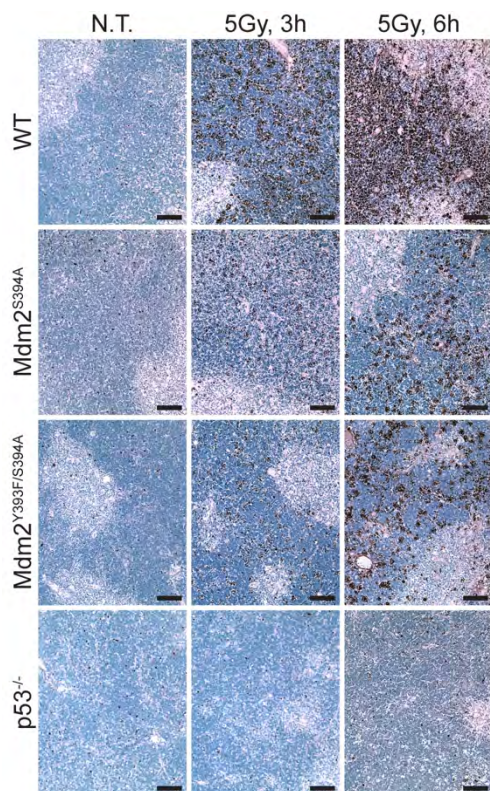


Figure 3.33. Apoptosis in irradiated Mdm2 mutant thymi. TUNEL staining of thymi from WT, *Mdm2*^{S394A}, *Mdm2*^{Y393F/S394A} and *p53*^{-/-} mice treated with 5 Gy IR and harvested at 3 and 6 hours.

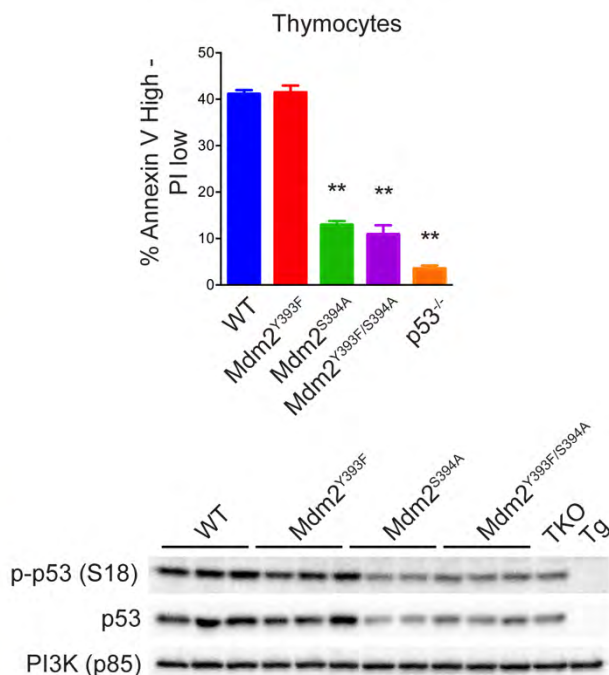


Figure 3.34. Quantification of apoptotic Mdm2 mutant thymocytes. Thymi were harvested from WT, *Mdm2*^{Y393F}, *Mdm2*^{S394A}, *Mdm2*^{Y393F/S394A} and *p53*^{-/-} mice 5 hours after treatment with 5 Gy IR and thymocytes were stained with AnnexinV-FITC and propidium iodide (PI) for FACS analysis (top). The percentage of Annexin V^{High} - PI^{Low} cells were quantified ($n = 3$, \pm SEM). ** $P < 0.01$ (Student's t -tests). Protein lysates generated from fractions of WT, *Mdm2*^{Y393F}, *Mdm2*^{S394A} and *Mdm2*^{Y393F/S394A} cell suspensions were analyzed for p53 and p-p53 (S18) protein levels (bottom).

Finally, we examined whether the radioresistant phenotypes observed in $Mdm2^{Y393F}$ and $Mdm2^{S394A}$ mice were exacerbated in $Mdm2^{Y393F/S394A}$ mice. $Mdm2^{S394A}$ and $Mdm2^{Y393F/S394A}$ mice were exposed to 9Gy whole-body IR (as utilized for $Mdm2^{Y393F}$ mice) and monitored for signs of morbidity (Figure 3.35). No significant difference in survival was observed between $Mdm2^{S394A}$ and $Mdm2^{Y393F/S394A}$ mice at this dose, with 82% of $Mdm2^{S394A}$ mice and 69% of $Mdm2^{Y393F/S394A}$ mice surviving at 4 weeks, respectively.

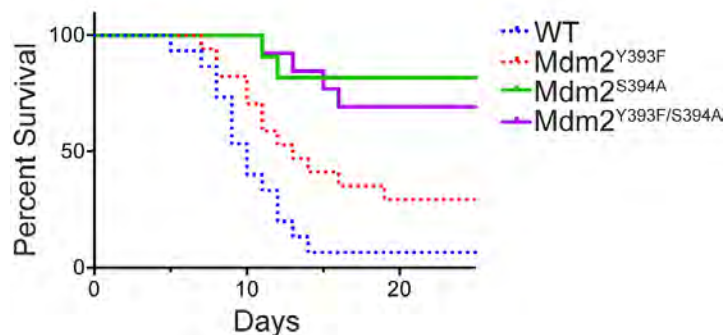


Figure 3.35. Radioresistance in Mdm2 mutant mice. Kaplan-Meier survival curves of WT ($n = 15$), $Mdm2^{Y393F}$ ($n = 17$), $Mdm2^{S394A}$ ($n = 11$), and $Mdm2^{Y393F/S394A}$ ($n = 13$) mice exposed to 9 Gy whole-body IR. Curves were compared by Log-rank test: WT to $Mdm2^{Y393F}$ ($P = 0.030$), WT to $Mdm2^{S394A}$ ($P < 0.0001$), WT to $Mdm2^{Y393F/S394A}$ ($P < 0.0001$), $Mdm2^{Y393F}$ to $Mdm2^{S394A}$ ($P = 0.010$), $Mdm2^{Y393F}$ to $Mdm2^{Y393F/S394A}$ ($P = 0.020$), $Mdm2^{S394A}$ to $Mdm2^{Y393F/S394A}$ (n.s.).

However, both genotypes are significantly more radioresistant than $Mdm2^{Y393F}$ mice, which are themselves significantly more radioresistant than WT mice at this dose. Thus, radioresistance resulting from the loss of either Mdm2 Tyr393 phosphorylation by c-Abl or Mdm2 Ser394 phosphorylation by ATM is not additive. Accordingly, IR-induced expression levels of p53 target genes in

irradiated bone marrow of $Mdm2^{S394A}$ and $Mdm2^{Y393F/S394A}$ mice are similarly reduced (Figure 3.36). The equivalent deficiency in the p53 response in $Mdm2^{S394A}$ and $Mdm2^{Y393F/S394A}$ bone marrow follows with comparably increased numbers of L⁻S⁻K HSPCs surviving in $Mdm2^{Y393F/S394A}$ bone marrow following IR (Figure 3.37). Furthermore, bone marrow cells from $Mdm2^{Y393F/S394A}$ or $Mdm2^{S394A}$ mice exhibit similar hematopoietic repopulating abilities *in vivo* (Figure 3.38). As was observed with $Mdm2^{Y393F}$ and $Mdm2^{S394A}$ mice, no differences were seen in the number of lineage-defined or L⁻S⁻K hematopoietic cells (Figures 3.39 and 3.40).

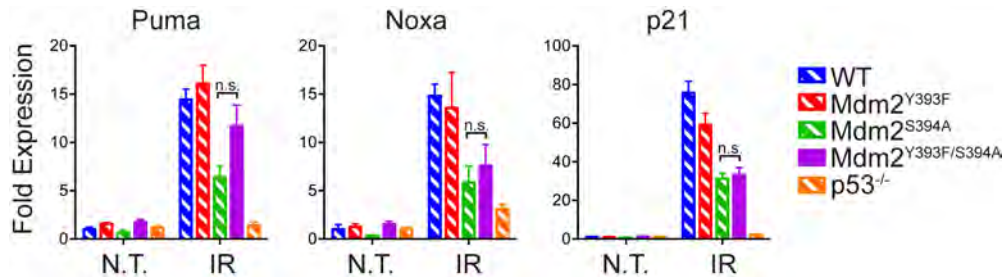


Figure 3.36. Gene expression in irradiated $Mdm2$ mutant bone marrow.

Fold expression of p53-target genes in bone marrow of WT, $Mdm2^{Y393F}$, $Mdm2^{S394A}$ and $p53^{-/-}$ mice, as shown in Figure 3.17, untreated and 6 hours after 5 Gy IR, including expression data from $Mdm2^{Y393F/S394A}$ bone marrow. ($n = 3-4$ mice, \pm SEM). No significant difference is observed between $Mdm2^{S394A}$ and $Mdm2^{Y393F/S394A}$ expression levels (Student's *t*-tests of $\Delta\Delta$ Ct values).

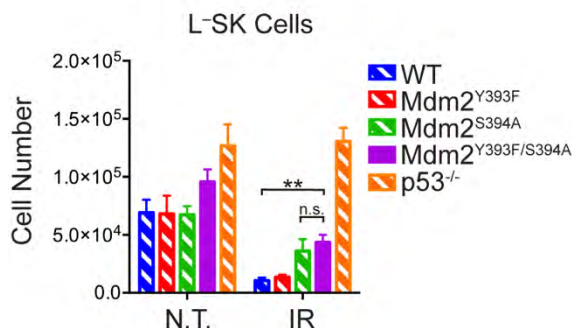


Figure 3.37. Quantification of L SK hematopoietic progenitor cells in *Mdm2* mutant bone marrow.

Bone marrow was harvested from mice untreated or 8 hours following 5 Gy IR ($n = 3-6$, \pm SEM). $**P < 0.01$ (Student's t -tests).

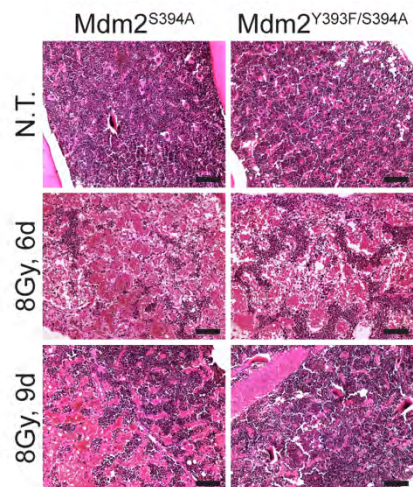


Figure 3.38. Haematoxylin and eosin stained *Mdm2*^{S394A} and *Mdm2*^{Y393F/S394A} bone marrow.

Mice were exposed to 8Gy IR. Scale bars represent 100 μ m.

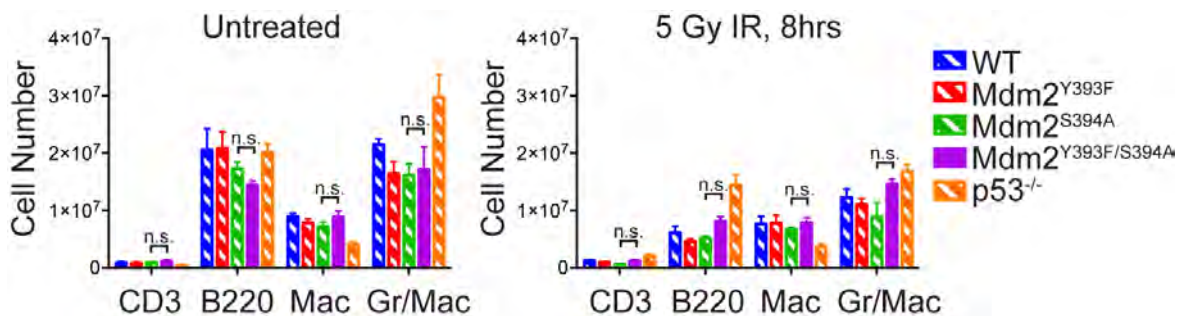


Figure 3.39. Quantification of lineage-defined hematopoietic cells in *Mdm2* mutant bone marrow.

Untreated bone marrow (top) or 8 hours after 5 Gy IR (bottom) from WT, *Mdm2*^{Y393F}, *Mdm2*^{S394A} and *p53*^{-/-} mice, as shown in Figure 3.19, including data from *Mdm2*^{Y393F/S394A} bone marrow ($n = 3-4$, \pm SEM). No significant difference is observed between *Mdm2*^{S394A} and *Mdm2*^{Y393F/S394A} lineage-defined cell numbers (Student's t -tests).

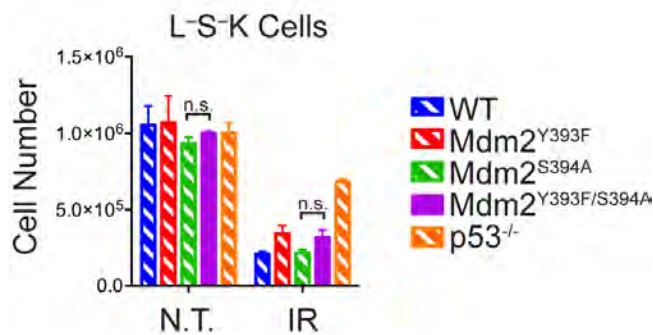


Figure 3.40. Quantification of L S K hematopoietic progenitor cells in *Mdm2* mutant bone marrow. Bone marrow from WT, *Mdm2*^{Y393F}, *Mdm2*^{S394A} and *p53*^{-/-} mice, as shown in Figure 3.20, either untreated or 8 hours after 5 Gy IR, including data from *Mdm2*^{Y393F/S394A} bone marrow ($n = 3-4$, \pm SEM). No significant difference is observed between *Mdm2*^{S394A} and *Mdm2*^{Y393F/S394A} L S K progenitor cell numbers (Student's *t*-tests).

Materials and Methods

Mice and Animal Studies

All animals described in this study were on a C57Bl/6 background. Mice and cells were irradiated with a cesium-137 source (Gammacell 40). The generation of *Mdm2*^{S394A} mice has been previously described (Gannon et al, 2012). *Eμ-myc* mice were a gift from Christine Eischen (Vanderbilt University). A detailed description of the generation and genotyping of *Mdm2*^{Y393F} and *Mdm2*^{Y393F/S394A} mice is provided below. All animals used in this study were maintained and assayed in accordance with federal guidelines and those established by the Institutional Animal Care and Use Committee at the University of Massachusetts Medical School.

Generation and Genotyping of *Mdm2*^{Y393F} and *Mdm2*^{Y393F/S394A} Mice

Targeting vectors were constructed from subcloned fragments of the *Mdm2* genomic sequence (129Sv strain). Site-directed mutagenesis was performed according to manufacturer instructions using a QuikChange II Site-Directed Mutagenesis Kit (Stratagene). Targeting vectors were sequenced to ensure only the desired mutations were introduced. Linearized targeting vectors were introduced into PC3 ES cells by electroporation. Targeted homologous recombination was detected by Southern blotting using 5' and 3' external probes after *SpeI* and *BamHI* restriction digests, respectively. Targeted cells were microinjected into E3.5 blastocysts (C57BL/6 strain), and embryos were

surgically implanted into pseudopregnant foster mice by standard procedures. Transmission of the knock-in allele and excision of the neo cassette in F1 and F2 offspring of male chimeric mice was confirmed by Southern blotting using the same 3' external probe and BamHI restriction digest strategy as in ES cells. *Mdm2*^{Y393F} and *Mdm2*^{Y393F/S394A} alleles were followed by genomic PCR using the primer pair: Forward 5'AAAGATGCTGGACCCTTCGTGAGA3' and Reverse 5'GCACACGTGAAACATGACATGAGG3', followed by BtsCI digest to identify the *Mdm2*^{Y393F} allele or AatII digest to identify the *Mdm2*^{Y393F/S394A} allele.

Immunoblotting

Tissues and cells were lysed in NP-40 lysis buffer (50 mM Tris-HCl [pH 7.5], 150 mM NaCl, 0.5% NP-40) supplemented with protease and phosphatase inhibitor cocktail tablets (Roche). Protein extracts (50 µg) were analyzed by direct western blotting with antibodies specific for Mdm2 (NBP1-02158; Novus), p53 (CM5; Novocastra), p-p53(S15) (#9284; Cell Signaling), α-tubulin (B-5-1-2; Sigma), Vinculin (hVin-1; Sigma) and PI3K p85 (06-496; Millipore). Blots were imaged on a Chemidoc MP (Bio-Rad) and relative band intensities determined by densitometry using Image Lab software (v4.1, Bio-Rad).

Quantification of Apoptosis

Animals were treated as described. Thymi and spleens were harvested and single cell suspensions generated by mechanical disruption and screening

through 70 μm mesh. Red blood cells were lysed in splenocyte samples by suspension in ammonium-chloride-potassium (ACK) buffer. Samples were stained using an Annexin V-FITC Apoptosis Detection Kit I (BD Pharmingen #556547) according to manufacturer protocol. Flow cytometry was performed by the UMASS Medical School Flow Cytometry Core Lab. Early apoptotic cells (Annexin V^{high} PI^{low}) were quantified using FlowJo software (Tree Star).

Cell Cycle Analysis

Treated MEFs were pulse labeled with 50 μM bromodeoxyuridine (BrdU) for 3 hours before being harvested by trypsinization and fixed in 70% ethanol overnight. Fixed cells were stained with FITC conjugated anti-BrdU antibody (Becton Dickinson #347583) and PI, and analyzed by flow cytometry by the UMASS Medical School Flow Cytometry Core Lab. Cell cycle populations were quantified using FlowJo software (Tree Star).

Gene Expression Analysis and Sequencing

Total RNA was isolated from tissues by RNeasy mini kit (QIAGEN) and cDNA synthesized by Superscript III First Strand Synthesis System (oligo-dT priming) (Invitrogen). Quantitative PCR was performed using SYBR Select Master Mix (Applied Biosystems) in conjunction with a 7300 Real-Time PCR System (Applied Biosystems). Thymus cDNA input was 10 ng and bone marrow cDNA input was 100 ng. Fold expression was calculated using the $\Delta\Delta\text{Ct}$ method

relative to untreated WT samples using *Rplp0* as internal reference. Primers used were as follows: *Puma*, 5'ACGACCTCAACGCGCAGTACG3' and 5'GAGGAGTCCCATGAAGAGATTG3'; *Noxa*, 5'CTCAGGAAGATCGGAGACAAAG3' and 5'GCACACTCGTCCTTCAAGT3'; *p21*, 5'CTGAGCGGCCTGAAGATT3' and 5'ATCTGCGCTTGGAGTGATAG3'; *Mdm2*, 5'AGTCTCTGGACTCGGAAGATTA3' and 5'CTGTATCGCTTTCTCCTGTCTG3'; *Rplp0*, 5'CTGAGTACACCTTCCCCTTAC3' and 5'CTCTTCCTTTGCTTCAGCTTTG3'. *Mdm2* message was amplified from spleen cDNA in overlapping fragments using two separate primer pairs: *Mdm2seq1*, 5'CCAGGCCAATGTGCAATACCAACA3' and 5'TCCTCAGCACATGGCTCTTTAGCA3'; *Mdm2seq2*, 5'TCTTGACGATGGCGTAAGTGAGCA3' and 5'TCCAAAGTCCTTCCAAGCGGAGAT3'. Amplified fragments were gel extracted (QIAGEN) and sequenced by Sequegen, Inc (Worcester, MA).

Histopathology

Tissues samples were fixed in 10% formalin for 24 hr. The UMMS Morphology Core Laboratory performed embedding, sectioning, and staining. TUNEL staining was performed using the In Situ Cell Death Detection Kit, POD (Roche) according to manufacturer's instructions. Immunohistochemistry was performed with antibodies specific for B220 (550286; BD Pharmingen) and CD3 (A0452; Dako). Naphthol chloroacetate esterase staining (Leder Stain) was performed to

detect cells with myeloid differentiation. Stained tissue was analyzed using an Olympus CX41 microscope fitted with a PixeLINK camera and software.

Bone Marrow Analysis

Total bone marrow from both hind limbs was harvested, RBCs were lysed, and single-cell suspensions were stained with cell-surface antibodies for Gr-1, CD11B, CD3, and B220. For LSK analysis, bone marrow cells were stained with a biotin lineage mixture, and antibodies for Sca-1, c-Kit, CD34, and Flk2. All samples were run on a BD LSRII flow cytometer (BD Bioscience) and analyzed using FlowJo software (Tree Star). A complete list of antibodies including clone numbers is given in Table 3.5.

Table 3.5. Antibodies used for flow cytometry in Chapter III

Antibody	Clone	Fluorophore	Source
CD3	145-2C11	Biotin, APC	BD Bioscience
B220	RA3-6B2	Biotin, PE	BD Bioscience
Ter119	TER-119	Biotin	Biolegend
Gr-1	RB6-8C5	Biotin, APC, PE	Biolegend
Mac-1	M1/70	Biotin, FITC	Biolegend
Sca-1	D7	APC/Cy7	Biolegend
CD117	2B8	APC	BD Bioscience
CD34	RAM34	FITC	BD Bioscience
Flk2	A2F10	PE	Biolegend
CD45.2	104	FITC, PE/Cy7	Biolegend
CD45.1	A20	PercP/Cy5.5	Biolegend

Statistical Analysis

Statistical analyses were performed using GraphPad Prism software, version 6.0d. Kaplan–Meier survival curves were analyzed by log-rank test. A *P*-value < 0.05 was considered statistically significant for Student's t-tests.

CHAPTER IV

Discussion

In response to DNA damage, numerous kinases become activated and phosphorylate various proteins involved in the DNA damage response, including the p53 tumor suppressor protein and its chief negative regulator, Mdm2. These signaling events have been proposed by many groups to activate p53 by interrupting Mdm2-inhibition of p53, thereby facilitating p53 transactivation of downstream target genes whose products regulate the cellular response to DNA damage. Previously, our lab and others have shown that phosphorylation of p53 following DNA damage has only a modest role in regulating p53 stabilization and activation, p53-mediated apoptosis and governing p53 tumor suppression *in vivo* (Wu et al., 2002; Chao et al., 2003; Sluss et al., 2004; MacPherson et al., 2004; Chao et al., 2006). However, having generated *Mdm2*^{S394A} knock-in mice, our lab has shown that ATM phosphorylation of Mdm2 Ser394 significantly regulates the amplitude and duration of the p53 response to DNA damage in mice, and alters p53 suppression of spontaneous tumorigenesis (Gannon et al., 2012). These studies demonstrate the *in vivo* importance of Mdm2 phosphorylation in the regulation of the p53 DNA damage response.

In Chapter II of this dissertation, we explore *in vivo* the mechanism by which Mdm2 Ser394 phosphorylation alters p53 functions, and examine whether ATM-Mdm2-p53 signaling regulates tumorigenesis in mice induced by activated

oncogenes or ionizing radiation. Our results indicate that Mdm2 Ser394 phosphorylation regulates Mdm2 stability and has dramatically different and stress-dependent effects in tumorigenesis, suppressing Myc-driven lymphomagenesis and promoting IR-induced lymphomagenesis. In Chapter III we present a novel knock-in mouse that cannot be phosphorylated at Mdm2 Tyr393 by c-Abl (*Mdm2^{Y393F}* mice). The study of these mice provides further evidence of the significance of Mdm2 phosphorylation by DNA damage activated kinases in regulating p53 dependent organismal responses. Though we observed no defects in the acute DNA damage-induced stabilization and activation of p53 in *Mdm2^{Y393F}* mice, they display increased spontaneous and oncogene-induced tumorigenesis and radioresistance. We also present a mouse model in which both the c-Abl target residue Mdm2 Tyr393 and the adjacent ATM target residue Mdm2 Ser394 are mutated (*Mdm2^{Y393F/S394A}*). Our study of these animals shows an apparent redundancy of the shared phenotypes between *Mdm2^{Y393F}* and *Mdm2^{S394A}* mice, with tumorigenesis and radioresistance in *Mdm2^{Y393F/S394A}* mice never exceeding that observed in *Mdm2^{S394A}* mice.

Effects of Mdm2 phosphorylation on Mdm2 stability

In Chapter II we show that Mdm2 is present at higher levels in the thymus and spleen of *Mdm2^{S394A}* mice following DNA damage (Figures 2.1, 2.2, 2.5). Elevated Mdm2 levels are the result of Mdm2^{S394A} being more stable following DNA damage (Figure 2.6). Differences in Mdm2 expression do not appear to

influence the observed Mdm2 protein levels, as Mdm2 transcript levels are equivalent or even slightly reduced in both untreated and IR-treated *Mdm2*^{S394A} thymi during this timeframe (Figure 2.3). This result provides direct, *in vivo* evidence that DNA damage-induced phosphorylation of Mdm2 at this single residue by ATM induces Mdm2 destabilization. Our results trend with previous *in vitro* studies that report a decrease in the half-life of Mdm2 after genotoxic stress (Stommel and Wahl, 2004; Itahana et al., 2007; Inuzuka et al. 2010). Furthermore, DNA damage-induced Mdm2 destabilization has been shown to be inhibited with the PIKK inhibitor wortmannin (Stommel and Wahl, 2004), and the analogous mutation of Ser395 in human Mdm2 has been shown to stabilize Mdm2 following DNA damage in transfection based assays (Stommel and Wahl, 2004, Lu et al., 2007).

The observed difference in the stability of phosphorylated Mdm2^{S394A} after DNA damage differs from what our lab has previously reported (Gannon et al., 2012). It is possible that this new finding is the result of our using different, better-validated Mdm2 antibodies. Our data also show that Mdm2 levels are elevated in thymi and spleens of *Mdm2*^{S394A} mice in the absence of acute, exogenous DNA damage (Figures 2.1, 2.2, 2.6), again departing from our lab's previous observations. We interpret this finding to be indicative of some basal level of ATM activity in unstressed tissues that exerts influence on Mdm2 protein stability.

It is presently unclear how Mdm2 phosphorylation facilitates Mdm2 destabilization. One study has suggested that Mdm2 stability is primarily mediated through self-ubiquitination (Stommel and Wahl, 2004). This study reached this conclusion by overexpressing an Mdm2 mutant with abrogated RING E3 activity ($Mdm2^{C464A}$) in U2OS cells and observing little Mdm2 destabilization following DNA damage. This led the authors of the study to speculate as to a possible DNA damage-induced switch between Mdm2-mediated degradation of p53 and itself. However, a subsequent study in which MEFs from the corresponding $Mdm2^{C462A}$ knock-in mice were examined showed that Mdm2 RING E3 activity was in fact dispensable for Mdm2 destabilization after IR (Itahana et al., 2007). These divergent results may be due to the differences in methodologies, and further emphasize the potential for disparities between transfection based studies and more endogenous conditions.

Degradation of Mdm2 in the absence of Mdm2 ubiquitin ligase function is indicative of other ubiquitin ligases being capable of regulating Mdm2 stability. One study has shown that the p300/CBP-associated factor (PCAF) is capable of promoting Mdm2 ubiquitination, and that PCAF can impact Mdm2 levels under unstressed conditions as well as Mdm2 destabilization in response to DNA damage (Linares et al., 2007). Similarly, the anaphase-promoting complex/cyclosome (APC/C) E3 ubiquitin ligase complex has been shown to ubiquitinate Mdm2, with siRNA-mediated depletion of APC2, the Mdm2-binding member of the APC/C complex, leading to Mdm2 accumulation and diminished

p53 stabilization in response to DNA damage (He et al., 2014). Other studies have identified the F-box proteins β -TRCP and FBXO31 as mediators of Mdm2 degradation by the SCF complex (Inuzuka et al. 2010; Malonia et al., 2015). β -TRCP mediated degradation of Mdm2 is dependent on Mdm2 phosphorylation by CK1 and promotes Mdm2 turnover in response to DNA damage (Inuzuka et al. 2010). This is seemingly in contradiction with previous studies showing hypophosphorylation of CK1 target residues on Mdm2 following DNA damage (Blattner et al., 2002). Notably, knockdown of β -TRCP does not appear to impact the initial DNA damage-induced stabilization of p53, but rather Mdm2 stability and p53 levels at later time points in the damage response (Inuzuka et al. 2010). It has subsequently been shown that ATM phosphorylates CK1, and that this promotes CK1 nuclear localization and Mdm2 degradation (Wang et al., 2012). It is conceivable that the phosphorylation state of Mdm2 at CK1 target residues has opposing effects on Mdm2 stability depending on the damage response phase and differing active signaling events. Contrastingly, FBXO31 knockdown in cell lines abolishes the initial Mdm2 destabilization and p53 stabilization following DNA damage (Malonia et al., 2015). FBXO31 can direct the polyubiquitination and degradation of Mdm2, and the FBXO31-Mdm2 interaction appears dependent on ATM phosphorylation of Mdm2 (Malonia et al., 2015). However, the requirement for ATM phosphorylation was determined through the expression of an Mdm2 protein lacking all 6 proposed ATM target residues, and conversely, the treatment of lysates with phosphatase or cells with an ATM kinase inhibitor.

Consequently, the precise mechanism of how ATM phosphorylation of Mdm2 Ser394 specifically promotes Mdm2 degradation under endogenous conditions remains to be determined.

The methods and results described in Chapter II provide a starting point from which to further examine the mechanism of Mdm2 destabilization following Mdm2 Ser394 phosphorylation under endogenous conditions. Preliminary co-immunoprecipitation experiments have not proven successful for examining Mdm2-FBXO31 interactions in whole tissues. However, further optimization of methods may allow for the examination of the impact of Mdm2 Ser394 phosphorylation on Mdm2 interaction with the different ubiquitinating complexes listed above.

In opposition to Mdm2 destabilization, a number of different mechanisms are proposed to promote Mdm2 stability. These mechanisms include modifications of Mdm2 with the small, ubiquitin-like proteins SUMO (Small ubiquitin-related modifier) and NEDD8 (Neural precursor cell expressed developmentally down-regulated protein 8), which are separately proposed to have Mdm2 stabilizing effects and to decrease in response to DNA damage (Buschmann et al., 2001; Watson et al., 2010). Additionally, Mdm2, MdmX and p53 can be deubiquitinated by the HAUSP (herpesvirus-associated ubiquitin-specific protease) protein (Li et al., 2002a; Li et al., 2004; Meulmeester et al., 2005). DNA damage has been shown to reduce the affinity of Mdm2 and MdmX for HAUSP, leading to their enhanced ubiquitination (Meulmeester et al., 2005).

A proposed mechanism for the dissociation of Mdm2 from HAUSP involves ATM phosphorylation of Daxx (death domain-associated protein 6) triggering its dissociation from Mdm2, and relieving Daxx mediated promotion of Mdm2-HAUSP interaction (Tang et al., 2006; Tang et al., 2013). MDM2 is also been reported to be deubiquitinated by the ubiquitin-specific proteases USP2a and USP15 (Stevenson et al., 2007; Zou et al., 2014). Notably, USP2a also acts as a deubiquitinating enzyme for MdmX, and is downregulated in response to cisplatin (Allende-Vega et al., 2010). Accordingly, determining whether the interaction of Mdm2 with any of its proposed stabilizing interactors is affected in *Mdm2*^{S394A} tissues or cells may also shed light on the destabilizing effect of Mdm2 Ser394 phosphorylation.

In Chapter III, in contrast to what was observed in *Mdm2*^{S394A} tissues, we observed no differences in the levels of Mdm2 protein in *Mdm2*^{Y393F} spleens or thymi following DNA damage (Figure 3.10). However, we did observe slightly higher basal Mdm2 levels in *Mdm2*^{Y393F} thymi. It is possible that although ionizing radiation has been shown to activate c-Abl, its activation is not relevant in the response to IR in the tissues examined. It is also possible that the additional proposed c-Abl targets (Tyr276 and Tyr405) are able to compensate for the absence of Mdm2 Tyr393 phosphorylation, at least in the acute response to DNA damage. Notably, Mdm2 levels are similarly elevated and display qualitatively similar degradation kinetics after IR in *Mdm2*^{Y393F/S394A} thymi as in *Mdm2*^{S394A} thymi (Figure 3.31). This follows with the lack of a contribution from

Mdm2 Tyr393 phosphorylation to Mdm2 destabilization after IR, and shows that it has no additive effects in conjunction with Mdm2 Ser394 phosphorylation. One caveat of our results is that we have not been able to successfully detect c-Abl activation following stress. Similarly, we have not been able to detect Mdm2 Tyr393 phosphorylation in wild-type tissues. We have been unsuccessful in detecting c-Abl activation by western blotting with antibodies specific for phosphorylated c-Abl (indicative of its activation), and no antibody is presently available that specifically detects Mdm2 phosphorylated at Tyr393. Additional experiments to confirm these events in the tissues examined would be useful. Immunoprecipitation of c-Abl followed by an *in vitro* kinase assay may be required to detect its activation. Similarly, immunoprecipitating Mdm2 and immunoblotting with an anti-phosphotyrosine antibody, or the reciprocal experiment, may allow for specific detection of Mdm2 tyrosine phosphorylation, and allow for a visualization of its reduction in *Mdm2*^{Y393F} tissues. As there is similarly no commercially available antibody that detects Mdm2 Ser394 phosphorylation in mouse tissues, this approach may also work for detection of Mdm2 Ser394 phosphorylation using an anti-phosphoserine antibody. Alternatively, the phosphorylation state of Mdm2 Tyr393 and Mdm2 Ser394 could be examined by mass spectrometry.

The proximity of Mdm2 Tyr393 and Mdm2 Ser394 raises the possibility that mutation of either residue may be interfering with the phosphorylation of the other, or impacting the recognition and dephosphorylation of the neighboring

residue by the relevant phosphatase. This could theoretically result in either mutation acting to promote a hypomorphic or hypermorphic effect at the neighboring residue, potentially muddling the phenotypes (or lack thereof) observed for either mutation. As such, it would be interesting to use the above proposed techniques to examine the phosphorylation status of the neighboring residue as well, in DNA damaged *Mdm2*^{Y393F} and *Mdm2*^{S394A} tissues. Furthermore, as Mdm2 Ser394 is known to be dephosphorylated by the Wip1 phosphatase (Lu et al., 2007), the interaction of Wip1 with *Mdm2*^{Y393F} could be examined.

While we have shown that Mdm2 Ser394 phosphorylation governs Mdm2 destabilization in response to ionizing radiation *in vivo*, and similar observations have been made in cell culture settings using IR and the radiomimetic neocarzinostatin (NCS) (Stommel and Wahl, 2004; Lu et al., 2007), another study has observed no effect of phosphorylation of this residue on Mdm2 destabilization in response to the topoisomerase inhibitor etoposide (Wang et al., 2012). Therefore, different DNA damaging agents may display differing levels of reliance on the phosphorylation of specific Mdm2 residues for the destabilization of Mdm2 and activation of p53. Further studies of the effects on Mdm2 stability and p53 activation in *Mdm2*^{Y393F}, *Mdm2*^{S394A} and *Mdm2*^{Y393F/S394A} mice or cells treated with an array of DNA damaging agents may identify specific damage responses with distinct or overlapping requirements for phosphorylation of either Mdm2 Tyr393 or Ser394.

Effects of Mdm2 phosphorylation on p53 stabilization and activation

In Chapter II, the increased levels of Mdm2 observed in the thymus and spleen of *Mdm2*^{S394A} mice after DNA damage correlate with a decrease in p53 levels, p53 target gene expression and apoptosis in these tissues (Figures 2.1-2.5). Previous studies have suggested that ATM phosphorylation of the analogous residue on human MDM2 (Ser395), either alone or in combination with several other ATM-target serine residues in the same region, impacts the ability of Mdm2 to promote p53 degradation and nuclear export, and governs Mdm2 RING-domain oligomerization and polyubiquitination of p53 (Maya et al., 2001; Cheng et al., 2009). DNA damage resulted in p53 stabilization in WT thymocytes, albeit after a brief period of p53 degradation (Figure 2.9). While the initial rate of p53 degradation does not appear affected in irradiated *Mdm2*^{S394A} thymocytes, we observed a prolonged period of p53 destabilization, ultimately resulting in lower relative levels of p53. This prolonged, rather than accelerated, p53 destabilization aligns more with the increased stability of *Mdm2*^{S394A} after DNA damage leading to increased Mdm2-bound p53 than with altered Mdm2 ubiquitination activity. This is supported by the increased relative amounts of Mdm2-bound p53 after IR observed in *Mdm2*^{S394A} thymi (Figure 2.10). However, an effect on Mdm2 ubiquitination activity cannot be ruled out, as the differing levels of Mdm2 and p53, and different rates of Mdm2 degradation in wild-type and *Mdm2*^{S394A} thymi preclude the accurate quantitation of relative p53 ubiquitination by Mdm2 *in vivo*.

It is likely that DNA damage-induced p53 activity is caused not only by reduced Mdm2-mediated p53 degradation (due to destabilization of Mdm2) but also by reduced Mdm2 steric inhibition of p53. As Mdm2 binds to the amino-terminal, transcriptional activation domain of p53 and inhibits p53 target gene expression, reduced Mdm2-p53 complex formation after Mdm2 phosphorylation by ATM may account for an increase in p53 activity even when p53 protein stability is only modestly altered (Momand et al., 1992; Oliner et al., 1993). Though visibly reduced in comparison to WT tissues, we still see moderate to significant levels of p53 stabilization in both *Mdm2*^{S394A} thymus and spleen (Figures 2.1 and 2.5). The greater relative differences in p53 target gene expression and protein levels in *Mdm2*^{S394A} tissues suggests further regulation of p53 activity beyond its stabilization (Figures 2.1, 2.3, 2.5). This is also supported by the increased relative amounts of Mdm2-bound p53 after IR observed in *Mdm2*^{S394A} thymi (Figure 2.10). As described above regarding the cause of decreased p53 stabilization in *Mdm2*^{S394A} tissues, definitively distinguishing whether increased Mdm2-p53 binding in *Mdm2*^{S394A} tissues is due to increased *Mdm2*^{S394A} levels, or a reduced affinity of phosphorylated Mdm2 for p53 would likely require moving to more controlled *in vitro* experiments.

In Chapter III, mirroring the absence of detectable differences in Mdm2 destabilization following IR, we observed no differences in p53 stabilization and p53 target gene expression in spleens and thymi of *Mdm2*^{Y393F} mice (Figures 3.10 and 3.11). Accordingly, no differences were detected in splenic or thymic

apoptosis in irradiated *Mdm2*^{Y393F} mice, or growth arrest in MEFs treated with IR or doxorubicin (Figures 3.12-3.14). As with IR-induced destabilization of Mdm2, no additive effects were observed in *Mdm2*^{Y393F/S394A} mice relative to *Mdm2*^{S394A} mice in the reduction of p53 stabilization and activity following IR (Figures 3.31-3.34). Again, additional studies employing different DNA damaging agents may expose unidentified damage-specific defects in p53 responses in *Mdm2*^{Y393F} mice.

Mdm2 phosphorylation in spontaneous tumor suppression

Our lab had previously published that *Mdm2*^{S394A} mice are prone to spontaneous tumors (Gannon et al., 2012). In Chapter III we report that *Mdm2*^{Y393F} mice are viable and display no developmental defects, yet they are significantly more prone to developing spontaneous tumors over their lifespan (Figure 3.6). The *Mdm2*^{Y393F} tumor spectrum, as well as latency, largely mirrors those observed with both p53^{+/-} and Mdm2-transgenic mice, with a large percentage of B cell lymphomas (Table 3.1, Figures 3.7 and 3.8) (Jones et al., 1998; Wang et al., 2008; Donehower and Lozano, 2009). We observed no synergistic effects of the loss of both Mdm2 Tyr393 and Ser394 phosphorylation on the incidence of spontaneous tumorigenesis. *Mdm2*^{Y393F/S394A} mice developed spontaneous tumors at a frequency and latency that nearly overlap what we have reported with *Mdm2*^{S394A} mice (Figure 3.28). Again the tumor spectrum, as well as latency, largely mirrors those observed with p53^{+/-} and Mdm2-transgenic mice,

with a large percentage of B cell lymphomas as well as sarcomas (Table 3.1, Figures 3.7 and 3.8). Thus, c-Abl phosphorylation of Mdm2 Tyr393 significantly impacts spontaneous tumor suppression, though to a lesser extent than Mdm2 Ser394 phosphorylation, and in an apparently redundant manner. This may reflect the proposed interdependence of c-Abl and ATM for their respective activities in response to DNA damage (Baskaran et al., 1997; Shafman et al., 1997; Wang et al., 2011a).

We infer that the observed increases in spontaneous tumorigenesis in *Mdm2*^{Y393F}, *Mdm2*^{S394A} and *Mdm2*^{Y393F/S394A} mice are the result of reduced p53-dependent functions. However, it is possible that the elevated basal Mdm2 protein levels observed in *Mdm2*^{S394A} and *Mdm2*^{Y393F/S394A} mice exert p53-independent oncogenic effects. A p53-independent oncogenic function of Mdm2 was first inferred from the altered tumor spectrum of *p53*^{-/-} mice expressing an *Mdm2* transgene (Jones et al., 1998). It was later shown that overexpression of Mdm2 inhibits DNA double-strand break repair independent of p53 and possibly through its interaction with Nbs1 (Alt et al., 2005), and B cells from *Mdm2*-transgenic mice display an increased frequency of chromosomal/chromatid breaks and/or aneuploidy (Wang et al., 2008). It would be interesting to generate *Mdm2*^{S394A} and *Mdm2*^{Y393F/S394A} mice on a *p53*^{-/-} background to examine whether the observed tumor suppressive effects of Mdm2 phosphorylation are dependent on p53. Relatedly, metaphases from splenocytes or purified B cells from these animals could be examined for differences in chromosomal stability. This same

approach could also be used to explore the p53-dependence of the reduced tumor suppression in response to activated Myc observed in *Mdm2*^{S394A} and *Mdm2*^{Y393F} mice (discussed below).

Mdm2 phosphorylation in Myc-driven tumorigenesis

The reduced level of p53 activity in *Mdm2*^{S394A} mice likely facilitates the more rapid *Eμ-myc*-driven B cell lymphomagenesis described in Chapter II (Figure 2.12). Both p53-dependent apoptosis and senescence have been shown to inhibit B-cell lymphomagenesis induced by aberrant Myc activity (Eischen et al., 1999; Eischen et al., 2001; Schmitt et al., 2002; Post et al., 2010). It has been previously demonstrated that activated oncogenes such as *Myc* result in elevated Arf expression, a result of hyperproliferative signaling (Zindy et al., 1998; Sherr et al., 2005). The importance of disrupting the Arf-Mdm2-p53 pathway in Myc-driven lymphomagenesis is evidenced by the fact that *Eμ-myc* driven tumors in mice face a selective pressure to inactivate the p53 pathway, by either p53 mutation, Mdm2 overexpression, or loss of Arf (Eischen et al., 1999). However, we observed a significant acceleration in the median time of tumor presentation in *Eμ-myc;Mdm2*^{S394A} mice in the absence of Mdm2 overexpression or p53 mutation in tumors (Figure 2.14). This suggests that the absence of Mdm2 Ser394 phosphorylation is sufficient to diminish p53 activity in response to oncogene activation and reduces the selective pressure to genetically disrupt the Mdm2-p53 signaling axis (Figure 2.15). Although loss of Arf was observed in a

subset of $E\mu\text{-myc};Mdm2^{S394A}$ tumors, this finding likely reflects the ability of Arf to prevent tumorigenesis in $E\mu\text{-myc}$ mice through an Mdm2-p53 independent mechanism.

As $Mdm2^{S394A}$ mice are deficient for an acute DNA damage-associated phosphorylation event, it is tempting to view the acceleration of lymphomagenesis in $E\mu\text{-myc};Mdm2^{S394A}$ mice as tied to the acute DNA damage response (Figure 2.15). However, Mdm2 protein levels are elevated in spleens of $Mdm2^{S394A}$ mice in the absence of acute DNA damage (Figure 2.5) and Mdm2-transgenic mice have been shown to develop accelerated $E\mu\text{-myc}$ -driven lymphomas displaying reduced selection for p53 inactivation (Wang et al., 2008). It cannot be ruled out that the accelerated lymphomagenesis observed in $E\mu\text{-myc};Mdm2^{S394A}$ mice is due to elevated Mdm2 levels resulting from impaired basal levels of Ser394 phosphorylation, and not the impaired acute DNA damage response of $Mdm2^{S394A}$ mice.

In Chapter III we report similarly accelerated B cell lymphomagenesis in $E\mu\text{-myc};Mdm2^{Y393F}$ mice as in $E\mu\text{-myc};Mdm2^{S394A}$ mice (Figure 3.9). As discussed above, we have observed no defects in p53-dependant apoptosis or growth arrest in $Mdm2^{Y393F}$ tissues and cells following DNA damage (Figures 3.12-3.14). It is conceivable that Mdm2 phosphorylation by c-Abl regulates p53 tumor suppressive functions other than apoptosis or growth arrest, or that that subtle differences in p53 functions, not detectable by acute damage in $Mdm2^{Y393F}$ mice, have a cumulative effect on p53 tumor suppression. Unlike $Mdm2^{S394A}$

mice, we have not observed significantly elevated basal levels of Mdm2 protein in *Mdm2*^{Y393F} spleens.

It would be informative to examine the status of the Arf-Mdm2-p53 pathway in *Eμ-myc;Mdm2*^{Y393F} tumors. If *Eμ-myc;Mdm2*^{Y393F} tumors similarly do not select for alterations in the Arf-Mdm2-p53 pathway, as was observed with *Eμ-myc;Mdm2*^{S394A} mice, it would support that the absence of Mdm2 Tyr393 phosphorylation leads to a deficiency in p53 function. Also, crossing *Mdm2*^{Y393F/S394A} mice with *Eμ-myc* mice would allow us to explore whether the accelerated lymphomagenesis in *Eμ-myc;Mdm2*^{Y393F} mice and *Eμ-myc;Mdm2*^{S394A} mice is occurring through similar pathways, and whether phosphorylation of Mdm2 Tyr393 and Ser394 have additive or redundant effects in suppressing oncogene-induced tumorigenesis.

It would also be interesting to examine Arf, Mdm2 and p53 protein levels in pre-neoplastic spleens or bone marrow, or cultured pre-B cells, from *Eμ-myc*, *Eμ-myc;Mdm2*^{Y393F} and *Eμ-myc;Mdm2*^{S394A} mice. Arf and p53 levels are elevated in pre-B cells in pre-neoplastic *Eμ-myc* mice (Eischen et al., 1999). Observing reduced levels of p53 in *Eμ-myc;Mdm2*^{Y393F} and/or *Eμ-myc;Mdm2*^{S394A} samples would support the p53-dependence of the observed accelerations in lymphomagenesis. This would also show whether the stress caused by activated oncogenes has any effect on Mdm2^{Y393F} or Mdm2^{S394A} protein levels. Relatedly, it would be interesting to determine whether any differences in apoptosis or senescence are detectable in these same tissues or cells.

Mdm2 phosphorylation in IR-induced lymphomagenesis and radioresistance

In Chapter II, to further explore a role for Mdm2 Ser394 phosphorylation in the DDR and in regulation of p53 tumor suppression, we examined lymphomagenesis induced by low level exposure of mice to ionizing radiation (Figures 2.16-2.18). In contrast to Myc-driven lymphomagenesis, *Mdm2*^{S394A} mice proved to be resistant to DNA damage-induced T cell lymphomagenesis, highlighting a stark difference in the effects of ATM-Mdm2-p53 signaling on lymphomas induced by different types of DNA damage-related stress.

The cell of origin in IR-induced lymphomas has historically been viewed as a stem/progenitor cell residing within the bone marrow (Kaplan, 1964), and IR-induced lymphomagenesis is significantly enhanced in the absence of functional p53 (Kemp et al., 1994). Subsequent studies examining the contribution of the p53-dependent pro-apoptotic genes *Puma* and *Noxa* made the paradoxical observation that *Puma*^{-/-} mice develop fewer IR-induced lymphomas (Labi et al., 2010; Michalak et al., 2010). This was attributed to increased survival of leukocytes in the bone marrow, which reduced the proliferative stress and/or propagation of lesions within progenitor cells tasked with repopulating the bone marrow. That *Noxa*^{-/-} mice displayed only modest radioprotection of L⁻SK cells and developed more lymphomas was interpreted as a failure to clear damaged progenitors, thereby promoting the survival of damaged stem/progenitor cells (Michalak et al., 2010). Despite a reduction of p53-dependent gene expression

of *Puma* and *Noxa* in total bone marrow of IR-damaged *Mdm2*^{S394} mice (Figure 2.19), we observed no defects in the attrition of mature hematopoietic cells or lineage-defined progenitor cells (CMPs) (Figures 2.22 and 2.23). Only the most primitive HSPCs display resistance to IR (Figure 2.23). Our finding that *Mdm2*^{S394A} mice are resistant to IR-induced lymphomas reveals that the effects of a reduced p53-dependent damage response in *Mdm2*^{S394A} mice does not mirror the ablation of either *Puma* or *Noxa* alone. Interestingly, a recent study by Kirsch and colleagues suggests that the tumor-initiating cell in IR-induced lymphomas is thymic in origin (Lee et al. 2015). Using mice in which p53 activity was temporally blocked during total-body irradiation, the authors propose that the IR-induced p53 response in bone marrow promotes lymphomagenesis by reducing HSPC fitness, thereby reducing the competition of cells originating from the bone marrow with thymocytes containing oncogenic lesions. The results we have observed with *Mdm2*^{S394A} mice align favorably with this model, as we have observed less p53 activity and increased HSPC fitness in *Mdm2*^{S394A} mice following threshold-lethal doses of radiation, and reduced incidence of T cell lymphomagenesis in *Mdm2*^{S394A} mice after IR exposure. The p53 dependence of the increased HSPC fitness in *Mdm2*^{S394A} mice is further intimated by studies which have observed increased bone marrow repopulation potential in bone marrow deficient for p53, both in the presence and absence of IR (reviewed in Pant *et al.*, 2012). Interestingly, a recent study has linked Mdm2 to enhanced stem-ness via association with the Polycomb Repressor Complex 2 (PRC2)

(Wienken et al., 2015). Further studies into the relative p53-dependent and p53-independent contributions of Mdm2 to HSPC fitness are clearly warranted.

In Chapter III, despite the absence of observable defects in p53 responses to DNA damage in *Mdm2*^{Y393F} thymus, spleen or MEFs, we show that *Mdm2*^{Y393F} mice are resistant to threshold-lethal doses of IR (Figure 3.16). This radioresistance parallels our previous observations with *Mdm2*^{S394A} mice, which display profound defects in p53-dependent apoptosis and growth arrest and tissues and cells. HSPC or bone marrow cells from both mutants display improved repopulating functions following IR exposure, albeit to a lesser extent in *Mdm2*^{Y393F} mice (Figure 3.22). In keeping with this difference, HSPCs in *Mdm2*^{S394A} bone marrow display a significant survival advantage following IR, whereas *Mdm2*^{Y393F} HSPCs display only a marginal possible increase in survival after DNA damage (Figure 3.21).

As with the acute p53 response to DNA damage and spontaneous tumorigenesis, we observed no additive effects on radioresistance when both Mdm2 Tyr393 and Ser394 were mutated. *Mdm2*^{Y393F/S394A} and *Mdm2*^{S394A} mice displayed comparable survival, HSPC numbers, and bone marrow reconstitution following whole body IR (Figures 3.35-3.38). Hence, there is an apparent redundancy of the shared phenotypes between *Mdm2*^{Y393F} and *Mdm2*^{S394A} mice, with tumorigenesis and radioresistance in *Mdm2*^{Y393F/S394A} mice never exceeding that observed in *Mdm2*^{S394A} mice. However, ATM phosphorylation of Mdm2-S394 clearly has a predominant effect on Mdm2-p53 signaling and p53 functions

relative to the effects induced by c-Abl phosphorylation of Mdm2 Tyr393.

We infer that a very slight increase in the survival of *Mdm2*^{Y393F} HSPCs may account for the increased bone marrow repopulation and radioresistance in *Mdm2*^{Y393F} mice, as *Mdm2*^{Y393F/S394A} and *Mdm2*^{S394A} mice display further increased bone marrow repopulation and radioresistance along with significantly higher levels of HSPCs after IR. However, it is possible that the improved repopulation in *Mdm2*^{Y393F} mice is the result of increased cycling of surviving HSPCs, possibly reflecting a different stress (such as reactive oxygen species) that c-Abl phosphorylation of Mdm2 plays a greater role in the response to. As such it would be interesting to perform cell cycle analysis on HSPCs from irradiated WT and Mdm2-mutant mice.

General Conclusions

This dissertation presents a number of findings that appreciably further our understanding of the significance of Mdm2 phosphorylation by DNA damage-responsive kinases on p53 responses and tumor suppression *in vivo*. We show that phosphorylation of different Mdm2 residues by kinases associated with the DNA damage response can profoundly impact Mdm2 stability, p53 stabilization and activation, and tumor suppression. The effects that we observed in response to ATM phosphorylation of Mdm2 Ser394 and c-Abl phosphorylation of Mdm2 Tyr393 were both overlapping and distinct (Figure 4.1).

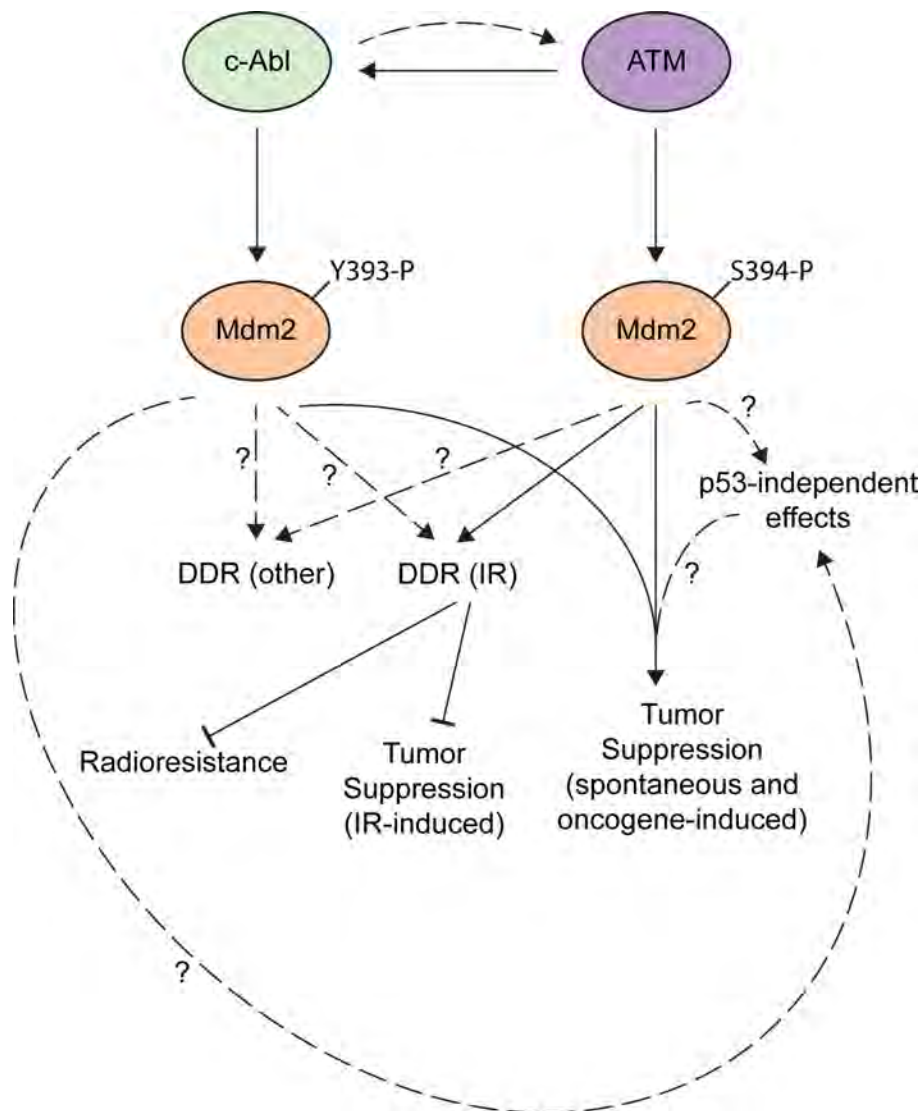


Figure 4.1. Graphical summary of the effects of Mdm2 Tyr393 and Mdm2 Ser394 phosphorylation on p53-dependent DNA damage responses and tumor suppression.

Our findings indicate the potential for an additional layer of pharmaceutical control of the p53 pathway. We have shown phosphorylation of Mdm2 Tyr393 and Mdm2 Ser394 to significantly impact the capacity of HSPCs to repopulate

bone marrow following irradiation and (in the case of Ser394 phosphorylation) simultaneously protect against lymphomagenesis induced by repeated IR exposure. While broad inhibition of DNA damage responsive kinases such as ATM and c-Abl would likely be undesirable due to their involvement in additional processes such as DNA repair, small-molecule therapeutics that inhibit DNA damage-induced Mdm2 phosphorylation events may be useful both in basic research and in the clinic. In patients undergoing radiotherapy, acute p53-dependent apoptosis in normal radiosensitive tissues is a major source of side effects. Transiently blocking DNA damage-induced Mdm2 phosphorylation may prove to be a useful manner of reducing unwanted side effects without compromising p53 tumor suppressive function.

Bibliography

- Adams, J.M., Harris, A.W., Pinkert, C.A., Corcoran, L.M., Alexander, W.S., Cory, S., Palmiter, R.D., and Brinster, R.L. (1985). The c-myc oncogene driven by immunoglobulin enhancers induces lymphoid malignancy in transgenic mice. *Nature* 318, 533–538.
- Agami, R., Blandino, G., Oren, M., and Shaul, Y. (1999). Interaction of c-Abl and p73alpha and their collaboration to induce apoptosis. *Nature* 399, 809–813.
- Allende-Vega, N., Dias, S., Milne, D., and Meek, D. (2005). Phosphorylation of the acidic domain of Mdm2 by protein kinase CK2. *Mol. Cell. Biochem.* 274, 85–90.
- Allende-Vega, N., Sparks, A., Lane, D.P., and Saville, M.K. (2010). MdmX is a substrate for the deubiquitinating enzyme USP2a. *Oncogene* 29, 432–441.
- Alt, J.R., Greiner, T.C., Cleveland, J.L., and Eischen, C.M. (2003). Mdm2 haplo-insufficiency profoundly inhibits Myc-induced lymphomagenesis. *EMBO J.* 22, 1442–1450.
- Alt, J.R., Bouska, A., Fernandez, M.R., Cerny, R.L., Xiao, H., and Eischen, C.M. (2005). Mdm2 binds to Nbs1 at sites of DNA damage and regulates double strand break repair. *J. Biol. Chem.* 280, 18771–18781.
- Armstrong, J.F., Kaufman, M.H., Harrison, D.J., and Clarke, A.R. (1995). High-frequency developmental abnormalities in p53-deficient mice. *Curr. Biol.* 5, 931–936.
- Atadja, P., Wong, H., Garkavtsev, I., Veillette, C., and Riabowol, K. (1995). Increased activity of p53 in senescing fibroblasts. *Proc. Natl. Acad. Sci.* 92, 8348–8352.
- Baker, S., Fearon, E., Nigro, J., Hamilton, Preisinger, A., Jessup, J., vanTuinen, P., Ledbetter, D., Barker, D., Nakamura, Y., et al. (1989). Chromosome 17 deletions and p53 gene mutations in colorectal carcinomas. *Science* 244, 217–221.
- Baker, S., Markowitz, S., Fearon, E., Willson, J., and Vogelstein, B. (1990). Suppression of human colorectal carcinoma cell growth by wild-type p53. *Science* 249, 912–915.

- Banin, S., Moyal, L., Shieh, S., Taya, Y., Anderson, C.W., Chessa, L., Smorodinsky, N.I., Prives, C., Reiss, Y., Shiloh, Y., et al. (1998). Enhanced phosphorylation of p53 by ATM in response to DNA damage. *Science* 281, 1674–1677.
- Baptiste, N., Friedlander, P., Chen, X., and Prives, C. (2002). The proline-rich domain of p53 is required for cooperation with anti-neoplastic agents to promote apoptosis of tumor cells. *Oncogene* 21, 9–21.
- Bargonetti, J., Manfredi, J.J., Chen, X., Marshak, D.R., and Prives, C. (1993). A proteolytic fragment from the central region of p53 has marked sequence-specific DNA-binding activity when generated from wild-type but not from oncogenic mutant p53 protein. *Genes Dev.* 7, 2565–2574.
- Barlow, C., Hirotsune, S., Paylor, R., Liyanage, M., Eckhaus, M., Collins, F., Shiloh, Y., Crawley, J.N., Ried, T., Tagle, D., et al. (1996). Atm-deficient mice: a paradigm of ataxia telangiectasia. *Cell* 86, 159–171.
- Bartel, F., Schulz, J., Bohnke, A., Blumke, K., Kappler, M., Bache, M., Schmidt, H., Wurl, P., Taubert, H., and Hauptmann, S. (2005). Significance of HDMX-S (or MDM4) mRNA splice variant overexpression and HDMX gene amplification on primary soft tissue sarcoma prognosis. *Int. J. Cancer* 117, 469–475.
- Baskaran, R., Wood, L.D., Whitaker, L.L., Canman, C.E., Morgan, S.E., Xu, Y., Barlow, C., Baltimore, D., Wynshaw-Boris, A., Kastan, M.B., et al. (1997). Ataxia telangiectasia mutant protein activates c-Abl tyrosine kinase in response to ionizing radiation. *Nature* 387, 516–519.
- Baudier, J., Delphin, C., Grunwald, D., Khochbin, S., and Lawrence, J.J. (1992). Characterization of the tumor suppressor protein p53 as a protein kinase C substrate and a S100b-binding protein. *Proc. Natl. Acad. Sci.* 89, 11627–11631.
- Ben David, Y., Prideaux, V.R., Chow, V., Benchimol, S., and Bernstein, A. (1988). Inactivation of the p53 oncogene by internal deletion or retroviral integration in erythroleukemic cell lines induced by Friend leukemia virus. *Oncogene* 3, 179–185.
- Bensaad, K., Tsuruta, A., Selak, M.A., Vidal, M.N.C., Nakano, K., Bartrons, R., Gottlieb, E., and Vousden, K.H. (2006). TIGAR, a p53-inducible regulator of glycolysis and apoptosis. *Cell* 126, 107–120.

- Berger, M., Sionov, R.V., Levine, A.J., and Haupt, Y. (2001). A role for the polyproline domain of p53 in its regulation by Mdm2. *J. Biol. Chem.* 276, 3785–3790.
- Bienz, B., Zakut-Houri, R., Givol, D., and Oren, M. (1984). Analysis of the gene coding for the murine cellular tumour antigen p53. *EMBO J.* 3, 2179–2183.
- Bischoff, J.R., Friedman, P.N., Marshak, D.R., Prives, C., and Beach, D. (1990). Human p53 is phosphorylated by p60-cdc2 and cyclin B-cdc2. *Proc. Natl. Acad. Sci.* 87, 4766–4770.
- Blattner, C., Hay, T., Meek, D.W., and Lane, D.P. (2002). Hypophosphorylation of Mdm2 augments p53 stability. *Mol. Cell. Biol.* 22, 6170–6182.
- Boehme, K.A., Kulikov, R., and Blattner, C. (2008). p53 stabilization in response to DNA damage requires Akt/PKB and DNA-PK. *Proc. Natl. Acad. Sci.* 105, 7785–7790.
- Bond, J., Houghton, M., Blaydes, J., Gire, V., Wynford-Thomas, D., and Wyllie, F. (1996). Evidence that transcriptional activation by p53 plays a direct role in the induction of cellular senescence. *Oncogene* 13, 2097–2104.
- Bond, J.A., Wyllie, F.S., and Wynford-Thomas, D. (1994). Escape from senescence in human diploid fibroblasts induced directly by mutant p53. *Oncogene* 9, 1885–1889.
- Boyd, S.D., Tsai, K.Y., and Jacks, T. (2000). An intact HDM2 RING-finger domain is required for nuclear exclusion of p53. *Nat. Cell Biol.* 2, 563–568.
- Brady, C.A., Jiang, D., Mello, S.S., Johnson, T.M., Jarvis, L.A., Kozak, M.M., Broz, D.K., Basak, S., Park, E.J., McLaughlin, M.E., et al. (2011). Distinct p53 transcriptional programs dictate acute DNA-damage responses and tumor suppression. *Cell* 145, 571–583.
- Brugarolas, J., Chandrasekaran, C., Gordon, J.I., Beach, D., Jacks, T., and Hannon, G.J. (1995). Radiation-induced cell cycle arrest compromised by p21 deficiency. *Nature* 377, 552–557.
- Budanov, A.V., Shoshani, T., Faerman, A., Zelin, E., Kamer, I., Kalinski, H., Gorodin, S., Fishman, A., Chajut, A., Einat, P., et al. (2002). Identification of a novel stress-responsive gene Hi95 involved in regulation of cell viability. *Oncogene* 21, 6017–6031.

- Budanov, A.V., Sablina, A.A., Feinstein, E., Koonin, E.V., and Chumakov, P.M. (2004). Regeneration of peroxiredoxins by p53-regulated sestrins, homologs of bacterial AhpD. *Science* 304, 596–600.
- Bueso-Ramos, C.E., Yang, Y., deLeon, E., McCown, P., Stass, S.A., and Albitar, M. (1993). The human MDM-2 oncogene is overexpressed in leukemias. *Blood* 82, 2617–2623.
- Buschmann, T., Lerner, D., Lee, C.-G., and Ronai, Z. 'ev (2001). The Mdm-2 amino terminus is required for Mdm2 binding and SUMO-1 conjugation by the E2 SUMO-1 conjugating enzyme Ubc9. *J. Biol. Chem.* 276, 40389–40395.
- Cahilly-Snyder, L., Yang-Feng, T., Francke, U., and George, D.L. (1987). Molecular analysis and chromosomal mapping of amplified genes isolated from a transformed mouse 3T3 cell line. *Somat. Cell Mol. Genet.* 13, 235–244.
- Candau, R., Scolnick, D.M., Darpino, P., Ying, C.Y., Halazonetis, T.D., and Berger, S.L. (1997). Two tandem and independent sub-activation domains in the amino terminus of p53 require the adaptor complex for activity. *Oncogene* 15, 807–816.
- Canman, C.E., Lim, D.S., Cimprich, K.A., Taya, Y., Tamai, K., Sakaguchi, K., Appella, E., Kastan, M.B., and Siliciano, J.D. (1998). Activation of the ATM kinase by ionizing radiation and phosphorylation of p53. *Science* 281, 1677–1679.
- Chang, C., Simmons, D.T., Martin, M.A., and Mora, P.T. (1979). Identification and partial characterization of new antigens from simian virus 40-transformed mouse cells. *J. Virol.* 31, 463–471.
- Chao, C., Hergenahm, M., Kaeser, M.D., Wu, Z., Saito, S. 'ichi, Iggo, R., Hollstein, M., Appella, E., and Xu, Y. (2003). Cell type- and promoter-specific roles of Ser18 phosphorylation in regulating p53 responses. *J. Biol. Chem.* 278, 41028–41033.
- Chao, C., Herr, D., Chun, J., and Xu, Y. (2006). Ser18 and 23 phosphorylation is required for p53-dependent apoptosis and tumor suppression. *EMBO J.* 25, 2615–2622.
- Chehab, N.H., Malikzay, A., Stavridi, E.S., and Halazonetis, T.D. (1999). Phosphorylation of Ser-20 mediates stabilization of human p53 in response to DNA damage. *Proc. Natl. Acad. Sci.* 96, 13777–13782.

- Chen, C.Y., Oliner, J.D., Zhan, Q., Fornace, A.J.J., Vogelstein, B., and Kastan, M.B. (1994). Interactions between p53 and MDM2 in a mammalian cell cycle checkpoint pathway. *Proc. Natl. Acad. Sci.* *91*, 2684–2688.
- Chen, J., Lin, J., and Levine, A.J. (1995). Regulation of transcription functions of the p53 tumor suppressor by the mdm-2 oncogene. *Mol. Med.* *1*, 142–152.
- Chen, J., Wu, X., Lin, J., and Levine, A.J. (1996). mdm-2 inhibits the G1 arrest and apoptosis functions of the p53 tumor suppressor protein. *Mol. Cell. Biol.* *16*, 2445–2452.
- Chen, L., Gilkes, D.M., Pan, Y., Lane, W.S., and Chen, J. (2005a). ATM and Chk2-dependent phosphorylation of MDMX contribute to p53 activation after DNA damage. *EMBO J.* *24*, 3411–3422.
- Chen, P., Chen, Y., Bookstein, R., and Lee, W. (1990). Genetic mechanisms of tumor suppression by the human p53 gene. *Science* *250*, 1576–1580.
- Chen, Z., Trotman, L.C., Shaffer, D., Lin, H.-K., Dotan, Z.A., Niki, M., Koutcher, J.A., Scher, H.I., Ludwig, T., Gerald, W., et al. (2005b). Crucial role of p53-dependent cellular senescence in suppression of Pten-deficient tumorigenesis. *Nature* *436*, 725–730.
- Cheng, Q., Chen, L., Li, Z., Lane, W.S., and Chen, J. (2009). ATM activates p53 by regulating MDM2 oligomerization and E3 processivity. *EMBO J.* *28*, 3857–3867.
- Cheng, Q., Cross, B., Li, B., Chen, L., Li, Z., and Chen, J. (2011). Regulation of MDM2 E3 ligase activity by phosphorylation after DNA damage. *Mol. Cell. Biol.* *31*, 4951–4963.
- Cheng, T., Rodrigues, N., Shen, H., Yang, Y., Dombkowski, D., Sykes, M., and Scadden, D.T. (2000). Hematopoietic stem cell quiescence maintained by p21cip1/waf1. *Science* *287*, 1804–1808.
- Cho, Y., Gorina, S., Jeffrey, P., and Pavletich, N. (1994). Crystal structure of a p53 tumor suppressor-DNA complex: understanding tumorigenic mutations. *Science* *265*, 346–355.
- Chow, V., Ben-David, Y., Bernstein, A., Benchimol, S., and Mowat, M. (1987). Multistage Friend erythroleukemia: independent origin of tumor clones with normal or rearranged p53 cellular oncogenes. *J. Virol.* *61*, 2777–2781.

- Ciccia, A., and Elledge, S.J. (2010). The DNA damage response: making it safe to play with knives. *Mol. Cell* 40, 179–204.
- Clarke, A.R., Purdie, C.A., Harrison, D.J., Morris, R.G., Bird, C.C., Hooper, M.L., and Wyllie, A.H. (1993). Thymocyte apoptosis induced by p53-dependent and independent pathways. *Nature* 362, 849–852.
- Clarke, A.R., Gledhill, S., Hooper, M.L., Bird, C.C., and Wyllie, A.H. (1994). p53 dependence of early apoptotic and proliferative responses within the mouse intestinal epithelium following gamma-irradiation. *Oncogene* 9, 1767–1773.
- Cordon-Cardo, C., Latres, E., Drobnjak, M., Oliva, M.R., Pollack, D., Woodruff, J.M., Marechal, V., Chen, J., Brennan, M.F., and Levine, A.J. (1994). Molecular abnormalities of mdm2 and p53 genes in adult soft tissue sarcomas. *Cancer Res.* 54, 794–799.
- Damalas, A., Kahan, S., Shtutman, M., Ben-Ze'ev, A., and Oren, M. (2001). Deregulated β -catenin induces a p53- and ARF-dependent growth arrest and cooperates with Ras in transformation. *EMBO J.* 20, 4912–4922.
- Dankort, D., Filenova, E., Collado, M., Serrano, M., Jones, K., and McMahon, M. (2007). A new mouse model to explore the initiation, progression, and therapy of BRAFV600E-induced lung tumors. *Genes Dev.* 21, 379–384.
- Danovi, D., Meulmeester, E., Pasini, D., Migliorini, D., Capra, M., Frenk, R., de Graaf, P., Francoz, S., Gasparini, P., Gobbi, A., et al. (2004). Amplification of Mdmx (or Mdm4) directly contributes to tumor formation by inhibiting p53 tumor suppressor activity. *Mol. Cell. Biol.* 24, 5835–5843.
- Debbas, M., and White, E. (1993). Wild-type p53 mediates apoptosis by E1A, which is inhibited by E1B. *Genes Dev.* 7, 546–554.
- Deng, C., Zhang, P., Harper, J.W., Elledge, S.J., and Leder, P. (1995). Mice lacking p21CIP1/WAF1 undergo normal development, but are defective in G1 checkpoint control. *Cell* 82, 675–684.
- Dias, S.S., Milne, D.M., and Meek, D.W. (2006). c-Abl phosphorylates Hdm2 at tyrosine 276 in response to DNA damage and regulates interaction with ARF. *Oncogene* 25, 6666–6671.

- Di Lello, P., Jenkins, L.M.M., Jones, T.N., Nguyen, B.D., Hara, T., Yamaguchi, H., Dikeakos, J.D., Appella, E., Legault, P., and Omichinski, J.G. (2006). Structure of the Tfb1/p53 complex: Insights into the interaction between the p62/Tfb1 subunit of TFIIH and the activation domain of p53. *Mol. Cell* 22, 731–740.
- Diller, L., Kassel, J., Nelson, C.E., Gryka, M.A., Litwak, G., Gebhardt, M., Bressac, B., Ozturk, M., Baker, S.J., and Vogelstein, B. (1990). p53 functions as a cell cycle control protein in osteosarcomas. *Mol. Cell. Biol.* 10, 5772–5781.
- Dimri, G.P., Itahana, K., Acosta, M., and Campisi, J. (2000). Regulation of a senescence checkpoint response by the E2F1 transcription factor and p14(ARF) tumor suppressor. *Mol. Cell. Biol.* 20, 273–285.
- Dixon, S.J., Lemberg, K.M., Lamprecht, M.R., Skouta, R., Zaitsev, E.M., Gleason, C.E., Patel, D.N., Bauer, A.J., Cantley, A.M., Yang, W.S., et al. (2012). Ferroptosis: an iron-dependent form of nonapoptotic cell death. *Cell* 149, 1060–1072.
- Donehower, L.A., and Lozano, G. (2009). 20 years studying p53 functions in genetically engineered mice. *Nat. Rev. Cancer* 9, 831–841.
- Donehower, L.A., Harvey, M., Slagle, B.L., McArthur, M.J., Montgomery, C.A.J., Butel, J.S., and Bradley, A. (1992). Mice deficient for p53 are developmentally normal but susceptible to spontaneous tumours. *Nature* 356, 215–221.
- Dornan, D., Shimizu, H., Burch, L., Smith, A.J., and Hupp, T.R. (2003). The proline repeat domain of p53 binds directly to the transcriptional coactivator p300 and allosterically controls DNA-dependent acetylation of p53. *Mol. Cell. Biol.* 23, 8846–8861.
- Dumaz, N., Milne, D.M., and Meek, D.W. (1999). Protein kinase CK1 is a p53-threonine 18 kinase which requires prior phosphorylation of serine 15. *FEBS Lett.* 463, 312–316.
- Eischen, C.M., Weber, J.D., Roussel, M.F., Sherr, C.J., and Cleveland, J.L. (1999). Disruption of the ARF-Mdm2-p53 tumor suppressor pathway in Myc-induced lymphomagenesis. *Genes Dev.* 13, 2658–2669.
- Eischen, C.M., Roussel, M.F., Korsmeyer, S.J., and Cleveland, J.L. (2001). Bax loss impairs Myc-induced apoptosis and circumvents the selection of p53 mutations during Myc-mediated lymphomagenesis. *Mol. Cell. Biol.* 21, 7653–7662.

- El-Deiry, W.S., Kern, S.E., Pietenpol, J.A., Kinzler, K.W., and Vogelstein, B. (1992). Definition of a consensus binding site for p53. *Nat. Genet.* 1, 45–49.
- El-Deiry, W.S., Tokino, T., Velculescu, V.E., Levy, D.B., Parsons, R., Trent, J.M., Lin, D., Mercer, W.E., Kinzler, K.W., and Vogelstein, B. (1993). WAF1, a potential mediator of p53 tumor suppression. *Cell* 75, 817–825.
- Eliyahu, D., Raz, A., Gruss, P., Givol, D., and Oren, M. (1984). Participation of p53 cellular tumour antigen in transformation of normal embryonic cells. *Nature* 312, 646–649.
- Eliyahu, D., Michalovitz, D., Eliyahu, S., Pinhasi-Kimhi, O., and Oren, M. (1989). Wild-type p53 can inhibit oncogene-mediated focus formation. *Proc. Natl. Acad. Sci.* 86, 8763–8767.
- Elson, A., Wang, Y., Daugherty, C.J., Morton, C.C., Zhou, F., Campos-Torres, J., and Leder, P. (1996). Pleiotropic defects in ataxia-telangiectasia protein-deficient mice. *Proc. Natl. Acad. Sci.* 93, 13084–13089.
- Evan, G.I., Wyllie, A.H., Gilbert, C.S., Littlewood, T.D., Land, H., Brooks, M., Waters, C.M., Penn, L.Z., and Hancock, D.C. (1992). Induction of apoptosis in fibroblasts by c-myc protein. *Cell* 69, 119–128.
- Fakharzadeh, S.S., Trusko, S.P., and George, D.L. (1991). Tumorigenic potential associated with enhanced expression of a gene that is amplified in a mouse tumor cell line. *EMBO J.* 10, 1565–1569.
- Fang, L., Igarashi, M., Leung, J., Sugrue, M.M., Lee, S.W., and Aaronson, S.A. (1999). p21Waf1/Cip1/Sdi1 induces permanent growth arrest with markers of replicative senescence in human tumor cells lacking functional p53. *Oncogene* 18, 2789–2797.
- Fang, S., Jensen, J.P., Ludwig, R.L., Vousden, K.H., and Weissman, A.M. (2000). Mdm2 is a RING finger-dependent ubiquitin protein ligase for itself and p53. *J. Biol. Chem.* 275, 8945–8951.
- Feng, J., Tamaskovic, R., Yang, Z., Brazil, D.P., Merlo, A., Hess, D., and Hemmings, B.A. (2004). Stabilization of Mdm2 via decreased ubiquitination is mediated by protein kinase B/Akt-dependent phosphorylation. *J. Biol. Chem.* 279, 35510–35517.
- Fields, S., and Jang, S. (1990). Presence of a potent transcription activating sequence in the p53 protein. *Science* 249, 1046–1049.

- Finch, R.A., Donoviel, D.B., Potter, D., Shi, M., Fan, A., Freed, D.D., Wang, C.-Y., Zambrowicz, B.P., Ramirez-Solis, R., Sands, A.T., et al. (2002). mdmx is a negative regulator of p53 activity in vivo. *Cancer Res.* 62, 3221–3225.
- Finlay, C.A. (1993). The mdm-2 oncogene can overcome wild-type p53 suppression of transformed cell growth. *Mol. Cell. Biol.* 13, 301–306.
- Finlay, C.A., Hinds, P.W., Tan, T.H., Eliyahu, D., Oren, M., and Levine, A.J. (1988). Activating mutations for transformation by p53 produce a gene product that forms an hsc70-p53 complex with an altered half-life. *Mol. Cell. Biol.* 8, 531–539.
- Finlay, C.A., Hinds, P.W., and Levine, A.J. (1989). The p53 proto-oncogene can act as a suppressor of transformation. *Cell* 57, 1083–1093.
- Friedler, A., Veprintsev, D.B., Freund, S.M.V., von Glos, K.I., and Fersht, A.R. (2005). Modulation of binding of DNA to the C-terminal domain of p53 by acetylation. *Structure* 13, 629–636.
- Friedman, P.N., Chen, X., Bargonetti, J., and Prives, C. (1993). The p53 protein is an unusually shaped tetramer that binds directly to DNA. *Proc. Natl. Acad. Sci.* 90, 3319–3323.
- Fritsche, M., Haessler, C., and Brandner, G. (1993). Induction of nuclear accumulation of the tumor-suppressor protein p53 by. *Oncogene* 8, 307–318.
- Funk, W.D., Pak, D.T., Karas, R.H., Wright, W.E., and Shay, J.W. (1992). A transcriptionally active DNA-binding site for human p53 protein complexes. *Mol. Cell. Biol.* 12, 2866–2871.
- Gamper, A.M., and Roeder, R.G. (2008). Multivalent binding of p53 to the STAGA complex mediates coactivator recruitment after UV damage. *Mol. Cell. Biol.* 28, 2517–2527.
- Gannon, H.S., and Jones, S.N. (2012). Using mouse models to explore MDM-p53 signaling in development, cell growth, and tumorigenesis. *Genes Cancer* 3, 209–218.
- Gannon, H.S., Woda, B.A., and Jones, S.N. (2012). ATM phosphorylation of Mdm2 Ser394 regulates the amplitude and duration of the DNA damage response in mice. *Cancer Cell* 21, 668–679.

- Garrison, S.P., Jeffers, J.R., Yang, C., Nilsson, J.A., Hall, M.A., Rehg, J.E., Yue, W., Yu, J., Zhang, L., Onciu, M., et al. (2008). Selection against PUMA gene expression in Myc-driven B-cell lymphomagenesis. *Mol. Cell. Biol.* 28, 5391–5402.
- Gembarska, A., Luciani, F., Fedele, C., Russell, E.A., Dewaele, M., Villar, S., Zwolinska, A., Haupt, S., de Lange, J., Yip, D., et al. (2012). MDM4 is a key therapeutic target in cutaneous melanoma. *Nat. Med.* 18, 1239–1247.
- Geyer, R.K., Yu, Z.K., and Maki, C.G. (2000). The MDM2 RING-finger domain is required to promote p53 nuclear export. *Nat. Cell Biol.* 2, 569–573.
- Goldberg, Z., Sionov, R.V., Berger, M., Zwang, Y., Perets, R., Van Etten, R.A., Oren, M., Taya, Y., and Haupt, Y. (2002). Tyrosine phosphorylation of Mdm2 by c-Abl: implications for p53 regulation. *EMBO J.* 21, 3715–3727.
- Gong, J., Costanzo, A., Yang, H.-Q., Melino, G., Kaelin, W.G., Levrero, M., and Wang, J.Y.J. (1999). The tyrosine kinase c-Abl regulates p73 in apoptotic response to cisplatin-induced DNA damage. *Nature* 399, 806–809.
- de Graaf, P., Little, N.A., Ramos, Y.F.M., Meulmeester, E., Letteboer, S.J.F., and Jochemsen, A.G. (2003). Hdmx protein stability is regulated by the ubiquitin ligase activity of Mdm2. *J. Biol. Chem.* 278, 38315–38324.
- Gu, W., and Roeder, R.G. (1997). Activation of p53 sequence-specific DNA binding by acetylation of the p53. *Cell* 90, 595–606.
- Gu, J., Nie, L., Wiederschain, D., and Yuan, Z.M. (2001). Identification of p53 sequence elements that are required for MDM2-mediated nuclear export. *Mol. Cell. Biol.* 21, 8533–8546.
- Gu, J., Kawai, H., Nie, L., Kitao, H., Wiederschain, D., Jochemsen, A.G., Parant, J., Lozano, G., and Yuan, Z.-M. (2002). Mutual dependence of MDM2 and MDMX in their functional inactivation of p53. *J. Biol. Chem.* 277, 19251–19254.
- Gu, W., Shi, X.L., and Roeder, R.G. (1997). Synergistic activation of transcription by CBP and p53. *Nature* 387, 819–823.
- Gudkov, A.V., and Komarova, E.A. (2003). The role of p53 in determining sensitivity to radiotherapy. *Nat. Rev. Cancer* 3, 117–129.
- Gurley, K.E., and Kemp, C.J. (2007). Ataxia-telangiectasia mutated is not required for p53 induction and apoptosis in irradiated epithelial tissues. *Mol. Cancer Res.* 5, 1312–1318.

- Harvey, D.M., and Levine, A.J. (1991). p53 alteration is a common event in the spontaneous immortalization of primary BALB/c murine embryo fibroblasts. *Genes Dev.* 5, 2375–2385.
- Harvey, M., McArthur, M.J., Montgomery, C.A.J., Butel, J.S., Bradley, A., and Donehower, L.A. (1993a). Spontaneous and carcinogen-induced tumorigenesis in p53-deficient mice. *Nat. Genet.* 5, 225–229.
- Harvey, M., Sands, A.T., Weiss, R.S., Hegi, M.E., Wiseman, R.W., Pantazis, P., Giovanella, B.C., Tainsky, M.A., Bradley, A., and Donehower, L.A. (1993b). In vitro growth characteristics of embryo fibroblasts isolated from p53-deficient mice. *Oncogene* 8, 2457–2467.
- Haupt, Y., Barak, Y., and Oren, M. (1996). Cell type-specific inhibition of p53-mediated apoptosis by mdm2. *EMBO J.* 15, 1596–1606.
- Haupt, Y., Maya, R., Kazaz, A., and Oren, M. (1997). Mdm2 promotes the rapid degradation of p53. *Nature* 387, 296–299.
- Hay, T.J., and Meek, D.W. (2000). Multiple sites of in vivo phosphorylation in the MDM2 oncoprotein cluster within two important functional domains. *FEBS Lett.* 478, 183–186.
- He, Y., Tollini, L., Kim, T.-H., Itahana, Y., and Zhang, Y. (2014). The anaphase-promoting complex/cyclosome is an E3 ubiquitin ligase for Mdm2. *Cell Cycle* 13, 2101–2109.
- Hemann, M.T., Zilfou, J.T., Zhao, Z., Burgess, D.J., Hannon, G.J., and Lowe, S.W. (2004). Suppression of tumorigenesis by the p53 target PUMA. *Proc. Natl. Acad. Sci.* 101, 9333–9338.
- Hermeking, H., and Eick, D. (1994). Mediation of c-Myc-induced apoptosis by p53. *Science* 265, 2091–2093.
- Hermeking, H., Lengauer, C., Polyak, K., He, T.C., Zhang, L., Thiagalingam, S., Kinzler, K.W., and Vogelstein, B. (1997). 14-3-3sigma is a p53-regulated inhibitor of G2/M progression. *Mol. Cell* 1, 3–11.
- Herzog, K.H., Chong, M.J., Kapsetaki, M., Morgan, J.I., and McKinnon, P.J. (1998). Requirement for Atm in ionizing radiation-induced cell death in the developing central nervous system. *Science* 280, 1089–1091.

- Higashimoto, Y., Saito, S., Tong, X.H., Hong, A., Sakaguchi, K., Appella, E., and Anderson, C.W. (2000). Human p53 is phosphorylated on serines 6 and 9 in response to DNA damage-inducing agents. *J. Biol. Chem.* *275*, 23199–23203.
- Hinds, P., Finlay, C., and Levine, A.J. (1989). Mutation is required to activate the p53 gene for cooperation with the ras oncogene and transformation. *J. Virol.* *63*, 739–746.
- Hinds, P., Finlay, C., Quartin, R., Baker, S., Fearon, E., Vogelstein, B., and Levine, A. (1990). Mutant p53 DNA clones from human colon carcinomas cooperate with ras in transforming primary rat cells: a comparison of the “hot spot” mutant phenotypes. *Cell Growth Differ.* *1*, 571–580.
- Hirao, A., Kong, Y.Y., Matsuoka, S., Wakeham, A., Ruland, J., Yoshida, H., Liu, D., Elledge, S.J., and Mak, T.W. (2000). DNA damage-induced activation of p53 by the checkpoint kinase Chk2. *Science* *287*, 1824–1827.
- Hjerrild, M., Milne, D., Dumaz, N., Hay, T., Issinger, O.G., and Meek, D. (2001). Phosphorylation of murine double minute clone 2 (MDM2) protein at serine-267 by protein kinase CK2 in vitro and in cultured cells. *Biochem. J.* *355*, 347–356.
- Ho, J., and Benchimol, S. (2003). Transcriptional repression mediated by the p53 tumour suppressor. *Cell Death Differ.* *10*, 404–408.
- Honda, R., and Yasuda, H. (1999). Association of p19(ARF) with Mdm2 inhibits ubiquitin ligase activity of Mdm2 for tumor suppressor p53. *EMBO J.* *18*, 22–27.
- Honda, R., and Yasuda, H. (2000). Activity of MDM2, a ubiquitin ligase, toward p53 or itself is dependent on the RING finger domain of the ligase. *Oncogene* *19*, 1473–1476.
- Honda, R., Tanaka, H., and Yasuda, H. (1997). Oncoprotein MDM2 is a ubiquitin ligase E3 for tumor suppressor p53. *FEBS Lett.* *420*, 25–27.
- Hu, W., Zhang, C., Wu, R., Sun, Y., Levine, A., and Feng, Z. (2010). Glutaminase 2, a novel p53 target gene regulating energy metabolism and antioxidant function. *Proc. Natl. Acad. Sci.* *107*, 7455–7460.
- Huang, L., Yan, Z., Liao, X., Li, Y., Yang, J., Wang, Z.-G., Zuo, Y., Kawai, H., Shadfan, M., Ganapathy, S., et al. (2011). The p53 inhibitors MDM2/MDMX complex is required for control of p53 activity in vivo. *Proc. Natl. Acad. Sci.* *108*, 12001–12006.

- Hupp, T.R., Meek, D.W., Midgley, C.A., and Lane, D.P. (1992). Regulation of the specific DNA binding function of p53. *Cell* 71, 875–886.
- Inuzuka, H., Tseng, A., Gao, D., Zhai, B., Zhang, Q., Shaik, S., Wan, L., Ang, X.L., Mock, C., Yin, H., et al. (2010). Phosphorylation by casein kinase I promotes the turnover of the Mdm2 oncoprotein via the SCF(beta-TRCP) ubiquitin ligase. *Cancer Cell* 18, 147–159.
- Itahana, K., Mao, H., Jin, A., Itahana, Y., Clegg, H.V., Lindström, M.S., Bhat, K.P., Godfrey, V.L., Evan, G.I., and Zhang, Y. (2007). Targeted inactivation of Mdm2 RING finger E3 ubiquitin ligase activity in the mouse reveals mechanistic insights into p53 regulation. *Cancer Cell* 12, 355–366.
- Jacks, T., Remington, L., Williams, B.O., Schmitt, E.M., Halachmi, S., Bronson, R.T., and Weinberg, R.A. (1994). Tumor spectrum analysis in p53-mutant mice. *Curr. Biol.* 4.
- Jackson, M.W., and Berberich, S.J. (2000). MdmX protects p53 from Mdm2-mediated degradation. *Mol. Cell. Biol.* 20, 1001–1007.
- Jackson, S.P., and Bartek, J. (2009). The DNA-damage response in human biology and disease. *Nature* 461, 1071–1078.
- Jenkins, J.R., Rudge, K., and Currie, G.A. (1984). Cellular immortalization by a cDNA clone encoding the transformation-associated phosphoprotein p53. *Nature* 312, 651–654.
- Jiang, L., Kon, N., Li, T., Wang, S.-J., Su, T., Hibshoosh, H., Baer, R., and Gu, W. (2015). Ferroptosis as a p53-mediated activity during tumour suppression. *Nature* 520, 57–62.
- Jones, S.N., Roe, A.E., Donehower, L.A., and Bradley, A. (1995). Rescue of embryonic lethality in Mdm2-deficient mice by absence of p53. *Nature* 378, 206–208.
- Jones, S.N., Hancock, A.R., Vogel, H., Donehower, L.A., and Bradley, A. (1998). Overexpression of Mdm2 in mice reveals a p53-independent role for Mdm2 in tumorigenesis. *Proc. Natl. Acad. Sci.* 95, 15608–15612.
- Kamijo, T., Weber, J.D., Zambetti, G., Zindy, F., Roussel, M.F., and Sherr, C.J. (1998). Functional and physical interactions of the ARF tumor suppressor with p53 and Mdm2. *Proc. Natl. Acad. Sci.* 95, 8292–8297.
- Kaplan, H.S. (1964). The role of radiation on experimental leukemogenesis. *Natl. Cancer Inst. Monogr.* 14, 207–220.

- Kaplan, H.S., and Brown, M.B. (1952). A quantitative dose-response study of lymphoid-tumor development in irradiated C 57 black mice. *J. Natl. Cancer Inst.* 13, 185–208.
- Kastan, M.B., Onyekwere, O., Sidransky, D., Vogelstein, B., and Craig, R.W. (1991). Participation of p53 protein in the cellular response to DNA damage. *Cancer Res.* 51, 6304–6311.
- Kastan, M.B., Zhan, Q., el-Deiry, W.S., Carrier, F., Jacks, T., Walsh, W.V., Plunkett, B.S., Vogelstein, B., and Fornace, A.J.J. (1992). A mammalian cell cycle checkpoint pathway utilizing p53 and GADD45 is defective in ataxia-telangiectasia. *Cell* 71, 587–597.
- Kawai, H., Wiederschain, D., Kitao, H., Stuart, J., Tsai, K.K.C., and Yuan, Z.-M. (2003). DNA damage-induced MDMX degradation is mediated by MDM2. *J. Biol. Chem.* 278, 45946–45953.
- Kawai, H., Lopez-Pajares, V., Kim, M.M., Wiederschain, D., and Yuan, Z.-M. (2007). RING domain-mediated interaction is a requirement for MDM2's E3 ligase activity. *Cancer Res.* 67, 6026–6030.
- Kemp, C.J., Wheldon, T., and Balmain, A. (1994). p53-deficient mice are extremely susceptible to radiation-induced tumorigenesis. *Nat. Genet.* 8, 66–69.
- Kern, S., Kinzler, K., Bruskin, A., Jarosz, D., Friedman, P., Prives, C., and Vogelstein, B. (1991). Identification of p53 as a sequence-specific DNA-binding protein. *Science* 252, 1708–1711.
- Kern, S., Pietenpol, J., Thiagalingam, S., Seymour, A., Kinzler, K., and Vogelstein, B. (1992). Oncogenic forms of p53 inhibit p53-regulated gene expression. *Science* 256, 827–830.
- Kharbanda, S., Ren, R., Pandey, P., Shafman, T.D., Feller, S.M., Weichselbaum, R.R., and Kufe, D.W. (1995). Activation of the c-Abl tyrosine kinase in the stress response to DNA-damaging agents. *Nature* 376, 785–788.
- Khosravi, R., Maya, R., Gottlieb, T., Oren, M., Shiloh, Y., and Shkedy, D. (1999). Rapid ATM-dependent phosphorylation of MDM2 precedes p53 accumulation in response to DNA damage. *Proc. Natl. Acad. Sci.* 96, 14973–14977.

- Kina, T., Ikuta, K., Takayama, E., Wada, K., Majumdar, A.S., Weissman, I.L., and Katsura, Y. (2000). The monoclonal antibody TER-119 recognizes a molecule associated with glycophorin A and specifically marks the late stages of murine erythroid lineage. *Brit. J. Haematol.* *109*, 280–287.
- Komarova, E.A., Christov, K., Faerman, A.I., and Gudkov, A.V. (2000). Different impact of p53 and p21 on the radiation response of mouse tissues. *Oncogene* *19*, 3791–3798.
- Komarova, E.A., Kondratov, R.V., Wang, K., Christov, K., Golovkina, T.V., Goldblum, J.R., and Gudkov, A.V. (2004). Dual effect of p53 on radiation sensitivity in vivo: p53 promotes hematopoietic injury, but protects from gastro-intestinal syndrome in mice. *Oncogene* *23*, 3265–3271.
- Kress, M., May, E., Cassingena, R., and May, P. (1979). Simian virus 40-transformed cells express new species of proteins precipitable by anti-simian virus 40 tumor serum. *J. Virol.* *31*, 472–483.
- Kubbutat, M.H.G., Jones, S.N., and Vousden, K.H. (1997). Regulation of p53 stability by Mdm2. *Nature* *387*, 299–303.
- Kuerbitz, S.J., Plunkett, B.S., Walsh, W.V., and Kastan, M.B. (1992). Wild-type p53 is a cell cycle checkpoint determinant following irradiation. *Proc. Natl. Acad. Sci.* *89*, 7491–7495.
- Kulikov, R., Boehme, K.A., and Blattner, C. (2005). Glycogen synthase kinase 3-dependent phosphorylation of Mdm2 regulates p53 abundance. *Mol. Cell. Biol.* *25*, 7170–7180.
- Kulju, K.S., and Lehman, J.M. (1995). Increased p53 protein associated with aging in human diploid fibroblasts. *Exp. Cell Res.* *217*, 336–345.
- Kussie, P.H., Gorina, S., Marechal, V., Elenbaas, B., Moreau, J., Levine, A.J., and Pavletich, N.P. (1996). Structure of the MDM2 oncoprotein bound to the p53 tumor suppressor transactivation domain. *Science* *274*, 948–953.
- Labi, V., Erlacher, M., Krumschnabel, G., Manzl, C., Tzankov, A., Pinon, J., Egle, A., and Villunger, A. (2010). Apoptosis of leukocytes triggered by acute DNA damage promotes lymphoma formation. *Genes Dev.* *24*, 1602–1607.
- Lane, D.P., and Crawford, L.V. (1979). T antigen is bound to a host protein in SY40-transformed cells. *Nature* *278*, 261–263.

- Laurie, N.A., Donovan, S.L., Shih, C.-S., Zhang, J., Mills, N., Fuller, C., Teunisse, A., Lam, S., Ramos, Y., Mohan, A., et al. (2006). Inactivation of the p53 pathway in retinoblastoma. *Nature* 444, 61–66.
- Leach, F.S., Tokino, T., Meltzer, P., Burrell, M., Oliner, J.D., Smith, S., Hill, D.E., Sidransky, D., Kinzler, K.W., and Vogelstein, B. (1993). p53 Mutation and MDM2 amplification in human soft tissue sarcomas. *Cancer Res.* 53, 2231–2234.
- LeBron, C., Chen, L., Gilkes, D.M., and Chen, J. (2006). Regulation of MDMX nuclear import and degradation by Chk2 and 14-3-3. *EMBO J.* 25, 1196–1206.
- Lee, C.-L., Castle, K.D., Moding, E.J., Blum, J.M., Williams, N., Luo, L., Ma, Y., Borst, L.B., Kim, Y., and Kirsch, D.G. (2015). Acute DNA damage activates the tumour suppressor p53 to promote radiation-induced lymphoma. *Nat. Commun.* 6.
- Lees-Miller, S.P., Sakaguchi, K., Ullrich, S.J., Appella, E., and Anderson, C.W. (1992). Human DNA-activated protein kinase phosphorylates serines 15 and 37 in the amino-terminal transactivation domain of human p53. *Mol. Cell. Biol.* 12, 5041–5049.
- Levav-Cohen, Y., Goldberg, Z., Zuckerman, V., Grossman, T., Haupt, S., and Haupt, Y. (2005). C-Abl as a modulator of p53. *Biochem. Biophys. Res. Commun.* 331, 737–749.
- Levine, A.J. (1997). p53, the cellular gatekeeper for growth and division. *Cell* 88, 323–331.
- Li, M., Chen, D., Shiloh, A., Luo, J., Nikolaev, A.Y., Qin, J., and Gu, W. (2002a). Deubiquitination of p53 by HAUSP is an important pathway for p53 stabilization. *Nature* 416, 648–653.
- Li, M., Luo, J., Brooks, C.L., and Gu, W. (2002b). Acetylation of p53 inhibits its ubiquitination by Mdm2. *J. Biol. Chem.* 277, 50607–50611.
- Li, M., Brooks, C.L., Wu-Baer, F., Chen, D., Baer, R., and Gu, W. (2003). Mono- versus polyubiquitination: differential control of p53 fate by Mdm2. *Science* 302, 1972–1975.
- Li, M., Brooks, C.L., Kon, N., and Gu, W. (2004). A dynamic role of HAUSP in the p53-Mdm2 pathway. *Mol. Cell* 13, 879–886.

- Li, T., Kon, N., Jiang, L., Tan, M., Ludwig, T., Zhao, Y., Baer, R., and Gu, W. (2012). Tumor suppression in the absence of p53-mediated cell cycle arrest, apoptosis, and senescence. *Cell* 149, 1269–1283.
- Linares, L.K., Hengstermann, A., Ciechanover, A., Muller, S., and Scheffner, M. (2003). HdmX stimulates Hdm2-mediated ubiquitination and degradation of p53. *Proc. Natl. Acad. Sci.* 100, 12009–12014.
- Linares, L.K., Kiernan, R., Triboulet, R., Chable-Bessia, C., Latreille, D., Cuvier, O., Lacroix, M., Le Cam, L., Coux, O., and Benkirane, M. (2007). Intrinsic ubiquitination activity of PCAF controls the stability of the oncoprotein Hdm2. *Nat. Cell Biol.* 9, 331–338.
- Linzer, D.I.H., and Levine, A.J. (1979). Characterization of a 54K Dalton cellular SV40 tumor antigen present in SV40-transformed cells and uninfected embryonal carcinoma cells. *Cell* 17, 43–52.
- Liu, T.-J., El-Naggar, A.K., McDonnell, T.J., Steck, K.D., Wang, M., Taylor, D.L., and Clayman, G.L. (1995). Apoptosis induction mediated by wild-type p53 adenoviral gene transfer in squamous cell carcinoma of the head and neck. *Cancer Res.* 55, 3117–3122.
- Liu, Z.-G., Baskaran, R., Lea-Chou, E.T., Wood, L.D., Chen, Y., Karin, M., and Wang, J.Y.J. (1996). Three distinct signalling responses by murine fibroblasts to genotoxic stress. *Nature* 384, 273–276.
- Lohrum, M.A., Woods, D.B., Ludwig, R.L., Balint, E., and Vousden, K.H. (2001). C-terminal ubiquitination of p53 contributes to nuclear export. *Mol. Cell Biol.* 21, 8521–8532.
- Lotem, J., and Sachs, L. (1993). Hematopoietic cells from mice deficient in wild-type p53 are more resistant to induction of apoptosis by some agents. *Blood* 82, 1092–1096.
- Loughery, J., Cox, M., Smith, L.M., and Meek, D.W. (2014). Critical role for p53-serine 15 phosphorylation in stimulating transactivation at p53-responsive promoters. *Nucleic Acids Res.* 42, 7666–7680.
- Lowe, S.W., and Ruley, H.E. (1993). Stabilization of the p53 tumor suppressor is induced by adenovirus 5 E1A and accompanies apoptosis. *Genes Dev.* 7, 535–545.
- Lowe, S.W., Ruley, H.E., Jacks, T., and Housman, D.E. (1993a). p53-dependent apoptosis modulates the cytotoxicity of anticancer agents. *Cell* 74, 957–967.

- Lowe, S.W., Schmitt, E.M., Smith, S.W., Osborne, B.A., and Jacks, T. (1993b). p53 is required for radiation-induced apoptosis in mouse thymocytes. *Nature* 362, 847–849.
- Lowe, S.W., Jacks, T., Housman, D.E., and Ruley, H.E. (1994). Abrogation of oncogene-associated apoptosis allows transformation of p53-deficient cells. *Proc. Natl. Acad. Sci.* 91, 2026–2030.
- Lu, H., and Levine, A.J. (1995). Human TAFII31 protein is a transcriptional coactivator of the p53 protein. *Proc. Natl. Acad. Sci.* 92, 5154–5158.
- Lu, X., Ma, O., Nguyen, T.-A., Jones, S.N., Oren, M., and Donehower, L.A. (2007). The Wip1 Phosphatase acts as a gatekeeper in the p53-Mdm2 autoregulatory loop. *Cancer Cell* 12, 342–354.
- Luo, J., Li, M., Tang, Y., Laszkowska, M., Roeder, R.G., and Gu, W. (2004). Acetylation of p53 augments its site-specific DNA binding both in vitro and in vivo. *Proc. Natl. Acad. Sci.* 101, 2259–2264.
- MacPherson, D., Kim, J., Kim, T., Rhee, B.K., van Oostrom, C.T.M., DiTullio, R.A., Venere, M., Halazonetis, T.D., Bronson, R., de Vries, A., et al. (2004). Defective apoptosis and B-cell lymphomas in mice with p53 point mutation at Ser 23. *EMBO J.* 23, 3689–3699.
- Malonia, S.K., Dutta, P., Santra, M.K., and Green, M.R. (2015). F-box protein FBXO31 directs degradation of MDM2 to facilitate p53-mediated growth arrest following genotoxic stress. *Proc. Natl. Acad. Sci.* 112, 8632–8637.
- Maltzman, W., and Czyzyk, L. (1984). UV irradiation stimulates levels of p53 cellular tumor antigen in nontransformed mouse cells. *Mol. Cell. Biol.* 4, 1689–1694.
- Martinez, J., Georgoff, I., Martinez, J., and Levine, A.J. (1991). Cellular localization and cell cycle regulation by a temperature-sensitive p53 protein. *Genes Dev.* 5, 151–159.
- Martins, C.P., Brown-Swigart, L., and Evan, G.I. (2006). Modeling the therapeutic efficacy of p53 restoration in tumors. *Cell* 127, 1323–1334.
- Matoba, S., Kang, J.-G., Patino, W.D., Wragg, A., Boehm, M., Gavrilova, O., Hurley, P.J., Bunz, F., and Hwang, P.M. (2006). p53 regulates mitochondrial respiration. *Science* 312, 1650–1653.

- Matsumura, T., Yoshihama, Y., Kimura, T., Shintani, S., and Alcalde, R.E. (1996). p53 and MDM2 expression in oral squamous cell carcinoma. *Oncology* 53, 308–312.
- Maya, R., Balass, M., Kim, S.-T., Shkedy, D., Leal, J.-F.M., Shifman, O., Moas, M., Buschmann, T., Ronai, Z. 'ev, Shiloh, Y., et al. (2001). ATM-dependent phosphorylation of Mdm2 on serine 395: role in p53 activation by DNA damage. *Genes Dev.* 15, 1067–1077.
- Mayo, L.D., and Donner, D.B. (2001). A phosphatidylinositol 3-kinase/Akt pathway promotes translocation of Mdm2 from the cytoplasm to the nucleus. *Proc. Natl. Acad. Sci.* 98, 11598–11603.
- McKinney, K., Mattia, M., Gottifredi, V., and Prives, C. (2004). p53 linear diffusion along DNA requires its C terminus. *Mol. Cell* 16, 413–424.
- Meek, D.W. (2015). Regulation of the p53 response and its relationship to cancer. *Biochem. J.* 469, 325–346.
- Meek, D.W., and Anderson, C.W. (2009). Posttranslational modification of p53: cooperative integrators of function. *Cold Spring Harb. Perspect. Biol.* 1, a000950.
- Melero, J., Stitt, D.T., Mangel, W.F., and Carroll, R.B. (1979). Identification of new polypeptide species (48–55K) immunoprecipitable by antiserum to purified large T antigen and present in SV40-infected and -transformed cells. *Virology* 93, 466–480.
- Mendrysa, S.M., McElwee, M.K., Michalowski, J., O'Leary, K.A., Young, K.M., and Perry, M.E. (2003). mdm2 is critical for inhibition of p53 during lymphopoiesis and the response to ionizing irradiation. *Mol. Cell. Biol.* 23, 462–472.
- Merritt, A.J., Potten, C.S., Kemp, C.J., Hickman, J.A., Balmain, A., Lane, D.P., and Hall, P.A. (1994). The role of p53 in spontaneous and radiation-induced apoptosis in the gastrointestinal tract of normal and p53-deficient mice. *Cancer Res.* 54, 614–617.
- Meulmeester, E., Maurice, M.M., Boutell, C., Teunisse, A.F.A.S., Ovaa, H., Abraham, T.E., Dirks, R.W., and Jochemsen, A.G. (2005). Loss of HAUSP-mediated deubiquitination contributes to DNA damage-induced destabilization of Hdmx and Hdm2. *Mol. Cell* 18, 565–576.

- Meyer, K.D., Lin, S.-C., Bernecky, C., Gao, Y., and Taatjes, D.J. (2010). p53 activates transcription by directing structural shifts in Mediator. *Nat. Struct. Mol. Biol.* 17, 753–760.
- Michalak, E., Jansen, E., Hoppo, L., Cragg, M., Tai, L., Smyth, G., Strasser, A., Adams, J., and Scott, C. (2009). Puma and to a lesser extent Noxa are suppressors of Myc-induced lymphomagenesis. *Cell Death Differ.* 16, 684–696.
- Michalak, E.M., Vandenberg, C.J., Delbridge, A.R.D., Wu, L., Scott, C.L., Adams, J.M., and Strasser, A. (2010). Apoptosis-promoted tumorigenesis: γ -irradiation-induced thymic lymphomagenesis requires Puma-driven leukocyte death. *Genes Dev.* 24, 1608–1613.
- Michalovitz, D., Halevy, O., and Oren, M. (1990). Conditional inhibition of transformation and of cell proliferation by a temperature-sensitive mutant of p53. *Cell* 62, 671–680.
- Midgley, C.A., Desterro, J.M., Saville, M.K., Howard, S., Sparks, A., Hay, R.T., and Lane, D.P. (2000). An N-terminal p14ARF peptide blocks Mdm2-dependent ubiquitination in vitro and can activate p53 in vivo. *Oncogene* 19, 2312–2323.
- Migliorini, D., Denchi, E.L., Danovi, D., Jochemsen, A., Capillo, M., Gobbi, A., Helin, K., Pelicci, P.G., and Marine, J.-C. (2002). Mdm4 (Mdmx) regulates p53-induced growth arrest and neuronal cell death during early embryonic mouse development. *Mol. Cell. Biol.* 22, 5527–5538.
- Miller, C.W., Aslo, A., Won, A., Tan, M., Lampkin, B., and Koeffler, H.P. (1996). Alterations of the p53, Rb and MDM2 genes in osteosarcoma. *J. Cancer Res. Clin. Oncol.* 122, 559–565.
- Momand, J., Zambetti, G.P., Olson, D.C., George, D., and Levine, A.J. (1992). The mdm-2 oncogene product forms a complex with the p53 protein and inhibits p53-mediated transactivation. *Cell* 69, 1237–1245.
- Momand, J., Jung, D., Wilczynski, S., and Niland, J. (1998). The MDM2 gene amplification database. *Nucleic Acids Res.* 26, 3453–3459.
- Montes de Oca Luna, R., Wagner, D.S., and Lozano, G. (1995). Rescue of early embryonic lethality in mdm2-deficient mice by deletion of p53. *Nature* 378, 203–206.

- Mowat, M., Cheng, A., Kimura, N., Bernstein, A., and Benchimol, S. (1985). Rearrangements of the cellular p53 gene in erythroleukaemic cells transformed by Friend virus. *Nature* 314, 633–636.
- Munroe, D.G., Rovinski, B., Bernstein, A., and Benchimol, S. (1988). Loss of a highly conserved domain on p53 as a result of gene deletion during Friend virus-induced erythroleukemia. *Oncogene* 2, 621–624.
- Nakamura, S., Roth, J.A., and Mukhopadhyay, T. (2000). Multiple lysine mutations in the C-terminal domain of p53 interfere with MDM2-dependent protein degradation and ubiquitination. *Mol. Cell. Biol.* 20, 9391–9398.
- Nakano, K., and Vousden, K.H. (2001). PUMA, a novel proapoptotic gene, is induced by p53. *Mol. Cell* 7, 683–694.
- Na Nakorn, T., Traver, D., Weissman, I.L., and Akashi, K. (2002). Myeloerythroid-restricted progenitors are sufficient to confer radioprotection and provide the majority of day 8 CFU-S. *J. Clin. Invest.* 109, 1579–1585.
- Nam, E.A., and Cortez, D. (2011). ATR signalling: more than meeting at the fork. *Biochem. J.* 436, 527–536.
- Noda, A., Ning, Y., Venable, S.F., Pereira-Smith, O.M., and Smith, J.R. (1994). Cloning of senescent cell-derived inhibitors of DNA synthesis using an expression screen. *Exp. Cell Res.* 211, 90–98.
- Oda, E., Ohki, R., Murasawa, H., Nemoto, J., Shibue, T., Yamashita, T., Tokino, T., Taniguchi, T., and Tanaka, N. (2000). Noxa, a BH3-only member of the Bcl-2 family and candidate mediator of p53-induced apoptosis. *Science* 288, 1053–1058.
- O’Gorman, S., Dagenais, N.A., Qian, M., and Marchuk, Y. (1997). Protamine-Cre recombinase transgenes efficiently recombine target sequences in the male germ line of mice, but not in embryonic stem cells. *Proc. Natl. Acad. Sci.* 94, 14602–14607.
- Ohki, R., Nemoto, J., Murasawa, H., Oda, E., Inazawa, J., Tanaka, N., and Taniguchi, T. (2000). Reprimo, a new candidate mediator of the p53-mediated cell cycle arrest at the G2 phase. *J. Biol. Chem.* 275, 22627–22630.

- Okamoto, K., Kashima, K., Pereg, Y., Ishida, M., Yamazaki, S., Nota, A., Teunisse, A., Migliorini, D., Kitabayashi, I., Marine, J.-C., et al. (2005). DNA damage-induced phosphorylation of MdmX at serine 367 activates p53 by targeting MdmX for Mdm2-dependent degradation. *Mol. Cell. Biol.* 25, 9608–9620.
- Oliner, J.D., Kinzler, K.W., Meltzer, P.S., George, D.L., and Vogelstein, B. (1992). Amplification of a gene encoding a p53-associated protein in human sarcomas. *Nature* 358, 80–83.
- Oliner, J.D., Pietenpol, J.A., Thiagalingam, S., Gyuris, J., Kinzler, K.W., and Vogelstein, B. (1993). Oncoprotein MDM2 conceals the activation domain of tumour suppressor p53. *Nature* 362, 857–860.
- van Os, R., Kamminga, L.M., Ausema, A., Bystrykh, L.V., Draijer, D.P., van Pelt, K., Dontje, B., and de Haan, G. (2007). A limited role for p21Cip1/Waf1 in maintaining normal hematopoietic stem cell functioning. *Stem Cells* 25, 836–843.
- Palmero, I., Pantoja, C., and Serrano, M. (1998). p19ARF links the tumour suppressor p53 to Ras. *Nature* 395, 125–126.
- Pan, Y., and Chen, J. (2003). MDM2 promotes ubiquitination and degradation of MDMX. *Mol. Cell. Biol.* 23, 5113–5121.
- Pant, V., Xiong, S., Iwakuma, T., Quintás-Cardama, A., and Lozano, G. (2011). Heterodimerization of Mdm2 and Mdm4 is critical for regulating p53 activity during embryogenesis but dispensable for p53 and Mdm2 stability. *Proc. Natl. Acad. Sci.* 108, 11995–12000.
- Pant, V., Quintás-Cardama, A., and Lozano, G. (2012). The p53 pathway in hematopoiesis: lessons from mouse models, implications for humans. *Blood* 120, 5118–5127.
- Pant, V., Xiong, S., Jackson, J.G., Post, S.M., Abbas, H.A., Quintás-Cardama, A., Hamir, A.N., and Lozano, G. (2013). The p53–Mdm2 feedback loop protects against DNA damage by inhibiting p53 activity but is dispensable for p53 stability, development, and longevity. *Genes Dev.* 27, 1857–1867.
- Parada, L.F., Land, H., Weinberg, R.A., Wolf, D., and Rotter, V. (1984). Cooperation between gene encoding p53 tumour antigen and ras in cellular transformation. *Nature* 312, 649–651.

- Parant, J., Chavez-Reyes, A., Little, N.A., Yan, W., Reinke, V., Jochemsen, A.G., and Lozano, G. (2001). Rescue of embryonic lethality in Mdm4-null mice by loss of Trp53 suggests a nonoverlapping pathway with MDM2 to regulate p53. *Nat. Genet.* 29, 92–95.
- Pavletich, N.P., Chambers, K.A., and Pabo, C.O. (1993). The DNA-binding domain of p53 contains the four conserved regions and the major mutation hot spots. *Genes Dev.* 7, 2556–2564.
- Peeters, H., Debeer, P., Bairoch, A., Wilquet, V., Huysmans, C., Parthoens, E., Fryns, J.P., Gewillig, M., Nakamura, Y., Niikawa, N., et al. (2003). PA26 is a candidate gene for heterotaxia in humans: identification of a novel. *Hum. Genet.* 112, 573–580.
- Pennica, D., Goeddel, D.V., Hayflick, J.S., Reich, N.C., Anderson, C.W., and Levine, A.J. (1984). The amino acid sequence of murine p53 determined from a c-DNA clone. *Virology* 134, 477–482.
- Pereg, Y., Shkedy, D., de Graaf, P., Meulmeester, E., Edelson-Averbukh, M., Salek, M., Biton, S., Teunisse, A.F.A.S., Lehmann, W.D., Jochemsen, A.G., et al. (2005). Phosphorylation of Hdmx mediates its Hdm2- and ATM-dependent degradation in response to DNA damage. *Proc. Natl. Acad. Sci.* 102, 5056–5061.
- Pereg, Y., Lam, S., Teunisse, A., Biton, S., Meulmeester, E., Mittelman, L., Buscemi, G., Okamoto, K., Taya, Y., Shiloh, Y., et al. (2006). Differential roles of ATM- and Chk2-mediated phosphorylations of Hdmx in response to DNA damage. *Mol. Cell. Biol.* 26, 6819–6831.
- Pierce, A.M., Gimenez-Conti, I.B., Schneider-Broussard, R., Martinez, L.A., Conti, C.J., and Johnson, D.G. (1998). Increased E2F1 activity induces skin tumors in mice heterozygous and nullizygous for p53. *Proc. Natl. Acad. Sci.* 95, 8858–8863.
- Polyak, K., Waldman, T., He, T.C., Kinzler, K.W., and Vogelstein, B. (1996). Genetic determinants of p53-induced apoptosis and growth arrest. *Genes Dev.* 10, 1945–1952.
- Pomerantz, J., Schreiber-Agus, N., Liegeois, N.J., Silverman, A., Alland, L., Chin, L., Potes, J., Chen, K., Orlow, I., Lee, H.W., et al. (1998). The Ink4a tumor suppressor gene product, p19Arf, interacts with MDM2 and neutralizes MDM2's inhibition of p53. *Cell* 92, 713–723.

- Post, S.M., Quintas-Cardama, A., Terzian, T., Smith, C., Eischen, C.M., and Lozano, G. (2010). p53-dependent senescence delays Emu-myc-induced B-cell lymphomagenesis. *Oncogene* 29, 1260–1269.
- Purdie, C.A., Harrison, D.J., Peter, A., Dobbie, L., White, S., Howie, S.E., Salter, D.M., Bird, C.C., Wyllie, A.H., and Hooper, M.L. (1994). Tumour incidence, spectrum and ploidy in mice with a large deletion in the p53 gene. *Oncogene* 9, 603–609.
- Raycroft, L., Wu, H., and Lozano, G. (1990). Transcriptional activation by wild-type but not transforming mutants of the p53 anti-oncogene. *Science* 249, 1049–1051.
- Reifenberger, G., Liu, L., Ichimura, K., Schmidt, E.E., and Collins, V.P. (1993). Amplification and overexpression of the MDM2 gene in a subset of human malignant gliomas without p53 mutations. *Cancer Res.* 53, 2736–2739.
- Riemenschneider, M.J., Knobbe, C.B., and Reifenberger, G. (2003). Refined mapping of 1q32 amplicons in malignant gliomas confirms MDM4 as the main amplification target. *Int. J. Cancer* 104, 752–757.
- Riley, T., Sontag, E., Chen, P., and Levine, A. (2008). Transcriptional control of human p53-regulated genes. *Nat. Rev. Mol. Cell Biol.* 9, 402–412.
- Rodriguez, M.S., Desterro, J.M.P., Lain, S., Lane, D.P., and Hay, R.T. (2000). Multiple C-terminal lysine residues target p53 for ubiquitin-proteasome-mediated degradation. *Mol. Cell. Biol.* 20, 8458–8467.
- Roth, J., Koch, P., Contente, A., and Dobbelstein, M. (2000). Tumor-derived mutations within the DNA-binding domain of p53 that phenotypically resemble the deletion of the proline-rich domain. *Oncogene* 19, 1834–1842.
- de Rozières, S., Maya, R., Oren, M., and Lozano, G. (2000). The loss of mdm2 induces p53-mediated apoptosis. *Oncogene* 19, 1691–1697.
- Sah, V.P., Attardi, L.D., Mulligan, G.J., Williams, B.O., Bronson, R.T., and Jacks, T. (1995). A subset of p53-deficient embryos exhibit exencephaly. *Nat. Genet.* 10, 175–180.
- Saito, S., Goodarzi, A.A., Higashimoto, Y., Noda, Y., Lees-Miller, S.P., Appella, E., and Anderson, C.W. (2002). ATM mediates phosphorylation at multiple p53 sites, including Ser(46), in response to ionizing radiation. *J. Biol. Chem.* 277, 12491–12494.

- Sakaguchi, K., Herrera, J.E., Saito, S., Miki, T., Bustin, M., Vassilev, A., Anderson, C.W., and Appella, E. (1998). DNA damage activates p53 through a phosphorylation-acetylation cascade. *Genes Dev.* 12, 2831–2841.
- Sakaguchi, K., Saito, S., Higashimoto, Y., Roy, S., Anderson, C.W., and Appella, E. (2000). Damage-mediated phosphorylation of human p53 threonine 18 through a cascade mediated by a casein 1-like kinase. Effect on Mdm2 binding. *J. Biol. Chem.* 275, 9278–9283.
- Sakamuro, D., Sabbatini, P., White, E., and Prendergast, G.C. (1997). The polyproline region of p53 is required to activate apoptosis but not growth arrest. *Oncogene* 15, 887–898.
- Santra, M.K., Wajapeyee, N., and Green, M.R. (2009). F-box protein FBXO31 mediates cyclin D1 degradation to induce G1 arrest after DNA damage. *Nature* 459, 722–725.
- Sawyers, C.L., McLaughlin, J., Goga, A., Havlik, M., and Witte, O. (1994). The nuclear tyrosine kinase c-Abl negatively regulates cell growth. *Cell* 77, 121–131.
- Schmitt, C.A., McCurrach, M.E., de Stanchina, E., Wallace-Brodeur, R.R., and Lowe, S.W. (1999). INK4a/ARF mutations accelerate lymphomagenesis and promote chemoresistance by disabling p53. *Genes Dev.* 13, 2670–2677.
- Schmitt, C.A., Fridman, J.S., Yang, M., Baranov, E., Hoffman, R.M., and Lowe, S.W. (2002). Dissecting p53 tumor suppressor functions in vivo. *Cancer Cell* 1, 289–298.
- Serrano, M., Lin, A.W., McCurrach, M.E., Beach, D., and Lowe, S.W. (1997). Oncogenic ras provokes premature cell senescence associated with accumulation of p53 and p16INK4a. *Cell* 88, 593–602.
- Shafman, T., Khanna, K.K., Kedar, P., Spring, K., Kozlov, S., Yen, T., Hobson, K., Gatei, M., Zhang, N., Watters, D., et al. (1997). Interaction between ATM protein and c-Abl in response to DNA damage. *Nature* 387, 520–523.
- Shao, L., Sun, Y., Zhang, Z., Feng, W., Gao, Y., Cai, Z., Wang, Z.Z., Look, A.T., and Wu, W.-S. (2010). Deletion of proapoptotic Puma selectively protects hematopoietic stem and progenitor cells against high-dose radiation. *Blood* 115, 4707–4714.

- Sharp, D.A., Kratowicz, S.A., Sank, M.J., and George, D.L. (1999). Stabilization of the MDM2 oncoprotein by interaction with the structurally related MDMX protein. *J. Biol. Chem.* *274*, 38189–38196.
- Shaulian, E., Zauberman, A., Ginsberg, D., and Oren, M. (1992). Identification of a minimal transforming domain of p53: negative dominance through abrogation of sequence-specific DNA binding. *Mol. Cell. Biol.* *12*, 5581–5592.
- Shaw, P., Bovey, R., Tardy, S., Sahli, R., Sordat, B., and Costa, J. (1992). Induction of apoptosis by wild-type p53 in a human colon tumor-derived cell line. *Proc. Natl. Acad. Sci.* *89*, 4495–4499.
- Sheikh, M.S., Shao, Z.M., Hussain, A., and Fontana, J.A. (1993). The p53-binding protein MDM2 gene is differentially expressed in human breast carcinoma. *Cancer Res.* *53*, 3226–3228.
- Sherr, C.J., Bertwistle, D., Den Besten, W., Kuo, M.-L., Sugimoto, M., Tago, K., Williams, R.T., Zindy, F., and Roussel, M.F. (2005). p53-Dependent and -independent functions of the Arf tumor suppressor. *Cold Spring Harb. Symp. Quant. Biol.* *70*, 129–137.
- Shieh, S.Y., Ikeda, M., Taya, Y., and Prives, C. (1997). DNA damage-induced phosphorylation of p53 alleviates inhibition by MDM2. *Cell* *91*, 325–334.
- Shieh, S.Y., Ahn, J., Tamai, K., Taya, Y., and Prives, C. (2000). The human homologs of checkpoint kinases Chk1 and Cds1 (Chk2) phosphorylate p53 at multiple DNA damage-inducible sites. *Genes Dev.* *14*, 289–300.
- Shiloh, Y., and Ziv, Y. (2013). The ATM protein kinase: regulating the cellular response to genotoxic stress, and more. *Nat Rev Mol Cell Biol* *14*, 197–210.
- Shvarts, A., Steegenga, W.T., Riteco, N., van Laar, T., Dekker, P., Bazuine, M., van Ham, R.C., van der Houven van Oordt, W., Hateboer, G., van der Eb, A.J., et al. (1996). MDMX: a novel p53-binding protein with some functional properties of MDM2. *EMBO J.* *15*, 5349–5357.
- Shvarts, A., Bazuine, M., Dekker, P., Ramos, Y.F., Steegenga, W.T., Merckx, G., van Ham, R.C., van der Houven van Oordt, W., van der Eb, A.J., and Jochemsen, A.G. (1997). Isolation and identification of the human homolog of a new p53-binding protein, Mdmx. *Genomics* *43*, 34–42.

- Siliciano, J.D., Canman, C.E., Taya, Y., Sakaguchi, K., Appella, E., and Kastan, M.B. (1997). DNA damage induces phosphorylation of the amino terminus of p53. *Genes Dev.* *11*, 3471–3481.
- Sionov, R.V., Moallem, E., Berger, M., Kazaz, A., Gerlitz, O., Ben-Neriah, Y., Oren, M., and Haupt, Y. (1999). c-Abl neutralizes the inhibitory effect of Mdm2 on p53. *J. Biol. Chem.* *274*, 8371–8374.
- Sionov, R.V., Coen, S., Goldberg, Z., Berger, M., Bercovich, B., Ben-Neriah, Y., Ciechanover, A., and Haupt, Y. (2001). c-Abl regulates p53 levels under normal and stress conditions by preventing its nuclear export and ubiquitination. *Mol. Cell. Biol.* *21*, 5869–5878.
- Sluss, H.K., Armata, H., Gallant, J., and Jones, S.N. (2004). Phosphorylation of serine 18 regulates distinct p53 functions in mice. *Mol. Cell. Biol.* *24*, 976–984.
- Sluss, H.K., Gannon, H., Coles, A.H., Shen, Q., Eischen, C.M., and Jones, S.N. (2010). Phosphorylation of p53 serine 18 upregulates apoptosis to suppress Myc-induced tumorigenesis. *Mol. Cancer Res.* *8*, 216–222.
- Soussi, T., and Beroud, C. (2001). Assessing TP53 status in human tumours to evaluate clinical outcome. *Nat. Rev. Cancer* *1*, 233–239.
- Stad, R., Ramos, Y.F., Little, N., Grivell, S., Attema, J., van Der Eb, A.J., and Jochemsen, A.G. (2000). Hdmx stabilizes Mdm2 and p53. *J. Biol. Chem.* *275*, 28039–28044.
- de Stanchina, E., McCurrach, M.E., Zindy, F., Shieh, S.Y., Ferbeyre, G., Samuelson, A.V., Prives, C., Roussel, M.F., Sherr, C.J., and Lowe, S.W. (1998). E1A signaling to p53 involves the p19(ARF) tumor suppressor. *Genes Dev.* *12*, 2434–2442.
- Steinman, H.A., Sluss, H.K., Sands, A.T., Pihan, G., and Jones, S.N. (2004). Absence of p21 partially rescues Mdm4 loss and uncovers an antiproliferative effect of Mdm4 on cell growth. *Oncogene* *23*, 303–306.
- Stenger, J.E., Mayr, G.A., Mann, K., and Tegtmeyer, P. (1992). Formation of stable p53 homotetramers and multiples of tetramers. *Mol. Carcinog.* *5*, 102–106.
- Stevenson, L.F., Sparks, A., Allende-Vega, N., Xirodimas, D.P., Lane, D.P., and Saville, M.K. (2007). The deubiquitinating enzyme USP2a regulates the p53 pathway by targeting Mdm2. *EMBO J.* *26*, 976–986.

- Stommel, J.M., and Wahl, G.M. (2004). Accelerated MDM2 auto-degradation induced by DNA-damage kinases is required for p53 activation. *EMBO J.* 23, 1547–1556.
- Stott, F.J., Bates, S., James, M.C., McConnell, B.B., Starborg, M., Brookes, S., Palmero, I., Ryan, K., Hara, E., Vousden, K.H., et al. (1998). The alternative product from the human CDKN2A locus, p14ARF, participates in a regulatory feedback loop with p53 and MDM2. *EMBO J.* 17, 5001–5014.
- Sturzbecher, H.W., Maimets, T., Chumakov, P., Brain, R., Addison, C., Simanis, V., Rudge, K., Philp, R., Grimaldi, M., and Court, W. (1990). p53 interacts with p34cdc2 in mammalian cells: implications for cell cycle control and oncogenesis. *Oncogene* 5, 795–781.
- Sturzbecher, H.W., Brain, R., Addison, C., Rudge, K., Remm, M., Grimaldi, M., Keenan, E., and Jenkins, J.R. (1992). A C-terminal alpha-helix plus basic region motif is the major structural determinant of p53 tetramerization. *Oncogene* 7, 1513–1523.
- Sugrue, M.M., Shin, D.Y., Lee, S.W., and Aaronson, S.A. (1997). Wild-type p53 triggers a rapid senescence program in human tumor cells lacking functional p53. *Proc. Natl. Acad. Sci.* 94, 9648–9653.
- Suzuki, S., Tanaka, T., Poyurovsky, M.V., Nagano, H., Mayama, T., Ohkubo, S., Lokshin, M., Hosokawa, H., Nakayama, T., Suzuki, Y., et al. (2010). Phosphate-activated glutaminase (GLS2), a p53-inducible regulator of glutamine metabolism and reactive oxygen species. *Proc. Natl. Acad. Sci.* 107, 7461–7466.
- Symonds, H., Krall, L., Remington, L., Saenz-Robles, M., Lowe, S., Jacks, T., and Van Dyke, T. (1994). p53-Dependent apoptosis suppresses tumor growth and progression in vivo. *Cell* 78, 703–711.
- Tang, J., Qu, L.-K., Zhang, J., Wang, W., Michaelson, J.S., Degenhardt, Y.Y., El-Deiry, W.S., and Yang, X. (2006). Critical role for Daxx in regulating Mdm2. *Nat Cell Biol* 8, 855–862.
- Tang, J., Agrawal, T., Cheng, Q., Qu, L., Brewer, M.D., Chen, J., and Yang, X. (2013). Phosphorylation of Daxx by ATM contributes to DNA damage-induced p53 activation. *PLoS One* 8, e55813.
- Tanimura, S., Ohtsuka, S., Mitsui, K., Shirouzu, K., Yoshimura, A., and Ohtsubo, M. (1999). MDM2 interacts with MDMX through their RING finger domains. *FEBS Lett.* 447, 5–9.

- Tao, W., and Levine, A.J. (1999). P19ARF stabilizes p53 by blocking nucleocytoplasmic shuttling of Mdm2. *Proc. Natl. Acad. Sci.* *96*, 6937–6941.
- Terzian, T., Wang, Y., Van Pelt, C.S., Box, N.F., Travis, E.L., and Lozano, G. (2007). Haploinsufficiency of Mdm2 and Mdm4 in tumorigenesis and development. *Mol. Cell. Biol.* *27*, 5479–5485.
- Teufel, D.P., Freund, S.M., Bycroft, M., and Fersht, A.R. (2007). Four domains of p300 each bind tightly to a sequence spanning both transactivation subdomains of p53. *Proc. Natl. Acad. Sci.* *104*, 7009–7014.
- Thut, C., Chen, J., Klemm, R., and Tjian, R. (1995). p53 transcriptional activation mediated by coactivators TAFII40 and TAFII60. *Science* *267*, 100–104.
- Toledo, F., Krummel, K.A., Lee, C.J., Liu, C.-W., Rodewald, L.-W., Tang, M., and Wahl, G.M. (2006). A mouse p53 mutant lacking the proline-rich domain rescues Mdm4 deficiency and provides insight into the Mdm2-Mdm4-p53 regulatory network. *Cancer Cell* *9*, 273–285.
- Toledo, F., Lee, C.J., Krummel, K.A., Rodewald, L.-W., Liu, C.-W., and Wahl, G.M. (2007). Mouse mutants reveal that putative protein interaction sites in the p53 proline-rich domain are dispensable for tumor suppression. *Mol. Cell. Biol.* *27*, 1425–1432.
- Tollini, L.A., Jin, A., Park, J., and Zhang, Y. (2014). Regulation of p53 by Mdm2 E3 ligase function is dispensable in embryogenesis and development, but essential in response to DNA damage. *Cancer Cell* *26*, 235–247.
- Toshiyuki, M., and Reed, J.C. (1995). Tumor suppressor p53 is a direct transcriptional activator of the human bax gene. *Cell* *80*, 293–299.
- Tsukada, T., Tomooka, Y., Takai, S., Ueda, Y., Nishikawa, S., Yagi, T., Tokunaga, T., Takeda, N., Suda, Y., and Abe, S. (1993). Enhanced proliferative potential in culture of cells from p53-deficient mice. *Oncogene* *8*, 3313–3322.
- Uchida, N., Aguila, H.L., Fleming, W.H., Jerabek, L., and Weissman, I.L. (1994). Rapid and sustained hematopoietic recovery in lethally irradiated mice transplanted with purified Thy-1.1lo Lin-Sca-1+ hematopoietic stem cells. *Blood* *83*, 3758–3779.
- Unger, T., Juven-Gershon, T., Moallem, E., Berger, M., Sionov, R.V., Lozano, G., Oren, M., and Haupt, Y. (1999). Critical role for Ser20 of human p53 in the negative regulation of p53 by Mdm2. *EMBO J.* *18*, 1805–1814.

- Valente, L.J., Gray, D.H.D., Michalak, E.M., Pinon-Hofbauer, J., Egle, A., Scott, C.L., Janic, A., and Strasser, A. (2013). p53 efficiently suppresses tumor development in the complete absence of its cell-cycle inhibitory and proapoptotic effectors p21, Puma, and Noxa. *Cell Rep.* 3, 1339–1345.
- Velasco-Miguel, S., Buckbinder, L., Jean, P., Gelbert, L., Talbott, R., Laidlaw, J., Seizinger, B., and Kley, N. (1999). PA26, a novel target of the p53 tumor suppressor and member of the GADD family of DNA damage and growth arrest inducible genes. *Oncogene* 18, 127–137.
- Venkatachalam, S., Shi, Y.P., Jones, S.N., Vogel, H., Bradley, A., Pinkel, D., and Donehower, L.A. (1998). Retention of wild-type p53 in tumors from p53 heterozygous mice: reduction of p53 dosage can promote cancer formation. *EMBO J.* 17, 4657–4667.
- Venkatachalam, S., Tyner, S.D., Pickering, C.R., Boley, S., Recio, L., French, J.E., and Donehower, L.A. (2001). Is p53 haploinsufficient for tumor suppression? Implications for the p53^{+/-} mouse model in carcinogenicity testing. *Toxicol. Pathol.* 29, 147–154.
- Venot, C., Maratrat, M., Sierra, V., Conseiller, E., and Debussche, L. (1999). Definition of a p53 transactivation function-deficient mutant and characterization of two independent p53 transactivation subdomains. *Oncogene* 18, 2405–2410.
- Ventura, A., Kirsch, D.G., McLaughlin, M.E., Tuveson, D.A., Grimm, J., Lintault, L., Newman, J., Reczek, E.E., Weissleder, R., and Jacks, T. (2007). Restoration of p53 function leads to tumour regression in vivo. *Nature* 445, 661–665.
- Vousden, K.H., and Lu, X. (2002). Live or let die: the cell's response to p53. *Nat. Rev. Cancer* 2, 594–604.
- Wagner, A.J., Kokontis, J.M., and Hay, N. (1994). Myc-mediated apoptosis requires wild-type p53 in a manner independent of cell cycle arrest and the ability of p53 to induce p21^{waf1/cip1}. *Genes Dev.* 8, 2817–2830.
- Walker, K.K., and Levine, A.J. (1996). Identification of a novel p53 functional domain that is necessary for efficient growth suppression. *Proc. Natl. Acad. Sci.* 93, 15335–15340.
- Wang, J.Y. (2014). The capable ABL: what is its biological function? *Mol. Cell. Biol.* 34, 1188–1197.

- Wang, X., Zeng, L., Wang, J., Chau, J.F.L., Lai, K.P., Jia, D., Poonepalli, A., Hande, M.P., Liu, H., He, G., et al. (2011a). A positive role for c-Abl in Atm and Atr activation in DNA damage response. *Cell Death Differ.* 18, 5–15.
- Wang, X., Wang, J., and Jiang, X. (2011b). MdmX protein is essential for Mdm2 protein-mediated p53 polyubiquitination. *J. Biol. Chem.* 286, 23725–23734.
- Wang, Y., Blandino, G., and Givol, D. (1999). Induced p21waf expression in H1299 cell line promotes cell senescence and protects against cytotoxic effect of radiation and doxorubicin. *Oncogene* 18, 2643–2649.
- Wang, Y.V., Leblanc, M., Wade, M., Jochemsen, A.G., and Wahl, G.M. (2009). Increased radio-resistance and accelerated B-cell lymphomas in mice with Mdmx mutations that prevent modifications by DNA damage-activated kinases. *Cancer Cell* 16, 33–43.
- Wang, Y.V., Leblanc, M., Fox, N., Mao, J.-H., Tinkum, K.L., Krummel, K., Engle, D., Piwnica-Worms, D., Piwnica-Worms, H., Balmain, A., et al. (2011c). Fine-tuning p53 activity through C-terminal modification significantly contributes to HSC homeostasis and mouse radiosensitivity. *Genes Dev.* 25, 1426–1438.
- Wang, Z., Inuzuka, H., Zhong, J., Fukushima, H., Wan, L., Liu, P., and Wei, W. (2012). DNA damage-induced activation of ATM promotes beta-TRCP-mediated Mdm2 ubiquitination and destruction. *Oncotarget* 3, 1026–1035.
- Waning, D.L., Lehman, J.A., Batuello, C.N., and Mayo, L.D. (2011). c-Abl phosphorylation of Mdm2 facilitates Mdm2-Mdmx complex formation. *J. Biol. Chem.* 286, 216–222.
- Watanabe, T., Hotta, T., Ichikawa, A., Kinoshita, T., Nagai, H., Uchida, T., Murate, T., and Saito, H. (1994). The MDM2 oncogene overexpression in chronic lymphocytic leukemia and low-grade lymphoma of B-cell origin. *Blood* 84, 3158–3165.
- Watson, I.R., Li, B.K., Roche, O., Blanch, A., Ohh, M., and Irwin, M.S. (2010). Chemotherapy induces NEDP1-mediated destabilization of MDM2. *Oncogene* 29, 297–304.
- Weber, J.D., Taylor, L.J., Roussel, M.F., Sherr, C.J., and Bar-Sagi, D. (1999). Nucleolar Arf sequesters Mdm2 and activates p53. *Nat. Cell Biol.* 1, 20–26.

- Wen, S.T., Jackson, P.K., and Van Etten, R.A. (1996). The cytostatic function of c-Abl is controlled by multiple nuclear localization signals and requires the p53 and Rb tumor suppressor gene products. *EMBO J.* 15, 1583–1595.
- Wienken, M., Dickmanns, A., Nemajerova, A., Kramer, D., Najafova, Z., Weiss, M., Karpiuk, O., Kassem, M., Zhang, Y., Lozano, G., et al. (2016). MDM2 associates with Polycomb Repressor Complex 2 and enhances stemness-promoting chromatin modifications independent of p53. *Mol. Cell* 61, 68–83.
- Winter, M., Milne, D., Dias, S., Kulikov, R., Knippschild, U., Blattner, C., and Meek, D. (2004). Protein kinase CK1delta phosphorylates key sites in the acidic domain of murine double-minute clone 2 protein (MDM2) that regulate p53 turnover. *Biochemistry* 43, 16356–16364.
- Wu, Z., Earle, J., Saito, S., Ichi, Anderson, C.W., Appella, E., and Xu, Y. (2002). Mutation of mouse p53 Ser23 and the response to DNA damage. *Mol. Cell. Biol.* 22, 2441–2449.
- Xu, Y., and Baltimore, D. (1996). Dual roles of ATM in the cellular response to radiation and in cell growth control. *Genes Dev.* 10, 2401–2410.
- Xue, W., Zender, L., Miething, C., Dickins, R.A., Hernando, E., Krizhanovsky, V., Cordon-Cardo, C., and Lowe, S.W. (2007). Senescence and tumour clearance is triggered by p53 restoration in murine liver carcinomas. *Nature* 445, 656–660.
- Yang, C., Cirielli, C., Capogrossi, M.C., and Passaniti, A. (1995). Adenovirus-mediated wild-type p53 expression induces apoptosis and suppresses tumorigenesis of prostatic tumor cells. *Cancer Res.* 55, 4210–4213.
- Yin, C., Knudson, C.M., Korsmeyer, S.J., and Dyke, T.V. (1997). Bax suppresses tumorigenesis and stimulates apoptosis in vivo. *Nature* 385, 637–640.
- Yonish-Rouach, E., Resnftzky, D., Lotem, J., Sachs, L., Kimchi, A., and Oren, M. (1991). Wild-type p53 induces apoptosis of myeloid leukaemic cells that is inhibited by interleukin-6. *Nature* 352, 345–347.
- Yoon, K.-A., Nakamura, Y., and Arakawa, H. (2004). Identification of ALDH4 as a p53-inducible gene and its protective role in cellular stresses. *J. Hum. Genet.* 49, 134–140.
- Yu, G.W., Rudiger, S., Veprintsev, D., Freund, S., Fernandez-Fernandez, M.R., and Fersht, A.R. (2006). The central region of HDM2 provides a second binding site for p53. *Proc. Natl. Acad. Sci.* 103, 1227–1232.

- Yu, H., Shen, H., Yuan, Y., XuFeng, R., Hu, X., Garrison, S.P., Zhang, L., Yu, J., Zambetti, G.P., and Cheng, T. (2010). Deletion of Puma protects hematopoietic stem cells and confers long-term survival in response to high-dose γ -irradiation. *Blood* 115, 3472–3480.
- Yu, J., Zhang, L., Hwang, P.M., Kinzler, K.W., and Vogelstein, B. (2001). PUMA induces the rapid apoptosis of colorectal cancer cells. *Mol. Cell* 7, 673–682.
- Yuan, Z.-M., Huang, Y., Ishiko, T., Kharbanda, S., Weichselbaum, R., and Kufe, D. (1997). Regulation of DNA damage-induced apoptosis by the c-Abl tyrosine kinase. *Proc. Natl. Acad. Sci.* 94, 1437–1440.
- Yuan, Z.-M., Shioya, H., Ishiko, T., Sun, X., Gu, J., Huang, Y., Lu, H., Kharbanda, S., Weichselbaum, R., and Kufe, D. (1999). p73 is regulated by tyrosine kinase c-Abl in the apoptotic response to DNA damage. *Nature* 399, 814–817.
- Zacchi, P., Gostissa, M., Uchida, T., Salvagno, C., Avolio, F., Volinia, S., Ronai, Z., Blandino, G., Schneider, C., and Del Sal, G. (2002). The prolyl isomerase Pin1 reveals a mechanism to control p53 functions after genotoxic insults. *Nature* 419, 853–857.
- Zambetti, G.P., Bargonetti, J., Walker, K., Prives, C., and Levine, A.J. (1992). Wild-type p53 mediates positive regulation of gene expression through a specific DNA sequence element. *Genes Dev.* 6, 1143–1152.
- Zhan, Q., Carrier, F., and Fornace, A.J. (1993). Induction of cellular p53 activity by DNA-damaging agents and growth arrest. *Mol. Cell. Biol.* 13, 4242–4250.
- Zhang, Y., Xiong, Y., and Yarbrough, W.G. (1998). ARF promotes MDM2 degradation and stabilizes p53: ARF-INK4a locus deletion impairs both the Rb and p53 tumor suppression pathways. *Cell* 92, 725–734.
- Zheng, H., You, H., Zhou, X.Z., Murray, S.A., Uchida, T., Wulf, G., Gu, L., Tang, X., Lu, K.P., and Xiao, Z.-X.J. (2002). The prolyl isomerase Pin1 is a regulator of p53 in genotoxic response. *Nature* 419, 849–853.
- Zhou, B.P., Liao, Y., Xia, W., Zou, Y., Spohn, B., and Hung, M.C. (2001). HER-2/neu induces p53 ubiquitination via Akt-mediated MDM2 phosphorylation. *Nat. Cell Biol.* 3, 973–982.

- Zhu, J., Zhou, W., Jiang, J., and Chen, X. (1998). Identification of a novel p53 functional domain that is necessary for mediating apoptosis. *J. Biol. Chem.* 273, 13030–13036.
- Zindy, F., Eischen, C.M., Randle, D.H., Kamijo, T., Cleveland, J.L., Sherr, C.J., and Roussel, M.F. (1998). Myc signaling via the ARF tumor suppressor regulates p53-dependent apoptosis and immortalization. *Genes Dev.* 12, 2424–2433.
- Zou, Q., Jin, J., Hu, H., Li, H.S., Romano, S., Xiao, Y., Nakaya, M., Zhou, X., Cheng, X., Yang, P., et al. (2014). USP15 stabilizes MDM2 to mediate cancer-cell survival and inhibit antitumor T cell responses. *Nat. Immunol.* 15, 562–570.
- Zuckerman, V., Lenos, K., Popowicz, G.M., Silberman, I., Grossman, T., Marine, J.-C., Holak, T.A., Jochemsen, A.G., and Haupt, Y. (2009). c-Abl phosphorylates Hdmx and regulates its interaction with p53. *J. Biol. Chem.* 284, 4031–4039.